Tensor lattice field theory for renormalization and quantum computing

Yannick Meurice

Department of Physics and Astronomy, The University of Iowa, Iowa City, Iowa 52242, USA

Ryo Sakai

Department of Physics and Astronomy, The University of Iowa, Iowa City, Iowa 52242, USA and Department of Physics, Syracuse University, Syracuse, New York 13244, USA

Judah Unmuth-Yockey

Department of Physics, Syracuse University, Syracuse, New York 13244, USA and Fermi National Accelerator Laboratory, Batavia, Illinois 60510, USA

(published 26 May 2022)

The successes and limitations of statistical sampling for a sequence of models studied in the context of lattice QCD are discussed and the need for new methods to deal with finite-density and real-time evolution is emphasized. It is shown that these lattice models can be reformulated using tensorial methods where the field integrations in the path-integral formalism are replaced by discrete sums. These formulations involve various types of duality and provide exact coarse-graining formulas that can be combined with truncations to obtain practical implementations of the Wilson renormalization group program. Tensor reformulations are naturally discrete and provide manageable transfer matrices. Truncations with the time continuum limit are combined, and Hamiltonians suitable for performing quantum simulation experiments, for instance, using cold atoms, or to be programmed on existing quantum computers, are derived. Recent progress concerning the tensor field theory treatment of noncompact scalar models, supersymmetric models, economical four-dimensional algorithms, noise-robust enforcement of Gauss's law, symmetry preserving truncations, and topological considerations are reviewed. Connections with other tensor network approaches are also discussed.

DOI: 10.1103/RevModPhys.94.025005

CONTENTS

I. INTRODUCTION

Quantum field theory models on space or spacetime lattices play an important role in our understanding of strongly interacting particles, nuclei, superconductivity, condensed matter, and phase transitions. In high-energy and nuclear physics, lattice quantum chromodynamics (QCD) provides an *ab initio* theory of strong interactions. In the QCD context, the lattice is a nonperturbative ultraviolet regularization that preserves local gauge invariance. As the lattice is not a physical feature, we need to approach the continuum limit where the lattice spacing is small compared to the physical length scales involved in the problem.

In the context of solid-state physics, lattice spacings of the order of a few angstroms are present, and atomic physicists can create optical lattices with a lattice spacing on the order of the laser wavelength; however, large correlation lengths appear near critical points and universal behavior independent of the microscopic details can be observed. It is also possible to create actual optical lattices in laboratories by trapping cold atoms in counterpropagating laser beams, and to tune the interaction in order to quantum simulate lattice models with interactions similar to Hubbard models (Bloch, Dalibard, and Zwerger, 2008). This is called an analog computing method or a quantum simulation experiment. Again, it is possible to tune the parameters to reach universal behaviors related to quantum phase transitions with large correlation lengths.

More generally, we are getting better control of the manipulation of small quantum systems evolving in small Hilbert spaces, and the idea of using physical quantum systems to study theoretical quantum models (Feynman, 1982) has generated many interesting developments (Georgescu, Ashhab, and Nori, 2014). As bits (which can be either on or off) can be thought of as the basic building blocks of classical computers, one can envision qubits that can each be used as a two-dimensional Hilbert space as the building blocks of a quantum computer. If we want to use the 2^N-dimensional Hilbert space provided by N qubits to represent the Hilbert space of a quantum field theory problem, we need to apply discretizations and truncations. Discretization of space can be achieved using the lattice approximation, while the discretization of continuous field integration can be done using character expansion, as is discussed extensively in this review, or by other methods that include gauge magnets and quantum links (Horn, 1981; Orland and Rohrlich, 1990; Brower, Chandrasekharan, and Wiese, 1999; Wiese, 2013), field digitization, or summation of discrete subgroups (Jordan, Lee, and Preskill, 2014; Alexandru, Bedaque, Harmalkar *et al.*, 2019; Hackett, Daniel *et al.*, 2019; Klco and Savage, 2019; Lamm, Lawrence, and Yamauchi, 2019).

General arguments (Lloyd, 1996) showed that for local interactions, a quantum computer will reduce the computational effort, for problems like the real-time evolution, to a polynomial in the size of the system rather than an exponential for a classical computer.

From a purely theoretical point of view, studying models with a large number of strongly correlated degrees of freedom is challenging. To deal with this situation, Kadanoff (1966) suggested considering the average field or spin in cells of variable sizes that are often called "blocks." The procedure is often called "block spinning" and it played a crucial role in the development of the renormalization group (RG) ideas (Wilson and Kogut, 1974). Sometimes great theoretical intuitions can take a long time to be practically realized. Despite its visual appeal, the block-spinning procedure is not easy to implement numerically. It typically involves approximations that are difficult to improve.

Successful applications of the RG idea were made possible without requiring numerical implementations of the original blocking idea. A well-known example is the discovery of asymptotic freedom (Gross and Wilczek, 1973; Politzer, 1973), which initially relied on a one-loop calculation of the Callan-Symanzik beta function. Typically, the interplay between small and large energy scales is more easily seen in the momentum representation. However, it is clear that if it were possible to design practical methods such that each step of the blocking could be performed within a reasonable amount of time and with a desired accuracy, the computational cost would scale like the number of blockings, in other words, the logarithm of the volume, since the size of a block after each blocking step doubles (Kadanoff, 1966). Achieving this goal is nontrivial and not guaranteed in general. We now explain the practical issues that have prevented the use of blocking for quantitative purposes and how new tensorial methods can be used to make progress in this direction.

A simple way of blocking consists of introducing 1 in the partition function in the following generic form:

$$\prod_{\mathfrak{B}} \int d\Phi_{\mathfrak{B}} \delta\left(\Phi_{\mathfrak{B}} - \sum_{x\in\mathfrak{B}} \phi_x\right) = 1, \tag{1}$$

where the blocks $\mathfrak{B}$ form a partition of the original lattice. For instance, in a three-dimensional cubic lattice, the blocks can be chosen as cubes with a linear size of two lattice spacings and contain eight sites. ϕ_x are the original lattice fields and $\Phi_{\mathfrak{B}}$ are the block fields that inherit new effective interactions after one performs the integration over the original fields. Conceptually, this sounds easy; however, in practice it appears to be more complicated than the original problem. As an example, one can try to write a simple algorithm for the two-dimensional Ising model on a square lattice by replacing four spins in a 2×2 square block with a single variable and writing an effective energy function (or at least some effective measure) for the new block variables. The procedure becomes more intricate as we proceed, and finding the effective energy function is nontrivial (Liu *et al.*, 2013).

For this reason approximate procedures were developed, such as the Migdal-Kadanoff approximation (Migdal, 1975; Kadanoff, 1976), the approximate recursion formula (Wilson and Kogut, 1974), and other hierarchical approximations (Dyson, 1969; Baker, 1972; Meurice, 2007), where no new interactions are generated by the blocking process. However, in these examples, the lack of a reference to an exact procedure to handle the original model with localized interactions makes the systematic improvement of these approximations difficult. Similar issues appear in nonperturbative functional methods based on the momentum space representation (Berges, Tetradis, and Wetterich, 2002), where the local potential approximation allows for high-accuracy estimates of the critical exponents (Bervillier, Juttner, and Litim, 2007), but its improvement with methods such as the derivative expansion remains difficult (Bervillier, 2013). For Ising models, it is possible to deal with the proliferation of couplings generated by the blocking process by starting with the most general set of interactions (Kadanoff, 1975; Kadanoff and Houghton, 1975; Niemeijer and van Leeuwen, 1976). They introduce the identity in terms of probabilities $P(\{\sigma'\},\{\sigma\})$ such that

$$\sum_{\{\sigma'\}} P(\{\sigma'\},\{\sigma\}) = 1, \tag{2}$$

where $\{\sigma'\}$ are new Ising spins associated with the blocks. As we later discuss, this special setup allows us to write formal expressions for the effective couplings as double partition functions and write RG equations. However, from a computational point of view the locality of the interactions is lost and additional assumptions are needed to proceed.

In contrast, reformulations of the partition function of classical spin models as the trace of a product of local tensors provide a new type of blocking procedure in configuration space called tensor RG (TRG) (Nishino and Okunishi, 1996; Levin and Nave, 2007; Gu and Wen, 2009; Xie *et al.*, 2009; Gu, Verstraete, and Wen, 2010; Xie *et al.*, 2012).

TRG procedures can be obtained by applying truncations to exact blocking formulas. The blocking unambiguously separates the degrees of freedom inside the block (which are integrated over) from those kept to communicate with the neighboring blocks (Meurice, 2013). However, the degrees of freedom remaining after the blocking are still microscopic, and finding a truncation that captures the low-energy physics and the entanglement is a nontrivial task.

In the early stages of TRG development, singular value decomposition (SVD) methods were used extensively. This was reviewed by Efrati *et al.* (2014). Some SVD procedures can be simplified by using character expansions (Liu *et al.*, 2013) when applied to most models studied in the context of lattice gauge theory (Liu *et al.*, 2013; Denbleyker *et al.*, 2014; Shimizu and Kuramashi, 2014a, 2018; Yu *et al.*, 2014; Zou *et al.*, 2014; Bazavov *et al.*, 2015; Takeda and Yoshimura, 2015; Kadoh *et al.*, 2018, 2019, 2020; Yoshimura *et al.*, 2018; Bazavov *et al.*, 2019; Kuramashi and Yoshimura, 2019; Nakamura, Oba, and Takeda, 2019; Unmuth-Yockey, 2019; Butt *et al.*, 2020). Tensorial methods are also used in the context of quantum gravity (Perez, 2013; Dittrich, Mizera, and Steinhaus, 2016; Asaduzzaman, Catterall, and Unmuth-Yockey, 2020).

In general, tensorial methods represent a new approach to lattice field theory that we call tensor lattice field theory (TLFT). TLFT can be used for purposes more general than the blocking procedure. In particular, TLFT provides a convenient, discrete framework to perform quantum computations or simulations. There are, additionally, continuous tensor network, or tensor-like, methods such as continuous matrix product states (Haegeman *et al.*, 2013; Campos, Sierra, and López, 2019).

In this review, we introduce TLFT for lattice models studied in the context of lattice gauge theory and report progress made for blocking and quantum computing, two competing methods that attempt to reduce the computing time logarithmically. The models targeted are introduced in Sec. II. We advocate a road map starting with the Ising model and culminating with QCD that we call the "Kogut sequence" (Kogut, 1979, 1983). This sequence is sometimes called a "ladder" and has been followed successfully in situations where importance-sampling methods such as the Metropolis algorithm are effective. Lattice QCD has become a reliable precision tool to study the static properties of hadrons. Currently we are roughly in the middle of the sequence, i.e., we have roughly half of the models in the sequence remaining to be studied thoroughly, with improvements and optimization on previous models still possible. However, we anticipate that recent progress on higher-dimensional algorithms (Kadoh and Nakayama, 2019; Adachi, Okubo, and Todo, 2020) could be combined with the methods that we describe to deal with gauge fields, fermions, and non-Abelian (noncommuting) symmetries in order to attempt calculations directly related to lattice QCD in the coming years.

In Sec. III, we discuss situations where importance sampling cannot be used and where quantum computations or simulations could provide alternate ways to perform computations. This includes unitary, real-time evolution and other situations where a sign problem is encountered. One important long-term goal with potential impact on the interpretation of high-energy collider data is doing *ab initio* real-time calculations relevant to fragmentation processes and parton distribution functions. In other words, starting with lattice QCD, we want to perform

calculations that would ultimately replace the use of event generators such as PYTHIA (Sjostrand *et al.*, 2015).

The simplest starting point for the real-time evolution is the evolution operator $\exp(-i\hat{H}t/\hbar)$ acting on the Hilbert space of the quantum Hamiltonian $\hat{H}$. We provide a first look at the transfer matrix that smoothly connects the "classical" Lagrangian approach to the Hilbert space used in the Hamiltonian formalism. We discuss various types of dualities (geometrical and topological) that are often used together and mistaken for one another.

For the models in the Kogut sequence, the bosonic field variables and the symmetry groups are *compact*. General mathematical theorems, namely, the Pontryagin duality (Pontryagin, 1939) and the Peter-Weyl theorem (Peter and Weyl, 1927), guarantee that functions over compact groups can be expanded in terms of *discrete* sums of representations. This is called the "character expansion" and was exploited to calculate strong coupling expansions (Balian, Drouffe, and Itzykson, 1975) or introduce new variables on geometrically dual lattice elements (Savit, 1980).

The discreteness of the character expansion provides a natural starting point for building approximate reformulations of lattice models suitable for quantum computing or quantum simulation experiments. The Ising model is an elementary example where the Hilbert space of the transfer matrix can be implemented with a set of qubits, the basic components of actual quantum computers that exist in a linear superposition of two states $|0\rangle$ and $|1\rangle$, rather than being just *on* or *off* like the bits of a classical computer. For models with continuous fields, character expansions allow us to perform the "hard integrals" analytically without needing to approximate the numerical discretizations that break the continuous symmetries. Demonstrating the power of the character expansion is one of the main goals of this review. Examples of quantum computations and simulations are provided at the end of Sec. III. In Sec. IV, we clarify the use of the terms "classical" and "quantum" in various contexts and make connections with other approaches (Schollwöck, 2011b; Haegeman and Verstraete, 2017; Ran *et al.*, 2020; Cirac *et al.*, 2021).

Section V introduces the tensor reformulation for the Ising model. SVD, truncation, and the TRG method are discussed in Sec. VI. Spin models with an $O(2)$ symmetry or with discrete subgroups are discussed in Sec. VII. In Sec. VIII, we derive expressions for local tensors in the simple case of a non-Abelian spin model with $O(3)$ symmetry. We also find tensor expressions for effective theories of gauge theories known as principal chiral models.

Models with local gauge symmetry are introduced in Sec. IX. We first consider Abelian gauge theories and work up in complexity to tensor expressions for non-Abelian gauge theories as well.

In Sec. X, tensor network expressions for the real and the complex ϕ^4 theory are derived. For models with noncompact fields such as the scalar ϕ^4 theory, the Gaussian quadrature rule can be used to extract discrete degrees of freedom, just as the gauge degrees of freedom are discretized via character expansions. The accuracy of the tensor network approach is shown for the real-field case, and an ability to deal with a severe sign problem is shown in the complex-field case.

In Sec. XI, we present tensor formulations for models with fermionic degrees of freedom. In general, fermions fit in well with the tensor (and discrete) approach thanks to the nilpotency of the Grassmann variables. In the section, various models that contain fermions such as pure fermions, gauged fermions, and fermions combined with scalars are discussed.

In Sec. XII, we rediscuss the transfer matrix using the tensor formalism and broaden the perspective. Recent TLFT developments regarding symmetries, topological solutions, and quantum gravity are discussed in Sec. XIII.

II. LATTICE FIELD THEORY

A. The Kogut sequence: From Ising to QCD

In the early 1970s, QCD appeared to be a strong candidate for a theory of strong interactions involving quarks and gluons. However, the perturbative methods that provided satisfactory ways to handle the electroweak interactions of leptons failed to explain confinement, mass gaps, and chiral symmetry breaking. A nonperturbative definition of QCD was needed. In 1974, Wilson proposed (Wilson, 1974) a lattice formulation of QCD where the $SU(3)$ local symmetry is exact. As this four-dimensional model is fairly difficult to handle numerically, a certain number of research groups started considering simpler lattice models in lower dimensions and then increased symmetry and dimensionality. This led to a sequence of models, sometimes called the "Kogut ladder," that appears in the reviews of Kogut (1979, 1983) and was later addressed with small modifications by Polyakov (1987) and Itzykson and Drouffe (1991).

The sequence is approximately the following:

(1) $D = 2$ Ising model
(2) $D = 3$ Ising model and its gauge dual
(3) $D = 2$ $O(2)$ spin and Abelian Higgs models
(4) $D = 2$ fermions and the Schwinger model
(5) $D = 3$ and 4 $U(1)$ gauge theory
(6) $D = 3$ and 4 non-Abelian gauge theories
(7) $D = 4$ lattice fermions
(8) $D = 4$ QCD

This sequence should not be understood in a rigid way as if each step is necessary for the next step. For instance, steps (3)–(5) can be interchanged, and the problems involving fermions have specific features that are not easily compared to those involving only bosonic fields. The message that we want to convey is that there is an approximate road map that has proven to be effective for the classical approach of lattice field theory in dealing with static problems using importance-sampling (Monte Carlo) methods. We advocate following a similar path to develop the quantum versions of these models and deal with real-time evolution and other problems not accessible with classical methods. The difference between quantum and classical is explained more precisely in Sec. IV.A. A similar path is followed to develop numerical coarse graining.

B. Classical lattice models and path integral

In this section we introduce lattice versions of classical field theory models. At this point, we point out that, while we provide definitions of the fields, notations, and acronyms or

initials used, more details on basic quantum field theory and lattice field theory can be found in textbooks and reviews by Kogut (1979), Itzykson and Drouffe (1991), Montvay and Münster (1994), and Peskin and Schroeder (1995). We use a Euclidean time and treat space and time on the same footing. The metric is simply a Kronecker delta in D dimensions. We then discretize space and time. We use a D-dimensional (hyper)cubic Euclidean spacetime lattice. The sites are denoted as $x = (x_1, x_2, \ldots, x_D)$, with $x_D = \tau$ the Euclidean-time direction. In lattice units, the spacetime sites are labeled with integers. In the following, the lattice units are implicit. The links between two nearest-neighbor lattice sites x and $x + \hat{\mu}$ are labeled as (x, μ) and the *plaquettes*, the smallest squares on a square or (hyper)cubic lattice, are delimited by four sites x, $x + \hat{\mu}$, $x + \hat{\mu} + \hat{\nu}$, while $x + \hat{\nu}$ are labeled as $(x, \mu\nu)$. By convention, we start with the lowest index when introducing a conventional circulation at the boundary of the plaquette. The total number of sites is denoted by V. Unless otherwise specified, periodic boundary conditions are assumed, and they preserve a discrete translational symmetry. If we take the time continuum limit, we obtain a quantum Hamiltonian formulation in $D-1$ spatial dimensions.

In the continuum, the Lagrangian density for N real scalar fields with an $\mathrm{O}(N)$ global symmetry reads

$$\mathcal{L}^{\mathrm{O}(N)}_{\mathrm{Euclidean}} = \tfrac{1}{2}\partial_\mu \vec{\phi} \cdot \partial_\nu \vec{\phi} \delta^{\mu\nu} + \lambda(\vec{\phi} \cdot \vec{\phi} - v^2)^2, \tag{3}$$

with $\vec{\phi}$ an N-dimensional vector. Here λ is a coupling constant whose size determines fluctuations of the $|\vec{\phi}|$ field around some value v. The potential has degenerate minima on an $(N-1)$-dimensional hypersphere S_{N-1} and a local maximum at $\vec{\phi} = 0$. For $N = 2$, the low-energy part of the potential has a shape similar to the bottom of a wine bottle. The degenerate minima form a circle at the bottom. We can study the small fluctuations about a given minimum on the circle. Note that the choice of a minimum breaks the $\mathrm{O}(2)$ symmetry. There are "soft" fluctuations along the circle that restore the symmetry and "hard" fluctuations in the radial direction.

We can extend this analysis to arbitrary N. We have one massive mode (fluctuations in the symmetry breaking direction) with mass $2\sqrt{2\lambda}v$ and $N-1$ massless modes [Nambu-Goldstone (NG) modes] that is the number of broken generators (Nambu, 1960; Goldstone, 1961; Goldstone, Salam, and Weinberg, 1962; Peskin and Schroeder, 1995).

We can write the Euclidean action for the NG modes on a D-dimensional lattice with isotropic lattice spacing a as

$$S_{\mathrm{NLSM}} = \frac{1}{2}\sum_x \sum_{\mu=1}^{D} a^{D-2}(\vec{\phi}_{x+\hat{\mu}} - \vec{\phi}_x) \cdot (\vec{\phi}_{x+\hat{\mu}} - \vec{\phi}_x). \tag{4}$$

This is called the nonlinear sigma model (NLSM) (Peskin and Schroeder, 1995). The constraint $\vec{\phi}_x \cdot \vec{\phi}_x = v^2$ (which enforces the "nonlinear" part of its name) can be expressed by introducing the unit vectors $\vec{\phi}_x = v\vec{\sigma}_x$ such that

$$\vec{\sigma}_x \cdot \vec{\sigma}_x = 1. \tag{5}$$

Redefining $a^{D-2}v^2 \equiv \beta$, we get the simple action

$$S_{\mathrm{NLSM}} = \beta \sum_{x,\mu} (1 - \vec{\sigma}_{x+\hat{\mu}} \cdot \vec{\sigma}_x). \tag{6}$$

These models are often called spin models as well. The first term in the action $\beta \sum_{x,\mu} 1$ is a constant that is often dropped. However, for large β the configurations with almost constant $\vec{\sigma_x}$ dominate the partition function and, since under these circumstances $\vec{\sigma}_{x+\hat{\mu}} \cdot \vec{\sigma}_x \simeq 1$, it is useful to subtract the constant in order to keep only the small fluctuations.

The case of $N = 1$ is the well-known Ising model with $\sigma_x = \pm 1$ (Ising, 1925). For $N = 2$, the terminologies "planar model" and "classical XY model" (Vaks and Larkin, 1965; Bowers and Joyce, 1967) are common, and if we use the circle parametrization

$$\sigma^{(1)}_x = \cos(\varphi_x), \qquad \sigma^{(2)}_x = \sin(\varphi_x), \tag{7}$$

then

$$\vec{\sigma}_{x+\hat{\mu}} \cdot \vec{\sigma}_x = \cos(\varphi_{x+\hat{\mu}} - \varphi_x), \tag{8}$$

with $\varphi_x \in [0, 2\pi)$.

There is another class of models that break the $\mathrm{O}(2)$ symmetry in Eq. (8) into a discrete $\mathbb{Z}_q$ symmetry; i.e., the possible angles are restricted to those of the qth roots of unity in the complex plane. They are called the q-state clock models (Potts, 1952). These models have the same action as Eq. (6) with identification of the angles being discrete,

$$\varphi_x = \frac{2\pi n_x}{q} \tag{9}$$

where $n_x = 0, 1, 2, \ldots, q-1$. With this identification, the $\mathrm{O}(2)$ model emerges as the $q \to \infty$ limit of the q-state clock models, and the Ising model is simply the $q = 2$ model.

For $N = 3$, the symmetry becomes non-Abelian and the model is sometimes called the "classical Heisenberg model." In the large-N limit, the model becomes solvable if we take the limit in such a way that $N/\beta(N) = \lambda$ remains constant (Coleman, Jackiw, and Politzer, 1974).

It is instructive to rewrite the $\mathrm{O}(2)$ model using the complex form

$$\Phi_x = e^{i\varphi_x}. \tag{10}$$

When the constant terms are dropped, the $\mathrm{O}(2)$ action reads

$$\begin{aligned} S_{\mathrm{O}(2)} &= \frac{\beta}{2}\sum_{x,\mu} (\Phi_{x+\hat{\mu}} - \Phi_x) \cdot (\Phi_{x+\hat{\mu}} - \Phi_x)^\star \\ &= \beta \sum_{x,\mu} [1 - \cos(\varphi_{x+\hat{\mu}} - \varphi_x)]. \end{aligned}$$

The $\mathrm{O}(2)$ model has a global symmetry

$$\varphi_x \to \varphi_x + \alpha. \tag{11}$$

With the complex notation, this transformation becomes

$$\Phi_x \to e^{i\alpha}\Phi_x. \tag{12}$$

We promote this symmetry to a local one

$$\Phi_x \to e^{i\alpha_x}\Phi_x, \tag{13}$$

i.e., one that is site dependent. This can be achieved by inserting a phase $U_{x,\mu}$ between $\Phi_x^\star$ and $\Phi_{x+\hat{\mu}}$, which transforms as

$$U_{x,\mu} \to e^{i\alpha_x}U_{x,\mu}e^{-i\alpha_{x+\hat{\mu}}}. \tag{14}$$

The procedure can be extended as follows for arbitrary N-dimensional complex vectors $\mathbf{\Phi}_x$ with a local transformation involving a U(N) matrix V_x:

$$\mathbf{\Phi}_x \to V_x\mathbf{\Phi}_x. \tag{15}$$

In addition, we can introduce U(N) matrices $\mathbf{U}_{x,\hat{\mu}}$ transforming as

$$\mathbf{U}_{x,\hat{\mu}} \to V_x\mathbf{U}_{x,\hat{\mu}}V^\dagger_{x+\hat{\mu}}. \tag{16}$$

The action

$$S_{\mathrm{U}(N)} = -\frac{\beta}{2}\sum_{x,\mu}(\mathbf{\Phi}^\dagger_x\mathbf{U}_{x,\hat{\mu}}\mathbf{\Phi}_{x+\hat{\mu}} + \mathrm{H.c.}) \tag{17}$$

has a local U(N) invariance that we call gauge invariance. If we consider two successive links in positive directions, then the local transformation at the middle site cancels and

$$\mathbf{U}_{x,\mu}\mathbf{U}_{x+\hat{\mu},\nu} \to V_x\mathbf{U}_{x,\mu}\mathbf{U}_{x+\hat{\mu},\nu}V^\dagger_{x+\hat{\mu}+\hat{\nu}}. \tag{18}$$

If the second link goes in the negative direction, we use the Hermitian conjugate and a similar property holds:

$$\mathbf{U}_{x,\mu}\mathbf{U}^\dagger_{x+\hat{\mu}-\hat{\nu},\nu} \to V_x\mathbf{U}_{x,\mu}\mathbf{U}^\dagger_{x+\hat{\mu}-\hat{\nu},\nu}V^\dagger_{x+\hat{\mu}-\hat{\nu}}. \tag{19}$$

We can pursue this process for an arbitrary path connecting x to some x_{final}. The transformation on the right-hand side is $V^\dagger_{x_{\mathrm{final}}}$. If we close the path and take the trace, we obtain a gauge-invariant quantity. We call these traces of products of gauge matrices over closed loops, "Wilson loops" (Wilson, 1974). In the case where the loop goes around the imaginary time direction, we often call it a "Polyakov loop" (Polyakov, 1978).

On a square, cubic, or hypercubic lattice, the smallest path that gives a nontrivial Wilson loop is a square. We call this square a plaquette. Claude Itzykson coined this terminology after Ken Wilson's seminar in Orsay in 1973. The corresponding matrix is

$$\mathbf{U}_{\mathrm{pl}} = \mathbf{U}_{x,\mu\nu} = \mathbf{U}_{x,\mu}\mathbf{U}_{x+\hat{\mu},\nu}\mathbf{U}^\dagger_{x+\hat{\nu},\mu}\mathbf{U}^\dagger_{x,\nu} \tag{20}$$

The simplest gauge-invariant lattice model has the following action, called Wilson's action:

$$S_{\mathrm{Wilson}} = \beta_{\mathrm{pl}}\sum_{\langle x,\mu\nu\rangle}\left[1 - \frac{1}{2N}\mathrm{Tr}[\mathbf{U}_{x,\mu\nu} + \mathrm{H.c.}]\right], \tag{21}$$

where $\sum_{\langle x,\mu\nu\rangle}$ indicates a sum over all plaquettes. Here each $\mathbf{U}_{x,\mu}$ is related to the vector potential, or gauge field, in the continuum theory through

$$\mathbf{U}_{x,\mu} = e^{i\mathbf{A}_{x,\mu}}. \tag{22}$$

On the lattice, both $\mathbf{U}_{x,\mu}$ and $\mathbf{A}_{x,\mu}$ are located on a link starting at x and going in the $\hat{\mu}$ positive direction. In the Abelian case ($N = 1$), the matrix reduces to a phase

$$U_{x,\mu} = e^{iA_{x,\mu}} \tag{23}$$

and there is no need to take the trace.

Another generalization of the $N = 1$ expression of the complex phase given in Eq. (10) consists of replacing Φ_x with an SU(N) matrix $\mathbf{U}_x$. This is called the principal chiral model (Gürsey, 1960; Green and Samuel, 1981; Samuel and Yee, 1985; Campostrini, Rossi, and Vicari, 1995; Peskin and Schroeder, 1995),

$$S_{\mathrm{PCM}} = -\frac{\beta}{2N}\sum_{x,\mu}[\mathrm{Tr}(\mathbf{U}^\dagger_{x+\hat{\mu}}\mathbf{U}_x) + \mathrm{H.c.}]. \tag{24}$$

This model has a global rotational symmetry under the U(N) group such that $\mathbf{U}_{x,\mu} \to \mathbf{U}_{x,\mu}{}' = V\mathbf{U}_{x,\mu}V^\dagger$, just as in Eq. (16) in the case of a uniform V in all of spacetime.

We can also consider the $N = 1$ case for Eq. (3) when the group is no longer compact; i.e., ϕ_x can take on the values of any real or complex number. The action on the lattice is then

$$S_{\mathrm{scalar}} = \sum_x\left(\frac{1}{2}\sum_{\mu=1}^{D}|\phi_{x+\hat{\mu}} - \phi_x|^2 + \lambda(|\phi_x|^2 - \nu^2)^2\right) \tag{25}$$

or, equivalently,

$$S_{\mathrm{scalar}} = \sum_x\left\{\frac{1}{2}\sum_{\mu=1}^{D}|\phi_{x+\hat{\mu}} - \phi_x|^2 - \frac{\mu_0^2}{2}|\phi_x|^2 + \frac{\lambda'}{4}|\phi_x|^4\right\}, \tag{26}$$

with the substitution $\mu_0^2/2 = 2\lambda\nu^2$ and $\lambda'/4 = \lambda$, and the overall constant is ignored.

Besides scalar fields, we also consider fermionic fields (or Grassmann fields on the lattice). In the case of free fermions, we can write a lattice action using a straightforward discretization due to Wilson (Wilson, 1974) as

$$S_{\mathrm{WD}} = \sum_x\overline{\psi}_x(D\psi)_x \tag{27}$$

with the Wilson-Dirac operator defined by

$$D_{xx'} = (am + rD)\delta_{x,x'} + \frac{1}{2}\sum_{\mu=1}^{D}\{(r-\gamma_\mu)\delta_{x',x+\hat{\mu}} + (r+\gamma_\mu)\delta_{x,x'+\hat{\mu}}\}, \tag{28}$$

where γ_μ are the gamma matrices in D dimensions and r is the "Wilson parameter" to control species doubling. This so-called doubling is the name given to the existence of extra copies of fermions (16 in the case of four dimensions), and they must be removed or gapped out appropriately. ψ_x and $\bar{\psi}_x$ are multicomponent Grassmann variables that *anticommute*, as opposed to classical bosonic variables which can be interchanged without a sign change.

There is another formulation of lattice fermions where different components of the fermion fields are located at different lattice sites, called staggered fermions. This comes about from a transformation that mixes the fermion components and spacetime components (Kogut and Susskind, 1975). The action for free fermion fields is given by

$$S_F = \frac{1}{2}\sum_{x=1}^{N}\sum_{\mu=1}^{D}\eta_{x,\mu}[\bar{\psi}_x\psi_{x+\hat{\mu}} - \bar{\psi}_{x+\hat{\mu}}\psi_x], \tag{29}$$

where

$$\eta_{x,\mu} = (-1)^{\sum_{\nu<\mu} x_\nu}, \tag{30}$$

with x_ν the coordinate in the νth direction. One can include gauge fields in a gauge-invariant manner by inserting $\mathbf{U}_{x,\mu}$ such that

$$S_F = \frac{1}{2}\sum_{x=1}^{N}\sum_{\mu=1}^{D}\eta_{x,\mu}[\bar{\psi}_x\mathbf{U}_{x,\mu}\psi_{x+\hat{\mu}} - \bar{\psi}_{x+\hat{\mu}}\mathbf{U}^\dagger_{x,\mu}\psi_x]. \tag{31}$$

These models will appear in the rest of the review and will be reintroduced in each section. As previously seen, the matter degrees of freedom are placed on each lattice site. When one considers a tensor network representation of a model, integer degrees of freedom will arise at each link on the lattice; see Fig. 1. As for lattice gauge theories where gauge degrees of freedom are initially placed on links, the character expansion will be used for generating integer at each plaquette. These points are made clear later in the review. The simplest example is the Ising model discussed in Sec. V.

C. Physical applications

The sequence of models described in Sec. II.A is designed to handle lattice QCD, which is currently our best definition of the theory describing strongly interacting particles observed in a large number of experiments. Some of the models discussed in Sec. II.B are also studied in condensed matter. For instance,

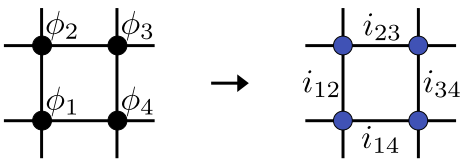

FIG. 1. Reinterpretation of physical degrees of freedom (ϕ) to tensor indices (i). After the reinterpretation, the partition function is expressed as a summation of tensor indices instead of the path integral.

the O(2) model with a chemical potential can be seen as an effective theory for the Bose-Hubbard model (Sachdev, 2001). U(1) gauge theories with either scalar or fermion fields are studied in the context of superconductivity (Herbut, 2007). Tight-binding approximations for solids lead to interesting lattice models: for instance, a sheet of graphene can be described with fermions on a hexagonal lattice having a dispersion relation similar to that for a massless Dirac fermion at half filling (Castro Neto *et al.*, 2009). Other interesting applications include spin liquids and topological phases (Anderson, 1973; Wen, 2004, 2017; Zhou, Kanoda, and Ng, 2017; Knolle and Moessner, 2019).

We point out that in the context of high-energy physics local Lagrangian densities have played a crucial role in the development of the standard model. In the continuum limit, models compatible with relativistic invariance, local gauge invariance, and renormalizability have a small number of free parameters provided that the interactions among the fields and their first derivatives are kept local. The standard model of electroweak and strong interactions has only 18 free parameters if we ignore the QCD vacuum angle and the additional parameters related to the masses and mixing of the neutrinos in extensions of the standard model. It is not possible to tweak the theory each time a new experiment is completed. This makes the standard model a predictive theory. In the lattice formulation, the local interactions involving derivatives in the continuum are replaced by interactions involving fields located on neighboring sites, links, and plaquettes and can be considered quasilocal. For these reasons, the idea that reformulations of lattice models and their coarse-grained versions can be kept local seems to be an important consideration.

D. Computational methods beyond perturbation theory

Besides the RG methods mentioned in the Introduction, lattice models have been studied with a variety of analytical and numerical methods. For example, expansions at small and large coupling for spin and gauge models (Kogut, 1979, 1983; Polyakov, 1987; Itzykson and Drouffe, 1991; Parisi, 1998) have been investigated extensively. As power series, they can be used to check numerical calculations in their respective limits; however, it is hard to capture nonperturbative effects such as the generation of a dynamical mass gap in the continuum limit. After Wilson's original proposal (Wilson, 1974) a suggestive Hamiltonian picture was developed by Kogut and Susskind (1975); however, it became clear that the size of the Hilbert space would make numerical calculations impractical.

In many practical situations, the path-integral formulation uses a real Euclidean action S_E. This allows importance sampling. A typical way to proceed is to start with a random field configuration and then apply some random changes on this configuration. If the new configuration has a lower action, it is accepted. If the new configuration has an action larger by δS_E, then it is accepted with a probability $\exp(-\delta S_E)$. The fact that the fields are connected to only a few neighboring fields makes the calculation of δS_E easy and the exploration of the important configurations controllable.

Mathematicians are often astounded that it is possible to obtain reliable results with this method (Villani, 2012). To date

this is the most reliable way to capture nonperturbative behavior while taking the continuum limit. Around 1978, Creutz (2001) studied numerical lattice gauge theory with simulations of the gauge Ising model on a 3^4 lattice using an HP 9830 calculator programmed in BASIC. This was rapidly followed by the study of other Abelian gauge theories (Creutz, Jacobs, and Rebbi, 1979) and other models. This was reviewed by Rebbi (1983).

Several decades after its inception, numerical lattice gauge theory has become an area of research where corrections on the order of a few percent are considered important. For instance, in heavy flavor physics the determination of the mixing angle $|V_{ub}|$ was quoted as $(3.72 \pm 0.16) \times 10^{-3}$ (Bailey *et al.*, 2015). This result was obtained using ensembles of lattices of various lattice spacings and sizes, some of them as large as $64^3 \times 192$. For a review of averages of numerical results with estimated errors, see the Flavour Lattice Averaging Group summary (Aoki *et al.*, 2020).

Given the success of importance sampling for static problems in QCD, not much has been done to develop efficient numerical Hamiltonian methods. On the other hand, in condensed matter the idea that it is possible to approximate low-energy states of the Hamiltonian with a significantly reduced Hilbert space has been successful in $1+1$ dimensions and shares some similarities with importance sampling. This idea appeared in the context of the density matrix renormalization group (DMRG) method (White, 1992; Schollwöck, 2005, 2011b; Haegeman and Verstraete, 2017) and the other methods discussed in Sec. IV.C. We expect that in the coming years great progress will be made in adapting related methods in the context of lattice gauge theory.

III. QUANTUM COMPUTING

A. Situations where importance sampling fails

The numerical successes of lattice gauge theory can be linked to the fact that when the action of the Euclidean-time path integral S_E is real, importance sampling works surprisingly well for the selection of configurations with a Boltzmann distribution $\exp(-S_E)$. However, if we return to real time or introduce a chemical potential that makes the action complex, this powerful tool becomes ineffective (de Forcrand, 2010). This is because in these instances the Boltzmann weights become complex, making their interpretation as probability weights impossible.

Real-time evolution can be set up by using a Hamiltonian acting on a Hilbert space that can be constructed by noticing that the Euclidean path integral can be recast as the trace of a transfer matrix (Wilson and Kogut, 1974; Creutz, 1977; Fradkin and Susskind, 1978; Kogut, 1979; Lüscher, 1990). In addition to the transfer-matrix method, one can also extract real-time observables, such as Green's functions, by generating functional methods in Minkowski spacetime. There are also other techniques for calculating off-equilibrium real-time observables requiring the use of the Keldysh contour (Keldysh, 1965).

Analysis of the exponential decays of correlations as the Euclidean time is increased is a standard tool to extract masses and form factors for momenta that are small compared to the lattice cutoff. On the other hand, real-time evolution and a large Hilbert space involving states with large momenta are needed to describe aspects of hadron fragmentation in real spacetime and deep-inelastic scattering (Lamm, Lawrence, and Yamauchi, 2020; Mueller, Tarasov, and Venugopalan, 2020; Nachman *et al.*, 2021). The real-time evolution operator does not provide a positive measure or a projection onto a small Hilbert space. Another situation where sampling methods are challenged is the construction of interpolating operators for nuclei as the number of Wick contractions grows rapidly with the number of light quarks involved (Detmold and Orginos, 2013).

One could consider the possibility of abandoning the Lagrangian formulation and directly considering the Kogut-Susskind Hamiltonian (Kogut and Susskind, 1975) for QCD and/or the standard many-body formalism in condensed matter and nuclear physics (Fetter and Walecka, 2003), where the Hilbert space is generated by creation operators on a Fock-space vacuum. For the sake of argument, we now consider the simple case of N conjugate pairs of fermionic creation and annihilation operators. They generate a Hilbert space of dimensions 2^N. The exponential growth of this number with N rapidly restricts our ability to store or manipulate the matrix elements of operators using brute-force methods with classical computers. Computations involving spatial lattices with 64^3 sites, made possible by the Lagrangian formulations, would be completely out of the question if we had to set up the entire quantum Hilbert space with existing classical computers. Note, however, that for a broad class of many-body problems it has been shown (Poulin *et al.*, 2011) that most states of the Hilbert space can be reached only after an exponentially long time. This suggests that tensor-network methods should allow one to express Hamiltonians and the ground state without needing to explore the full Hilbert space.

B. Qubits and other quantum platforms

The building blocks of an ordinary (classical) computer memory are bits taking the value 0 or 1. In some designs of DRAM devices, this is achieved by using small capacitors that are either on or off. The typical units of capacitance are femtofarads with voltages of the order of 1 V. These capacitors store a few thousand electrons and can be charged or discharged in times of the order of 10^{-15} sec. The limit of miniaturization where electrons, atoms, or photons can be manipulated individually and where the peculiarities of the quantum behavior become prominent was discussed by Lloyd (1996).

Following the physical examples of the electron spin or the photon polarization, one could envision an ideal and generic quantum system where the on-off concept for bits is replaced by the linear superposition of the two states. This basic unit of quantum computing is often called a qubit (Schumacher, 1995) and can be represented as

$$|\text{qubit}\rangle = \alpha_0|0\rangle + \alpha_1|1\rangle, \tag{32}$$

with two complex numbers α_0 and α_1 such that $|\alpha_0|^2 + |\alpha_1|^2 = 1$. A set of N qubits spans a Hilbert space of dimension 2^N. If we use a classical computer to apply a

dense unitary matrix representing the real-time evolution on an arbitrary state, we need to perform on the order of 2^{2N} operations. On the other hand, if the Hamiltonian is such that any qubit is connected to only a restricted number of other qubits that are fixed by the dimensionality of space and the internal symmetries, then it is possible to design a method that performs the evolution with a number of quantum manipulations that scale polynomially only with N (Lloyd, 1996). This is discussed in Sec. III.F. Presently commercial quantum computers provide sets of qubits and the possibility of preparing, evolving, and measuring quantum states. The limitations of the current hardware are discussed in Sec. III.G.

More generally, the idea that quantum devices can be used to perform computations for quantum problems involving many degrees of freedom is appealing (Feynman, 1982). Physical systems involving cold atoms [see Jaksch *et al.* (1998) and Bloch, Dalibard, and Zwerger (2008) for reviews of the early developments] or trapped ions [see Leibfried *et al.* (2003) for early developments and Debnath *et al.* (2016) for a recent example] can be used to mimic the behavior of simplified many-body models such as various types of spin chains or Hubbard models. In addition, superconducting circuits (Devoret and Schoelkopf, 2013), Rydberg atoms (Bernien *et al.*, 2017; Wu *et al.*, 2021), and photonic systems (Wang *et al.*, 2020) also provide interesting opportunities.

C. From Euclidean transfer matrices to Hilbert spaces

For the lattice models introduced in Sec. II.B, the Euclidean time was treated on an equal footing with the $D-1$ spatial dimensions. To discuss real-time evolution, we first need to single out the time direction. Evolution then occurs along this direction according to a transfer matrix. The key ingredient then is to connect the Lagrangian formulation to the Hamiltonian formalism and to identify the Hilbert space from the transfer matrix introduced in Eq. (33). The general idea is to organize the partition function sums or integrals into operations performed on successive time slices (Wilson and Kogut, 1974; Creutz, 1977; Fradkin and Susskind, 1978; Kogut, 1979). A general procedure to construct the transfer matrix of lattice models in configuration space in the general context of scattering theory was presented by Lüscher (1990). A dual method based on character expansions that are at the heart of TLFT are discussed in Sec. XII, where we illustrate these two possibilities with examples. Note that in this section Euclidean-time methods are used to derive a Hamiltonian that can later be used to do real-time calculations.

Turning to the transfer matrix, with generic notations for a lattice model with N_τ sites in the Euclidean-time direction,

$$Z = \int \mathcal{D}\Phi e^{-S[\Phi]_E} = \mathrm{Tr}(\mathbb{T}^{N_\tau}). \tag{33}$$

If the lattice spacing a_τ in the Euclidean-time direction is small compared to the physical timescales involved, we have

$$\mathbb{T} \propto e^{-a_\tau \hat{H}}. \tag{34}$$

For N_τ large enough, the use of Euclidean time provides a projection in the low-energy sector of the Hilbert space. This property remains effective if we insert operators that create and destroy states with nontrivial quantum numbers.

The simplest possible example is the following one-dimensional Ising model:

$$S_{\mathrm{Ising}} = \beta \sum_\tau (1 - \sigma_{\tau+1}\sigma_\tau) \tag{35}$$

$$= \frac{\beta}{2} \sum_\tau (\sigma_{\tau+1} - \sigma_\tau)^2 \tag{36}$$

with partition function

$$Z = \sum_{\{\sigma\}} e^{-S}. \tag{37}$$

This is a product of exponentials that each share one spin variable with the next factor. We can then write the partition function as

$$Z = \mathrm{Tr}[\mathbb{T}^{N_\tau}], \tag{38}$$

with

$$\mathbb{T}_{\alpha\alpha'} = \exp\left\{-\frac{\beta}{2}(\sigma^{(\alpha)}_{\tau+1} - \sigma^{(\alpha')}_\tau)^2\right\} \tag{39}$$

and $\sigma^{(\alpha)} = 1, -1$ for $\alpha = 0, 1$, respectively. Along the diagonal of the transfer matrix we see only unity. On the off diagonal, a spin flip comes with weight $e^{-2\beta}$. To leading order in the temporal lattice spacing, $\mathbb{T} \simeq 1 - a_\tau \hat{H} + \cdots$, which allows us to identify

$$\hat{H} = -h_x \hat{\sigma}^x, \tag{40}$$

with $h_x \equiv e^{-2\beta}/a_\tau$ and $\hat{\sigma}^x$ the x Pauli matrix. In this case, to extract a Hamiltonian from the original Lagrangian formulation, we required the coupling β to go to infinity to match the temporal lattice spacing ($e^{-2\beta} \propto a_\tau$).

In this way we found the Hamiltonian and Hilbert space in configuration space; however, one can use a dual method as well by expanding the original Boltzmann weights. Consider the following action for the Ising model in Eq. (35) with the constant dropped:

$$S_{\mathrm{Ising}} = -\beta \sum_\tau \sigma_{\tau+1}\sigma_\tau. \tag{41}$$

The Boltzmann weight can be expanded in the form

$$\mathbb{T}_{\alpha\alpha'} = e^{\beta \sigma^{(\alpha)}_{\tau+1}\sigma^{(\alpha')}_\tau} \tag{42}$$

$$= \cosh(\beta) \sum_{n=0}^{1} (\sigma^{(\alpha)}_{\tau+1}\sigma^{(\alpha')}_\tau)^n \tanh^n(\beta), \tag{43}$$

which is simply the Euler identity for imaginary angles. Ignoring the factor out front since it does not affect the Hamiltonian, in this form we can easily do the summation

over the values of α at all lattice sites. The transfer matrix becomes a diagonal matrix with matrix elements labeled as follows with the integers n from each Boltzmann factor:

$$\mathbb{T}_{nn'} = \begin{pmatrix} 1 & 0 \\ 0 & \tanh(\beta) \end{pmatrix}. \tag{44}$$

In the literature, the integers n are often called dual variables or character indices. The terminology is discussed more systematically in Sec. III.D. To recover a Hamiltonian, the transfer matrix must have the form $1 - a_\tau \hat{H} + \cdots$ for small times. This is found by taking $\beta \to \infty$ and recalling $\tanh\beta = 1\text{–}2e^{-2\beta} + \cdots$ for large β. The Hamiltonian in these new variables then takes the form

$$\hat{H} = h_z(1 - \hat{\sigma}^z), \tag{45}$$

with $h_z \equiv e^{-2\beta}/a_\tau$ and $\hat{\sigma}^z$ the z Pauli matrix. These are two distinct procedures that give Hamiltonians in the time continuum limit: one in the original configuration variables and the second in the dual variables.

The transfer matrix of the Ising model in higher dimensions can be constructed in a similar manner (Kaufman, 1949). The action for the Ising model in dimension D is the $N = 1$ case of Eq. (6). In higher dimensions there are now two types of interactions. If we consider a particular time slice, we can first collect all the time links connected to the next time slice, each with a representation given in Eq. (35). In addition, we have all the spatial links in the time slice with nearest-neighbor interactions. We can represent any spin configuration in a time slice as an element of a tensor product of eigenstates of the Pauli matrix $\sigma^z_{\mathbf{x}}$, with $\mathbf{x}$ denoting the spatial indices, as follows:

$$\{\text{configurations}\} = \bigotimes_{\mathbf{x}} |\pm 1\rangle_{\mathbf{x}}. \tag{46}$$

We can introduce operators $\hat{\sigma}^z_{\mathbf{x}}$ and $\hat{\sigma}^x_{\mathbf{x}}$ acting on this Hilbert space, which can be identified with a set of qubits. Following Kaufman (1949), we can collect the two types of interactions in two matrices. Using

$$e^{\beta\sigma_{\alpha'}\sigma_\alpha} = [2\sinh(2\beta)]^{1/2}[\exp(\tilde{\beta}\sigma^x)]_{\alpha'\alpha}, \tag{47}$$

where $\tilde{\beta}$ is the dual inverse temperature introduced by Kramers and Wannier (1941) that satisfies the relation $\tanh(\tilde{\beta}) = e^{-2\beta}$, the contribution of time links can be summarized as follows with the matrix connecting the configuration of the two time slices:

$$\mathbb{V}_1 = [2/\sinh(2\tilde{\beta})]^{N_s^{D-1}/2} e^{\tilde{\beta}\sum_{\mathbf{x}} \hat{\sigma}^x_{\mathbf{x}}}. \tag{48}$$

On the other hand, the spatial links can be recast in the diagonal matrix as

$$\mathbb{V}_2 = e^{\beta \sum_{\mathbf{x},j} \hat{\sigma}^z_{\mathbf{x}} \hat{\sigma}^z_{\mathbf{x}+\hat{j}}}, \tag{49}$$

with $\hat{j}$ a unit vector pointing along one of the $D-1$ directions on the lattice. We can now write the transfer matrix as

$$\mathbb{T} = \mathbb{V}_2^{1/2} \mathbb{V}_1 \mathbb{V}_2^{1/2}, \tag{50}$$

where the matrix indices label the spatial configurations. Geometrically, the Hilbert space is located on the time slices. Illustrations of the time slices and the location of the Hilbert space can be found in Sec. XII.

Alternatively, we can work in the following dual representation where the $\sigma^x_{\mathbf{x}}$ are diagonal:

$$\tilde{\mathbb{T}} = \mathbb{V}_1^{1/2} \mathbb{V}_2 \mathbb{V}_1^{1/2}, \tag{51}$$

where the matrix indices label sets of group characters. Geometrically, the Hilbert space is located between the time slices. Graphical illustrations of this situation will be provided in Sec. XII. The construction generalizes easily for finite Abelian groups and in a nontrivial way for continuous and compact Abelian groups. The advantage of using the second (dual) representation is that it remains discrete and, as we see in Sec. XIII.A, it preserves the symmetry when truncations are applied (Meurice, 2019, 2020a).

D. Topological and geometrical dualities

In Sec. III.C we used the concept of duality on two occasions. The first was the relation between β and $\tilde{\beta}$, which interchanges their low and large value regimes. The second occasion was the discussion of the two ways to represent the transfer matrix. In addition, in Secs. VII.C and IX.A.2 we use the geometrical duality reviewed by Savit (1980). Duality is a general concept used in many branches of mathematics. According to Atiyah (2007) duality gives "two different points of view of looking at the same object." In the following we clarify the various usages of the concepts in the rest of this review.

An important notion of duality is the so-called Pontryagin duality (Pontryagin, 1939) used in the study of topological groups. It relates an Abelian group and its characters (for instance, Fourier modes). It states that if the former is compact, the later is discrete and vice versa. The simplest situation is a finite group that is compact and discrete. In the case of finite cyclic Abelian groups the characters form a finite group that is isomorphic to the group itself (Serre, 1973). A simple example is $\mathbb{Z}_q$, the additive group of integers modulo q. If x denotes an element of $\mathbb{Z}_q$, the characters (see Appendix A.1) have the form

$$\chi_k(x) = \exp\left(i\frac{2\pi}{q}kx\right) \tag{52}$$

and satisfy the character property

$$\chi_k(x + x') = \chi_k(x)\chi_k(x'). \tag{53}$$

The product of two characters is another character

$$\chi_k(x)\chi_{k'}(x) = \chi_{k+k'}(x), \tag{54}$$

and one sees that they also form a $\mathbb{Z}_q$ group. They obey the orthogonality relations

$$\frac{1}{q}\sum_{x=0}^{q-1}\chi_k(x)\chi_{k'}^{\star}(x)=\delta_{k,k'} \tag{55}$$

and

$$\frac{1}{q}\sum_{k=0}^{q-1}\chi_k(x)\chi_{k}^{\star}(x')=\delta_{x,x'}. \tag{56}$$

A simple example of a continuous (nondiscrete) and compact group is U(1), the multiplicative group of complex numbers with modulus 1. The group properties can be reformulated in an additive manner by introducing the phases $z=e^{i\varphi}$, which are added modulo 2π. Topologically it is a circle that is a compact manifold. Its characters are discrete and labeled by the integers. They are the usual Fourier modes $e^{in\varphi}$. The orthogonality relations appear in the following asymmetric way:

$$\int_{-\pi}^{\pi}\frac{d\varphi}{2\pi}e^{in\varphi}(e^{in\varphi})^{\star}=\delta_{n,n'}, \tag{57}$$

$$\sum_{n=-\infty}^{\infty}e^{in\varphi}(e^{in\varphi'})^{\star}=2\pi\sum_{m=-\infty}^{\infty}\delta(\varphi-\varphi'+2\pi m). \tag{58}$$

In practice, a deep understanding of the previous mathematical statements is not necessary, and we simply need to remember a few character expansions. For the Ising models we have functions over the multiplicative group $\sigma=\pm1$, and we can recall the expansion from Sec. III.C as a character expansion

$$\langle\sigma_{\alpha'}|\mathbb{T}|\sigma_{\alpha}\rangle=\exp(\beta\sigma_{\alpha'}\sigma_{\alpha})$$

$$=\frac{1}{2}\sum_{n=0}^{1}\lambda_n(\beta)(\sigma_{\alpha'}\sigma_{\alpha})^n \tag{59}$$

$$=\cosh(\beta)+\sigma_{\alpha'}\sigma_{\alpha}\sinh(\beta). \tag{60}$$

A similar representation can be obtained for the $\mathbb{Z}_q$ spin models. If we replace the discrete angle variables $(2\pi/q)x$ with continuous ones φ, we obtain a "matrix" with continuous elements that can be calculated using the standard Fourier transform

$$\langle\varphi'|\mathbb{T}|\varphi\rangle=\exp[\beta\cos(\varphi'-\varphi)] \tag{61}$$

$$=\sum_{n=-\infty}^{+\infty}I_n(\beta)\exp[in(\varphi'-\varphi)], \tag{62}$$

where $I_n(\beta)$ is the modified Bessel function of order n. We show in Sec. VII.B that finite versions of this expansion hold for the finite $\mathbb{Z}_q$ subgroups.

Generalizations of Pontryagin duality to compact non-Abelian groups appear in the Peter-Weyl theorem (Peter and Weyl, 1927). As an example, this translates into expansions in spherical harmonics for problems involving the O(3) symmetry. Related methods were used for tensor networks with continuous symmetries (Tagliacozzo, Celi, and Lewenstein, 2014; Zohar and Burrello, 2015).

From the point of view of quantum computing, we see that using compact fields guarantees that we can replace the continuous integrals by discrete sums. Our strategy is to associate the indices of these sums with quantum states. One important aspect of TLFT is that when the fields are compact, we do not need to discretize the integrals using numerical approximations. Instead, we can use character expansions such as Eq. (62), where some integrals have been done exactly and result in Bessel functions that we can input with any desired accuracy. In other words, the difficult part of the classical path-integral approach can be done efficiently with classical methods. After that, the original integrals reduce to orthogonality relations and can be performed exactly.

Another notion of duality is of a geometrical nature. It is related to the Levi-Civita tensor $\epsilon^{\mu_1\cdots\mu_D}$. Its meaning is dimension dependent and relates objects of dimension d to objects of dimension $D-d$. For instance, in $D=4$ a dual field-strength tensor with two indices is obtained by contracting the original field-strength tensor with the Levi-Civita tensor. This duality transformation interchanges the electric and magnetic fields and reduces to the identity when repeated twice. It also relates sites to four-dimensional hypercubes, and plaquettes to plaquettes. In $D=3$ it relates the field-strength tensor to a divergenceless pseudovector $\epsilon^{ijk}\partial_j A_k$, links to plaquettes and sites to cubes.

The various notions of duality are often used simultaneously. A common example is the "dual formulation" of the Ising model. As we explain in Sec. V.B, the new set of indices from Eq. (60), which is a consequence of Pontryagin duality, leads to a representation in terms of paths. We can then try to represent these paths as the boundaries of surfaces, which brings the geometrical duality and new "dual variables" together (Savit, 1980).

There are also occasions where the phrase dual variables has become associated with generic integer fields, regardless or their origin or their relation to the previously mentioned concepts of duality (Bruckmann *et al.*, 2015, 2016; Gattringer, Kloiber, and Müller-Preussker, 2015; Gattringer, Göschl, and Sulejmanpašić, 2018; Marchis and Gattringer, 2018). These integer fields can arise from a Taylor series of the Boltzmann weight, such as in the case of the Ising model,

$$e^{\beta\sigma\sigma'}=\sum_{q=0}^{\infty}\frac{\beta^q}{q!}(\sigma\sigma')^q. \tag{63}$$

Equation (63) associates a natural number with the links of the lattice, similar to the character expansion from before. Also just as before, this expansion allows one to perform the path-integral sums over the σ fields, leaving one with a theory of constrained, positive integer fields on the links of the lattice. However, instead of two values, i.e., $n=0,1$, these integers can take on an infinite number of values. Thus, while this expansion accomplishes similar feats, it can be seen as a less economical parametrization of the model. The character expansion from before can be found within the Taylor expansion by summing the even and odd integers, respectively, leaving one with two terms (0 and 1).

E. Real-time evolution with qubits

We now discuss the possibility of using quantum devices to represent states of the Hilbert space emerging from the transfer-matrix construction and to design methods to apply unitary transformations corresponding to the real-time evolution. For definiteness, we assume that we have at our disposal a set of qubits. For the spin Ising model, the construction of the transfer matrix leads to a Hilbert space with the qubit structure given by Eq. (46). The method to take the time continuum limit and identify a Hamiltonian using Eq. (33) is well known (Fradkin and Susskind, 1978; Kogut, 1979): we deform the original transfer matrix by increasing β in the time direction (which makes the dual value $\tilde{\beta}$ small) and decreasing β in the spatial directions. The arguments of the exponentials in $\mathbb{V}_1$ and $\mathbb{V}_2$ become infinitesimal and provide the two noncommuting pieces of the "quantum Hamiltonian." The role played by $\mathbb{V}_1$ is special in the intuitive picture that we are drawing: it acts only on single qubits without connecting them. Consequently, working in the representation where $\hat{\sigma}^x_{\mathbf{x}}$ is diagonal is a good starting point. Next we can "turn on" the terms in $\mathbb{V}_2$. At lowest order in the time lattice spacing they connect only those qubits that are nearest neighbors. We show in Sec. III.F that this type of situation permits quantum computation in a time scaling polynomially with the size of the system (Lloyd, 1996).

Character expansions and TLFT provide natural tools to perform similar constructions for the models presented in Sec. II.B. A first step consists of isolating building blocks that are localized in space and have a simple real-time evolution. The models have interactions associated with links and plaquettes. As a first approximation we set the interactions on spatial links and space-space plaquettes to zero.

For spin models, this results in a collection of N_s^{D-1} isolated one-dimensional spin models. These isolated models are the building blocks. They are solvable and it is easy to calculate their evolution in real time. For gauge models we also have electric degrees of freedom that can be associated with the spatial links of a given time slice of the lattice. They are required to satisfy a constraint called Gauss's law; however, when this condition is satisfied, the real-time evolution in the previously described isolation limit is straightforward, as we explain in Sec. XII.C. The Hilbert space of the isolated building blocks depends on the model considered. For the Ising spin models, a single qubit is all we need. For models with continuous symmetries, the exact treatment requires an infinite Hilbert space; however, small size truncations provide good approximations and preserve the symmetries of the models (Meurice, 2019, 2020a). This is an attractive feature of TLFT that is discussed in Sec. XIII.A. Having set up a finite Hilbert space with isolated building blocks, our next step is to restore the interactions associated with the spatial links and the space-space plaquettes. This is done for a variety of models in Sec. XII. Independent of the model-specific aspect of this procedure, it is clear that each building block is connected to only a limited numbers of other building blocks. For instance, for a spin model, there are two connections for each spatial direction. This quasilocality is crucial to implement real-time evolution with a quantum computer.

F. Lloyd-Suzuki-Trotter product formula

An important motivation for using a quantum computer is to calculate the real-time evolution for systems with many degrees of freedom having quasilocal interactions in the sense discussed in Sec. III.E. Ideally, the time to perform computations should scale polynomially with the size of the system rather than exponentially. A general argument leading to these conclusions was put forward by Lloyd (1996), who stated, "Feynman's 1982 conjecture, that quantum computers can be programmed to simulate any local quantum system, is shown to be correct." The proof is based on the basic idea behind the Suzuki-Trotter product formula (Trotter, 1959; Suzuki, 1976; Reed and Simon, 1980), namely, that, for two noncommuting operators $\hat{A}$ and $\hat{B}$ and sufficiently small ϵ,

$$e^{i\epsilon(\hat{A}+\hat{B})} \simeq e^{i\epsilon\hat{A}} e^{i\epsilon\hat{B}} + \mathcal{O}(\epsilon^2). \tag{64}$$

In the standard construction of the path integral in quantum mechanics, it is applied to the kinetic and potential energy, but it can also be applied to all the quasilocal parts of the Hamiltonian.

The argument goes as follows (Lloyd, 1996). Consider a system composed of N variables with Hamiltonian

$$\hat{H} = \sum_{j=1}^{\ell} \hat{H}_j, \tag{65}$$

where each $\hat{H}_j$ acts on a space that involves at most $k_{\max}$ of the variables. It is assumed that ℓ increases linearly with N but that $k_{\max}$ is fixed by the dimension and the symmetries and independent of N. The individual H_j can be represented as finite matrices in their local subspace. Under these assumptions, it was shown (Lloyd, 1996) that the error associated with the approximation

$$e^{i\hat{H}t} \simeq (e^{i\hat{H}_1 t/n} \cdots e^{i\hat{H}_\ell t/n})^n + \cdots \tag{66}$$

can be controlled by taking n large enough. In addition, once the accuracy goal is determined, the computing time scales linearly in N and t.

To fix the ideas, for most of the available quantum computers the $\hat{H}_j$ act on one or two qubits and can be represented by 2×2 or 4×4 matrices in this restricted space. A simple quantum circuit for the quantum Ising model used by Gustafson, Meurice, and Unmuth-Yockey (2019) and Gustafson, Dreher *et al.* (2021) is displayed in Fig. 2. The basic elements are rotations generated by $\hat{\sigma}^x_j$ or $\hat{\sigma}^z_j$ and acting on the jth qubit only and CNOT gates acting on a pair of qubits and flipping the target qubit when the control qubit is in the $|1\rangle$ state. The circuit can be repeated in the space (vertical) and time (horizontal) directions and conveys the previously mentioned linear scalings. More evolved circuits can be designed with the purpose of creating energy eigenstates (Verstraete, Cirac, and Latorre, 2009; Cervera-Lierta, 2018).

It is instructive to compare the computational resources to perform the unitary rotation $\exp(i\theta\hat{\sigma}^x_j\hat{\sigma}^x_k)$, in which the operator in the exponential flips the jth and kth qubits and

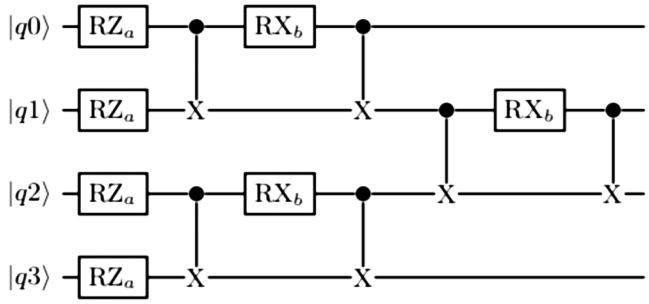

FIG. 2. Circuit for four qubits with open boundary conditions used by Gustafson, Meurice, and Unmuth-Yockey (2019). Here RZ and RX are rotations about the z and x axes, respectively.

does not act on the rest of the system. With a quantum computer, one would expect this operation to keep the coherence of the qubits with the rest of the system, present in the original state, but the cost ideally is independent of the size of the system. On the other hand, the same operation on an arbitrary state performed with a classical computer involves a matrix with 2^N nonzero and nondiagonal matrix elements, and the resources necessary increase exponentially with the size of the system.

G. Dealing with noise in the NISQ era

The discussion in Sec. III.F considers algorithmic aspects in an idealized situation where computer errors or noise can be neglected. Quantum computing technology is still in its early development. The current noisy intermediate-scale quantum (NISQ) computer hardware platforms can accommodate only small-depth circuits and sources of errors need to be understood in detail (Preskill, 2018). Understanding these errors and their noise, adjusting, and contriving algorithms to lessen these errors is the goal of error mitigation in quantum computing.

Various types of noise affect the single-qubit gates in a way that can be parametrized (Nielsen and Chuang, 2000) in terms of the density matrix $\hat{\rho}$:

$$\mathcal{E}(\hat{\rho}; p_x, p_y, p_z) = (1-p)\hat{\rho} + p_x\hat{\sigma}^x\hat{\rho}\hat{\sigma}^x + p_y\hat{\sigma}^y\hat{\rho}\hat{\sigma}^y + p_z\hat{\sigma}^z\hat{\rho}\hat{\sigma}^z. \tag{67}$$

In Eq. (67) $\mathcal{E}$ is a quantum operation and the values p_x, p_y, and p_z correspond to the probabilities of a σ^x, σ^y, or σ^z error, respectively, occurring and $p = p_x + p_y + p_z$. The error channel for two-qubit gates is given by $\mathcal{E}^{(2)} = \mathcal{E} \otimes \mathcal{E}$. Modeling the error in this way neglects spatial and temporal correlations and two-qubit correlations and assumes that the errors are identical and evenly distributed. In practice, if a classical simulation of the qubit evolution is performed, each unitary evolution operation needs to be followed by applying one of the four possibilities ($\hat{1}, \hat{\sigma}^x, \hat{\sigma}^y$, or $\hat{\sigma}^z$) with respective probabilities $1-p$, p_x, p_y, and p_z on the qubits involved. The probability distribution of errors is manifest only after averaging over an ensemble of runs.

In addition, readout errors (misidentifying $|1\rangle$ for $|0\rangle$ or vice versa) should be taken into account for all current quantum computing platforms. Given estimates of the probabilities for these errors, it is possible to correct the actual measurements by a multiplicative factor (Kandala *et al.*, 2019).

A common NISQ strategy for error mitigation is to increase the source of error in a controllable way and then extrapolate to the limit where the error is not present. Examples with superconducting qubits were given by Temme, Bravyi, and Gambetta (2017), Klco *et al.* (2018), Gustafson, Meurice, and Unmuth-Yockey (2019), Kandala *et al.* (2019), and Gustafson, Dreher *et al.* (2021). A simple way to increase the error is to insert two successive CNOT gates. Their exact multiplication is the identity; however, for a NISQ device it increases the chance of errors. Note that mitigation methods can also be used for quantum variational methods (Li and Benjamin, 2017).

In this context, the choice of the Trotter step δt is crucial because the number of steps is limited by the loss of coherence and the noise. A concrete discussion was given by Gustafson, Dreher *et al.* (2021) for the quantum Ising model in one spatial dimension with four sites. If we pick a small δt with good control on the $(\delta t)^2$ error, we may not be able to reach a timescale relevant for what we want to learn. However, it appears that by picking a significantly larger δt the rigorous bound is not sharp and the empirical bound is much tighter, as shown in Fig. 3, where we plot the operator norm of the Trotter error

$$\Delta_2 U \equiv e^{-i(h_T\hat{H}_T + J\hat{H}_{NN})\delta t} - e^{-ih_T\hat{H}_T\delta t}e^{-iJ\hat{H}_{NN}\delta t} \simeq \frac{h_T J}{2}[\hat{H}_T, \hat{H}_{NN}](\delta t)^2, \tag{68}$$

with

$$\hat{H}_T = -\sum_{j=1}^{4}\hat{\sigma}_j^z, \qquad \hat{H}_{NN} = -\sum_{j=1}^{3}\hat{\sigma}_j^x\hat{\sigma}_{j+1}^x. \tag{69}$$

The nonlinear aspects of the error are quite interesting and may involve resonances (Gustafson, Dreher *et al.*, 2021). For other recent developments see Gustafson (2020), Mishra *et al.* (2020), Gustafson *et al.* (2021), Gustafson, Dreher *et al.* (2021), Gustafson and Lamm (2021), Gustafson, Zhu *et al.*

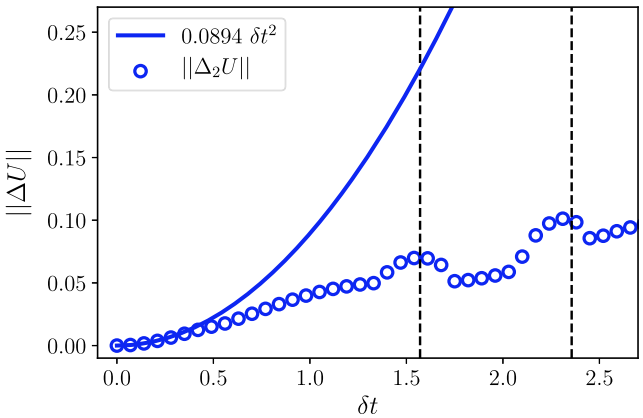

FIG. 3. $||\Delta_2 U||$ vs δt for the quantum Ising model with $h_T = 1$ and $J = 0.02$. The vertical lines are at $\pi/2$, $3\pi/4$…. For details see Meurice (2020b).

(2021), Rahman *et al.* (2021), Sewell and Jordan (2021), Funcke *et al.* (2022), and Honda *et al.* (2022).

H. Quantum computations and simulations

The idea of using quantum devices to mimic or study theoretical quantum models has been a subject of intense activity in recent years. Here we mention theoretical and experimental studies of the Ising model, and lattice gauge theories, in the context of quantum computation and quantum simulation.

1. Ising model

As previously stressed, the $(1+1)$-dimensional Ising model is the quintessential model to use to check computational tools and proposed algorithms. This is because the model possesses nontrivial features but has been solved exactly. It is not surprising then that this is one of the first models to be tried and tested in different forms of quantum computation. There have been various investigations into how to simulate the model on a quantum computer, and what interesting observables to measure (such as phase shift and thermodynamics) (Lidar and Biham, 1997; Mostame and Schützhold, 2008; You, Geller, and Stancil, 2013; Gustafson, Meurice, and Unmuth-Yockey, 2019). The following approaches have been considered: superconducting qubit machines, trapped-ion machines, cold atoms trapped in optical lattices, and Rydberg atom simulators.

On the superconducting qubit front, Hebenstreit *et al.* (2017) and Zhang *et al.* (2017) made initial simulations, and in some cases at relatively large system sizes. Their calculations of various spin observables matched the corresponding quantities in exact diagonalization well. Cervera-Lierta (2018) also carried out a simulation of the Ising model using a few spins, and a comparison between theory and computation was made for the average magnetization. Smith *et al.* (2019) and Gustafson, Dreher *et al.* (2021) simulated the Ising model using a few qubits on IBM's machines. It was shown that the Richardson extrapolation could be used to mitigate the noise in the regime where the nonlinear effects are not too large (Gustafson, Dreher *et al.*, 2021). In addition, Chen *et al.* (2020) took a quantum-classical approach that used a variational algorithm to compute the ground-state wave function: so-called variational quantum computing, where the quantum computer prepares a state with a circuit ansatz depending on some number of parameters. The expectation value of the energy is computed from this state, and circuit parameters are then tuned classically based on the quantum expectation value in order to minimize the energy.

Using trapped ions, Friedenauer *et al.*, 2008 completed the first work, followed by extensive investigations from student's work (Friedenauer, 2010; Korenblit, 2013). These are pioneering investigations into the trapped-ion platform. Edwards *et al.* (2010), Kim *et al.* (2010, 2011), and Islam *et al.* (2011) looked at the phase structure of the model by simulating a few spins. They calculated the phase diagram of the model using the probability of the state to be in a ferromagnetic state, or moments of the magnetization. There were also attempts to measure the Rényi entropy using digital quantum gates. Linke *et al.* (2018) considered a two-site antiferromagnetic Ising model and, using the SWAP gate, measured the parity of two copies of the system (Johri, Steiger, and Troyer, 2017). Islam *et al.* (2015) used bosonic many-body states and interfered the copies to extract subsystem parities. They then calculated the Rényi entropy from subsystem parities.

Finally, another promising approach is to use highly excited Rydberg states of atoms, which allows for strong atom-atom interactions across relatively large distances. Kim *et al.* (2017) used a chain of 19 rubidium atoms, whose interactions they controlled by tuning the lattice parameters to simulate the model. Guardado-Sanchez *et al.* (2018) explored out-of-equilibrium dynamics through a quench using an array of lithium atoms, again placed in a Rydberg state. Simon *et al.* (2011) used trapped rubidium atoms to simulate the antiferromagnetic Ising model. They were able to identify a phase transition between the paramagnetic and antiferromagnetic phases and observe magnetic domains using a site-resolved atomic microscope and noise correlation measurements. Bernien *et al.* (2017) demonstrated the use of configurable and programmable arrays of atoms and simulated an Ising-like model on 51 qubits. They observed a phase transition between symmetric and ordered phases and discussed out-of-equilibrium properties of spin models (Keesling *et al.*, 2019). For reviews of this topic see Schauss (2018) and Browaeys and Lahaye (2020).

2. Gauge theories

The use of optical lattices (Bloch, Dalibard, and Zwerger, 2008) to quantum simulate lattice gauge theories has been extensively developed. Proposals for the quantum simulation of lattice gauge theories beginning with early work on Abelian models were made by Zohar and Reznik (2011), Banerjee *et al.* (2012), Zohar, Cirac, and Reznik (2012, 2013b), and Tagliacozzo, Celi, Zamora, and Lewenstein (2013) and were made for digital quantum devices by Zohar *et al.* (2017a, 2017b). In the case of non-Abelian models, proposals were made by Banerjee *et al.* (2013), Tagliacozzo, Celi, Orland, and Lewenstein (2013), and Zohar, Cirac, and Reznik (2013a). For reviews see Wiese (2013), Zohar, Cirac, and Reznik (2016), Bañuls and Cichy (2020), and Bañuls *et al.* (2020). Byrnes and Yamamoto (2006) produced a useful early reference on quantum computing for non-Abelian gauge theories. For recent developments combining condensed matter and gauge theory ideas, see Li *et al.* (2016), Kasper *et al.* (2017), Clark *et al.* (2018), and Schweizer *et al.* (2019). Trapped ions (Leibfried *et al.*, 2003) have provided new opportunities to approach lattice gauge theory models (Davoudi *et al.*, 2020). Rydberg atoms offer a versatile platform for gauge theories (Celi *et al.*, 2020; Surace *et al.*, 2020; Meurice, 2021).

The Schwinger model is often the first target to develop new approaches (Martinez *et al.*, 2016; Kasper *et al.*, 2017; Klco *et al.*, 2018; Davoudi *et al.*, 2020; Kharzeev and Kikuchi, 2020; Magnifico *et al.*, 2020; Surace *et al.*, 2020). For recent work on non-Abelian models, see Silvi, Sauer *et al.* (2019), Raychowdhury and Stryker (2020a, 2020b), Davoudi, Raychowdhury, and Shaw (2021), and Dasgupta and Raychowdhury (2022), and .

IV. THE MEANING OF QUANTUM VERSUS CLASSICAL

In this section, we discuss the meaning of classical and quantum for models, phase transitions, and tensor networks.

A. Models

In textbooks on quantum mechanics, it is a common procedure to start with the Hamiltonian formulation and derive a path-integral representation that can be extended to field theory. The path-integral formalism allows for formulations that are manifestly gauge invariant and treats space and time on an equal footing. For these reasons, it can be argued that the fundamental definition of relativistic models should be given in terms of the action and the measure of integration over all the possible configurations without reference to a Hamiltonian. Examples of such actions are given in Sec. II.B.

It is common to call models formulated with the path-integral classical, while the corresponding formulation using a Hamiltonian acting on a Hilbert space is called quantum. However, except for possible discretization artifacts, the two formulations describe the same quantum behavior. In the path-integral formulation for bosonic fields, the action is calculated in terms of c numbers, as in the classical formulation, but the sum over all the configurations provides a quantum description that amounts to more than the classical equations of motion. In other words, the path integral is an alternate method of quantization that is convenient in Euclidean time.

Starting with a classical action, a Hamiltonian can be constructed from the action by using the transfer-matrix formalism. This was demonstrated in Sec. III.C and is discussed in detail in Sec. XII for the models that were introduced in Sec. II.B. A discussion with detailed references on the connection between statistical mechanics in D dimensions and quantum Hamiltonians in $D-1$ dimensions appeared in the classic work of Wilson and Kogut (1974).

B. Phase transitions

The actions for spin and gauge models introduced in Sec. II.B contain the parameter β, or $\beta_{\rm pl}$ for pure gauge theories, that is often called the "inverse classical temperature," or "coupling constant," and can be associated with "classical phase transitions." For instance, the $D=2$ classical Ising model has a spontaneous magnetization when $\beta > \beta_c = (1/2)\ln(1+\sqrt{2})$.

In contrast, given a Hamiltonian $\hat{H}$, we can define a thermal quantum partition function with temperature $T_{\rm qu}$ in the usual way,

$$Z(T_{\rm qu}) = \mathrm{Tr}[e^{-\hat{H}/T_{\rm qu}}], \tag{70}$$

where $T_{\rm qu}$ has in general a different meaning than $1/\beta$ in the classical formulation. With the lattice formulation at Euclidean time as a starting point, we have the identification

$$1/T_{\rm qu} = N_\tau a_\tau, \tag{71}$$

and the nonzero temperature is associated with the finite extent of the temporal dimension. A typical situation of interest is to start in an ordered phase at $T_{\rm qu}=0$ corresponding to the infinite Euclidean-time limit and induce a finite-temperature phase transition into a disordered phase by taking a sufficiently small temporal extent. In this way, the temporal extent of the lattice is responsible for a finite-temperature phase transition, as opposed to the coupling β, which is unrelated to the temperature in the quantum partition function. Transitions related to the couplings at $T_{\rm qu}=0$ are quantum phase transitions. The transition can sometimes be understood in terms of the classical phase diagram in $D-1$ dimensions. A more detailed discussion was given in Cardy's monograph (Cardy, 1996)

C. Tensor networks

In Secs. V–XI we introduce "classical tensors" in order to reformulate classical models as defined in Sec. IV.A. The partition function of these models can be visualized as an assembly obtained by "wiring" (tracing) together objects carrying multiple "legs" (tensor indices) and attached to the sites, links, or plaquettes of a Euclidean spacetime lattice. This type of classical construction was inspired by (Levin and Nave, 2007; Gu and Wen, 2009) various quantum tensor networks (Fannes, Nachtergaele, and Werner, 1992; Vidal, 2003, 2004, 2007; Verstraete and Cirac, 2004a; Shi, Duan, and Vidal, 2006; Perez-Garcia *et al.*, 2007; Verstraete, Murg, and Cirac, 2008), developed in various contexts often related to the DMRG method (White, 1992). There is an abundant literature on the subject, including Schollwöck (2005, 2011a), Cirac and Verstraete (2009), Orus (2014), Montangero (2018), Silvi, Tschirsich *et al.* (2019), and Ran *et al.* (2020).

One important idea is the representation of quantum states by matrix product states (MPSs) that appeared in several of the aforementioned references. As an example, for a one-dimensional quantum chain problem with N_s sites, an arbitrary element of the Hilbert space can be written as

$$|\psi\rangle = \sum_{i_1,\ldots,i_{N_s}} c_{i_1,\ldots,i_{N_s}} |i_1,\ldots,i_{N_s}\rangle, \tag{72}$$

where

$$|i_1,\ldots,i_{N_s}\rangle = |i_1\rangle \otimes \cdots \otimes |i_{N_s}\rangle \tag{73}$$

and each of the indices runs over a local Hilbert space of dimension d_H attached to a site. The dimension of the Hilbert space is $d_H^{N_s}$. It represents an exponential growth with the size of the system that rapidly becomes computationally unmanageable. For a MPS, one assumes the form

$$c_{i_1,\ldots,i_{N_s}} = \mathrm{Tr}[A_{i_1},\ldots,A_{i_{N_s}}], \tag{74}$$

where the A_{i_j} are $d_B \times d_B$ matrices for each value of i_j. d_B is called the bond dimension. A graphical representation of such a state is shown in Fig. 4 for open boundary conditions. The filled circles represent the matrices, the vertical lines represent open indices with d_H values, and the horizontal lines indicate traced indices with d_B values. The size of the

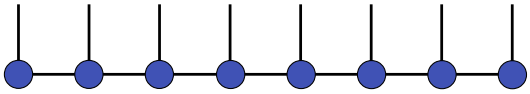

FIG. 4. Illustration of states in the MPS approach.

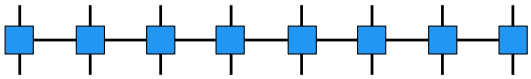

FIG. 5. Illustration of operators in the MPS approach.

MPS "subset"[1] is growing only like $N_s \times d_B^2 \times d_H$, and thus linearly with the size of the system. Similarly, one can represent operators using the trace of N_s $d_B \times d_B$ matrices $A_{i_j}^{i'_j}$ with two indices in the one-site Hilbert space at a computational cost scaling as $N_s \times d_B^2 \times d_H^2$. This is illustrated in Fig. 5. Objects with similar shapes appear as "time slices" of the classical construction. In the case where the indices take an infinite number of values and the sums are truncated in such a way that the number of indices kept in the time direction (like d_H) is the same as the number in the space direction (like d_B), we use the isotropic notation D_{cut} (one can leave the number of states in the temporal and spatial directions independent of each other). On the other hand, we discuss the anisotropic situation where the time direction is singled out to define the transfer matrix and the Hamiltonian in Sec. XII.

MPSs and the DMRG have been used in studies of $(1+1)$-dimensional models such as the Bose-Hubbard model (Bonnes, Charrier, and Läuchli, 2014), the Schwinger model (Bañuls *et al.*, 2013; Byrnes *et al.*, 2002; Buyens *et al.*, 2014, 2016) (see Sec. XI.G for more information), SU(2) gauge theory (Kühn, Cirac, and Bañuls, 2015; Bañuls *et al.*, 2017b), and the O(3) nonlinear sigma model (Bruckmann, Jansen, and Kühn, 2019). Fermionic tensor network studies and the Hubbard model were discussed by Barthel, Pineda, and Eisert (2009) and Corboz *et al.* (2010). Tensor network techniques for lattice gauge theories were discussed by Rico *et al.* (2014), Tagliacozzo, Celi, and Lewenstein (2014), Zohar and Burrello (2015), Pichler *et al.* (2016), Silvi *et al.* (2017), and Silvi, Sauer *et al.* (2019) and reviewed by Bañuls *et al.* (2018) and Bañuls and Cichy (2020). For a review of matrix product operators and their relations with the transfer matrix, see Haegeman and Verstraete (2017). Section XII.G includes references on tensor network studies in $2+1$ and $3+1$ dimensions using generalizations of MPSs.

The MPS framework can also be used to perform real-time calculations based on the Suzuki-Trotter approximation. An example of this method is called the time-evolving block decimation reviewed by Paeckel *et al.* (2019).

The success and limitations of the MPS approach can be analyzed in terms of "area laws" (Plenio *et al.*, 2005; Verstraete *et al.*, 2006). Following a short pedagogical discussion (Schollwöck, 2011a), if a bipartition of a system is introduced, one would expect that the entanglement entropy between the two parts to scale like the size of their boundary with possible logarithmic corrections. In one spatial dimension, we can separate a MPS into two parts by cutting a single bound carrying a maximal entropy $\ln_2 d_B$. Consequently, d_B needs to increase only as the size of the system to capture a possibly logarithmic entanglement. On the other hand, if we fill a two-dimensional surface with a one-dimensional MPS, the entanglement grows at least like the linear size of the system that forces d_b to grow exponentially with this size. Projected entangled pair states (PEPSs) were proposed (Verstraete and Cirac, 2004b) to overcome this difficulty.

We also now mention that tensor methods have been applied (Nishino and Okunishi, 1996) to the transfer-matrix treatment of a classical statistical model such as the problem involving monomers and dimers on a rectangular lattice (Baxter, 1968), where variational methods can be applied and compared to the DMRG approach. This approach is called the corner transfer-matrix renormalization group method. Pioneering work connecting the DMRG and the transfer martix of the Ising model was conducted by Nishino and Okunishi (1996). Related results and their connections with MPSs were reviewed by Haegeman and Verstraete (2017).

For a recent and comprehensive review on MPSs and related topics, see Cirac *et al.* (2021).

V. TENSOR METHODS EXPLAINED WITH THE ISING MODEL

A. Tensor formulation

In this section we construct a tensor formulation for the Ising model in D dimensions. The partition function for the Ising model is

$$Z_{\text{Ising}} = \prod_x \sum_{\sigma_x=\pm 1} e^{\beta \sum_{x,\mu} \sigma_{x+\hat{\mu}} \sigma_x}. \tag{75}$$

For each link (x,μ) we use the expansion

$$e^{\beta \sigma_{x+\hat{\mu}} \sigma_x} = \cosh(\beta) \sum_{n_{x,\mu}=0,1} [\sigma_{x+\hat{\mu}} \sqrt{\tanh(\beta)} \sigma_x \sqrt{\tanh(\beta)}]^{n_{x,\mu}}. \tag{76}$$

Equation (76) attaches an index $n_{x,\mu}$ at each link (x,μ). It is then possible to pull together the various factors of $[\sqrt{\tanh(\beta)}\sigma_x]^{n_{x,\mu}}$ from links coming from a single site x and to sum over σ_x,

$$\begin{aligned} &\sum_{\sigma_x=\pm 1} \prod_{\mu=1}^{D} [\sqrt{\tanh(\beta)}\sigma_x]^{n_{x-\hat{\mu},\mu}+n_{x,\mu}} \\ &= \sqrt{\tanh(\beta)}^{\sum_\mu n_{x-\hat{\mu},\mu}+n_{x,\mu}} \\ &\quad \times 2\delta\left(\text{mod}\left[\sum_\mu n_{x-\hat{\mu},\mu} + n_{x,\mu}, 2\right]\right), \end{aligned} \tag{77}$$

using

[1]The sum of two MPSs is not a MPS, so we do not call it a subspace.

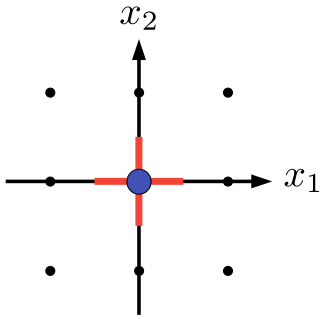

FIG. 6. Basic tensor for $D = 2$. The indices of the tensor are shown as thick lines (red online) emanating from a circular body at the central site of the lattice. Diagrams of tensors designed this way are ubiquitous in the literature. The neighboring lattice sites are indicated as black dots.

$$\sum_{\sigma_x=\pm 1} \sigma_x^n = 2\delta(\mathrm{mod}[n,2]) \tag{78}$$

at every site on the lattice. The expression $\delta(\mathrm{mod}[n,2])$ equals 1 when n is even (0 modulo 2) and 0 otherwise. We can rewrite the partition function as the following trace of a tensor product:

$$Z = 2^V[\cosh(\beta)]^{VD}\mathrm{Tr}\left[\prod_x T^{(x)}_{n_{x-\hat{1},1},n_{x,1},\ldots,n_{x,D}}\right]. \tag{79}$$

Tr indicates contractions (sums over 0 and 1) over the link indices (the $n_{x,\mu}$'s). The local tensor $T^{(x)}$ has $2D$ indices. The explicit form is

$$T^{(x)}_{n_{x-\hat{1},1},n_{x,1},\ldots,n_{x-\hat{D},D},n_{x,D}} = [\sqrt{\tanh(\beta)}]^{n_{x,\mathrm{in}}+n_{x,\mathrm{out}}} \times \delta(\mathrm{mod}[n_{x,\mathrm{in}} + n_{x,\mathrm{out}}, 2]), \tag{80}$$

with the definitions

$$n_{x,\mathrm{in}} \equiv \sum_{\mu=1}^{D} n_{x-\hat{\mu},\mu}, \qquad n_{x,\mathrm{out}} \equiv \sum_{\mu=1}^{D} n_{x,\mu}. \tag{81}$$

The notions of "in" and "out" refer to the position of the link with respect to the positive direction. The basic tensors and their assemblies in two and three dimensions are illustrated in Figs. 6–9.

Any kind of boundary condition can be accommodated by adapting the method of integration to the link configuration at the boundary. This is discussed in Sec. V.C.

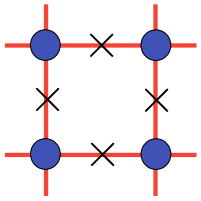

FIG. 7. Tensor assembly for $D = 2$. The crosses indicate contraction.

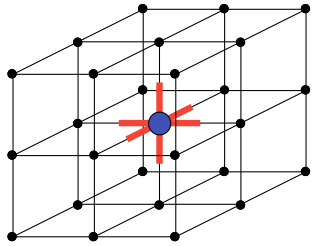

FIG. 8. Basic tensor for $D = 3$. The six indices of the local tensor are shown as thicker lines (red online) emanating from a circular body at the central site of the lattice, and they live along the links of the lattice.

The Kronecker delta in Eq. (80) implies the discrete conservation law

$$\sum_{\mu}(n_{x,\mu} - n_{x-\hat{\mu},\mu}) = 0 \ \mathrm{mod}\ 2, \tag{82}$$

which we also call the "tensor selection rule." It implies that only an even number of n's are allowed to take on the value 1. For instance, for $D = 2$, there are in principle 16 tensor values; however, only eight are nonzero, one with all four indices as zero [zeroth order in $\tanh(\beta)$], six with two 0's and two 1's [linear in $\tanh(\beta)$], and one with four 1's [quadratic in $\tanh(\beta)$]. Note that if a symmetry breaking term like a magnetic field coupling to the total spin is introduced, then all 16 tensor elements will generally be nonzero.

There are also tensor formulations that use the singular value decomposition (see Appendix A.3) on each nearest-neighbor Boltzmann factor to factorize the spins. The nearest-neighbor interactions can be represented as the following matrix, whose indices are the spin variables themselves:

$$e^{\beta\sigma_{x+\hat{\mu}}\sigma_x} = \begin{pmatrix} e^{\beta} & e^{-\beta} \\ e^{-\beta} & e^{\beta} \end{pmatrix}_{(x,\mu)}. \tag{83}$$

One can then perform the singular value decomposition to get

$$e^{\beta\sigma_{x+\hat{\mu}}\sigma_x} = \sum_{\alpha,\beta} U_{\sigma_{x+\hat{\mu}}\alpha}\lambda_{\alpha\beta}U^T_{\beta\sigma_x}, \tag{84}$$

and in the case of the Ising model the singular value decomposition has the same left and right unitary matrices. This factorizes the spins and allows for the following definition of the matrix:

$$W_{\sigma_x\alpha} \equiv U_{\sigma_x\alpha}\sqrt{\lambda_\alpha}. \tag{85}$$

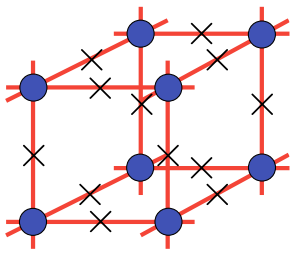

FIG. 9. Tensor assembly for $D = 3$. The crosses indicate contraction.

The main local tensor is then the contraction of all W matrices that have a common spin,

$$T_{ij\cdots N} = \sum_{\sigma_x} W_{\sigma_x i} W_{\sigma_x j} \cdots W_{\sigma_x N}. \tag{86}$$

In fact, the singular value decomposition in this case can be completely related to the expansion in Eq. (77). Consider the following character expansion from Sec. V.A for the nearest-neighbor interaction:

$$e^{\beta\sigma_{x+\hat{\mu}}\sigma_x} = \sum_{n_{x,\mu}=0}^{1} H_{x+\hat{\mu}} C_{n_{x,\mu}}(\beta) H_x, \tag{87}$$

with matrices

$$H_x \equiv \frac{1}{\sqrt{2}} \begin{pmatrix} 1 & 1 \\ 1 & -1 \end{pmatrix}, \tag{88}$$

whose columns are the normalized eigenvectors of the Pauli x matrix, $C_0 = 2\cosh\beta$, and $C_1 = 2\sinh\beta$. The elements of this matrix are from the four values that $n_{x,\mu}$ and σ_x can take normalized to be unitary. Since the variables are compact, their operators have a discrete spectrum, and the character expansion is the exact spectrum decomposition for this matrix. For any matrix M, by definition the singular value decomposition is determined using the eigenvalues and eigenvectors of $MM^\dagger$ and $M^\dagger M$. In this case (we drop any specific spacetime lattice indices for these steps since they are completely general),

$$\begin{aligned} \sum_{\sigma_j} e^{\beta\sigma_i\sigma_j} e^{\beta\sigma_j\sigma_k} &= \sum_{\sigma_j} \sum_{n,m} \sigma_i^n C_n \sigma_j^n \sigma_j^m C_m \sigma_k^m \\ &= \sum_{n,m} \sigma_i^n C_n C_m \sigma_k^m \delta_{n,m} \\ &= \sum_{n} \sigma_i^n C_n^2 \sigma_k^n. \end{aligned} \tag{89}$$

The singular values are then given by $\lambda_1 = 2|\cosh\beta|$ and $\lambda_2 = 2|\sinh\beta|$, as one would expect from Eqs. (84) and (87).

B. The forms of duality

The tensor representation can be used to reproduce the set of closed paths appearing in the expansion in powers of $\tanh(\beta)$ (Itzykson and Drouffe, 1991; Parisi, 1998) for the Ising model. The links associated with the set of indices $n_{x,\mu} = 1$ form a graph (a set of sites connected by links). The selection rule means that each site is attached to an even number of nonzero links. These graphs are closed paths with specific connectivity, which can in principle be enumerated order by order in their length using geometric constructions and combinatorial techniques.

One can try to construct these closed paths by assembling the most elementary contributions, namely, closed loops on a single plaquette. The way they can be assembled depends on the dimension. For instance, for $D = 2$ we can decide that when two loops around two plaquettes share a link, this link is "erased" from the path. Alternatively, one can introduce the dual variables originally conceived by Kramers and Wannier (1941), which are spins on the dual lattice located at the centers of the plaquettes. Each dual spin is then associated with a closed plaquette loop around it on the original lattice.

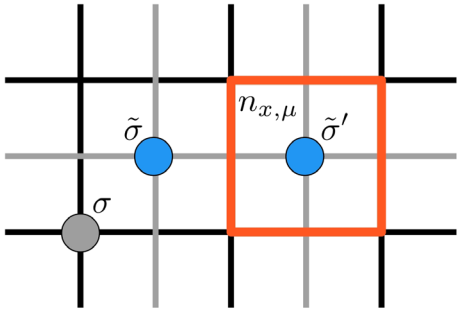

FIG. 10. The distinct dual variables shown on the original lattice (black lines) and the dual lattice (gray lines). Two dual spins are denoted with a tilde on the dual sites, an original spin σ on the original lattice, and the Pontryagin dual on the original lattice crossing a dual link. A closed loop of Pontryagin duals is generally shown on the original lattice encircling $\sim\sigma'$.

Furthermore, the Pontryagin dual variables $n_{x,\mu}$ can be expressed as $(1 - \tilde{\sigma}\tilde{\sigma}')/2$, with $\tilde{\sigma}$ and $\tilde{\sigma}'$ the two dual spin variables connected by a dual link crossing the original link. A depiction of the dual variables in their different locations is shown in Fig. 10. This illustrates that the notions of duality are often combined in a manner that may appear confusing at first sight. Note that the dual domains with a given dual spin have boundaries that can be interpreted as the closed paths of the original model. The questions of completeness and multiplicity need to be addressed using specific boundary conditions.

Similarly, in higher dimensions it is possible to introduce dual spins with interactions involving $2(D-1)$ spins. For $D = 3$, this leads to a gauge theory with plaquette interactions (Wegner, 1971). It is also possible to introduce dual variables for Ising models with arbitrary all-to-all spin interactions (Meurice, 1994). Duality questions related to Gauss's law are discussed in Sec. XII.D.

C. Boundary conditions

In Eq. (79), the trace is a sum over all the link indices. We need to specify the boundary conditions. Periodic boundary conditions (PBCs) allow us to keep a discrete translational invariance: the tensors themselves are translation invariant and assembled in the same way at every site. Open boundary conditions (OBCs) may also be implemented by introducing new tensors that can be placed at the boundary. Their construction is similar to the tensors in the bulk. The only difference is that the "outside links" that would be attached at sites on the boundary have an index set to zero. Using the normalization introduced in Eq. (77), one finds that the indices carrying a zero index carry a unit weight. This construction can be understood as decoupling the system from a larger environment by setting β on the links connecting to this environment to zero since $\tanh(0)^0 = 1$ and $\tanh(0) = 0$. This is illustrated in Fig. 11.

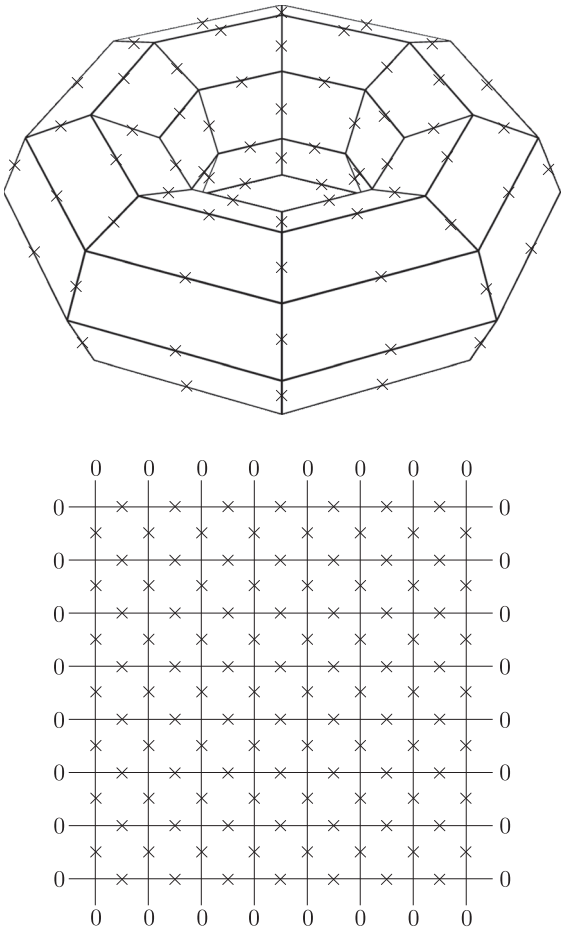

FIG. 11. Assembling the translation-invariant tensor with PBCs (top), or when using new tensors at the boundary for OBCs (bottom). Tensors are assumed to be put on each lattice site.

D. Exact blocking

An important feature of the tensor representation presented in Sec. V.A is that it allows an exact local blocking procedure, in contrast to what can be done in configuration space.[2] We divide the original lattice into cells having a linear size of two lattice spacings (blocks) in such a way that the boundaries are halfway between lattice sites. In other words, the boundaries are normal to links and cut them in the middle. As an example, for $D = 2$ the blocks are squares enclosing four sites, and their four sides cross eight links. This cell partition separates the link degrees of freedom into two disjoint categories: those completely inside the block, which can be integrated over, and those shared by neighboring blocks and kept to communicate between the blocks. This is a generic feature of the method (Meurice, 2013) that motivated a systematic study of lattice models (Liu *et al.*, 2013). Note that when translation invariance is present, all the blocks are identical and we need to do only one calculation.

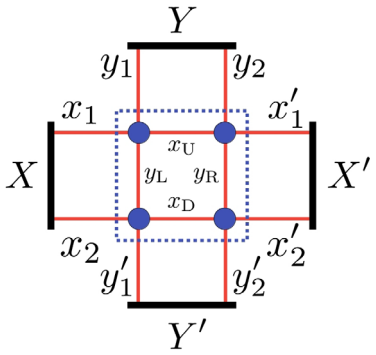

FIG. 12. Graphical representation of the block (dotted square) and $T'_{XX'YY'}$. From Meurice, 2013.

We now explicitly describe this exact blocking for $D = 2$ using generic notations inspired by those of Xie *et al.* (2012) and Meurice (2013). The extension to higher dimensions on hypercubic lattices is straightforward. We contract the four tensors located at the four sites inside the block along the four indices located strictly inside the block as well. The remaining eight indices associated with the eight links piercing the block are left as new degrees of freedom. By taking the tensor product between the two indices in each of the four directions coming out of the block, we obtain a new rank-4 tensor $T'_{XX'YY'}$. In the case of the Ising model [see Eq. (80)], each index now takes four values. This provides the following simple isotropic formula:

$$T'_{X(x_1x_2)X'(x'_1x'_2)Y(y_1y_2)Y'(y'_1y'_2)} = \sum_{x_U,x_D,x_R,x_L} T_{x_1x_Uy_1y_L} T_{x_Ux'_1y_2y_R} T_{x_Dx'_2y_Ry'_2} T_{x_2x_Dy_Ly'_1}, \quad (90)$$

where $X(x_1x_2)$ is a notation for the product states; i.e., if we group the indices with the same parity together, $X(00) = 1, X(11) = 2, X(10) = 3, X(01) = 4$. This contraction and redefinition relative to the block is illustrated in Fig. 12.

After this blocking, the partition function can be written as

$$Z = \mathrm{Tr} \prod_{2x} T'^{(2x)}_{XX'YY'},$$

where $2x$ denotes the sites of the coarser lattice with twice the lattice spacing of the original lattice. This coarse graining provides an exact representation of the original partition function. However, the number of states associated with each index is the square of the number of states in the original tensor. If this exact procedure had to be carried out numerically, this rapid growth would quickly run into practical limitations. Truncations are thus necessary. It is important to appreciate that truncations are the only approximations that will be needed. We now discuss truncations.

[2]We want to make clear that this section is describing not a RG transformation but rather an exact reorganization of the computation of the partition function in a way that performs the integration of some degrees of freedom corresponding to increasing distance scales. As explained in Sec. VI, truncations need to be applied to define a RG transformation.

VI. TENSOR RENORMALIZATION GROUP

A. Block spinning through SVD

Once partition functions and physical quantities are expressed as tensor networks, one needs to contract them to obtain numerical values. However, contracting exactly requires an extraordinary amount of computational resources. In this section we work through the original idea of how one can perform tensor contractions approximately, and how truncations appear in this approximation. To do so a coarse-graining algorithm for tensor networks is introduced. The original idea of such an approach was proposed by Levin and Nave (2007), where tensor networks are coarse grained simply by using the SVD; see Appendix A.3. This method is similar in spirit to the real-space renormalization group approach, and in this sense it is called the tensor renormalization group.[3]

In the standard renormalization group procedure (Wilson and Kogut, 1974), the blocking process is supplemented by a sorting of the resulting information according to its degree of relevance. As far as universal properties characterizing the continuum limit are concerned, it is acceptable to discard the information that reflects only microscopic details of a specific lattice formulation. In the context of the previously discussed tensor formulation, this means that, possibly after a certain number of exact contractions, we need to restrict the number of states associated with the tensor indices to a fixed number D_{cut}. We are then mapping a tensor with D_{cut}^{2D} entries into another tensor of the same shape, and the question of fixed points becomes meaningful. An important goal of the renormalization procedure is to identify fixed points. Note that the updated tensor remains a local object that supersedes the notion of action or Hamiltonian.

Here we assume that a partition function is expressed as a two-dimensional tensor network with bond dimension D_{cut},

$$Z = \mathrm{Tr}\prod_x T^{(x)}_{xx'yy'}, \tag{91}$$

and that periodic boundary conditions are imposed in all directions. Later in this section, we explain the algorithm of the original TRG proposed by Levin and Nave.[4]

The tensor T can first be regarded as a $D_{\mathrm{cut}}^2 \times D_{\mathrm{cut}}^2$ matrix and then can be approximately decomposed using the SVD in two ways:

$$T_{x'yxy'} = M^{[13]}_{(x'y)(xy')} \approx \sum_{m=1}^{D_{\mathrm{cut}}} S^{[1]}_{(x'y)m} \lambda^{[13]}_m S^{[3]}_{m(xy')}, \tag{92}$$

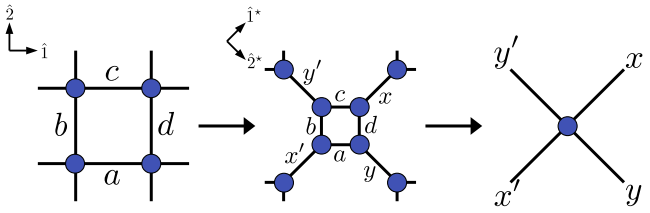

FIG. 13. A coarse-graining step for the tensor network. Circles represent tensors and closed indices should be contracted. The definitions of the unit vectors for the original and the coarse-grained network are also shown. The tensor indices are shown in the same manner as in Eq. (94).

$$T_{y'x'yx} = M^{[24]}_{(y'x')(yx)} \approx \sum_{m=1}^{D_{\mathrm{cut}}} S^{[2]}_{(y'x')m} \lambda^{[24]}_m S^{[4]}_{m(yx)}, \tag{93}$$

where $\lambda^{[13]}$ and $\lambda^{[24]}$ are the singular values (assumed to be in descending order: $\lambda_1 \geq \lambda_2 \geq \cdots \geq \lambda_{D_{\mathrm{cut}}^2} \geq 0$), and $S^{[1]}$, $S^{[2]}$, $S^{[3]}$, and $S^{[4]}$ are unitary matrices. Here the degree of the approximation is set at D_{cut} for simplicity. One can freely choose this parameter, and it becomes the bond dimension of the coarse-grained tensors.

When the decomposed tensors $S^{[i]}$ ($i = 1$, 2, 3, and 4) are used, a coarse-grained tensor is defined by

$$T^{\mathrm{new}}_{xx'yy'} = \sqrt{\lambda^{[13]}_x \lambda^{[24]}_y \lambda^{[13]}_{x'} \lambda^{[24]}_{y'}} \sum_{a,b,c,d=1}^{D_{\mathrm{cut}}} S^{[3]}_{x(cd)} S^{[4]}_{y(da)} S^{[1]}_{(ab)x'} S^{[2]}_{(bc)y'}. \tag{94}$$

The number of tensors on the network is now reduced by $1/2$, and the bond dimension of T^{new} is a free parameter and here set to be the same as that of T: D_{cut}. Repeating this procedure, one can make an effective tensor network that consists of a few tensors and then take the contraction of the tensor indices. A graphical explanation of the TRG is given in Fig. 13.

After a coarse-graining step, the network is rotated by 45°, and how one defines the new unit vectors is then one's choice. One possible way is to define them by $\hat{1}^\star = \hat{1} + \hat{2}$ and $\hat{2}^\star = \hat{1} - \hat{2}$, where $\hat{1}$ ($\hat{2}$) and $\hat{1}^\star$ ($\hat{2}^\star$) are the unit vectors along the $\hat{1}$ ($\hat{2}$) direction of the original lattice and that of the coarse-grained lattice, respectively; see Fig. 13. Using this definition, the orientation of the network is recovered after every two coarse-graining steps, i.e., $\hat{1}^{\star\star} = \hat{1}^\star + \hat{2}^\star = 2 \cdot \hat{1}$ and $\hat{2}^{\star\star} = \hat{1}^\star - \hat{2}^\star = 2 \cdot \hat{2}$.

In this procedure the relevant degrees of freedom are decided by the SVD during the decomposition of the T tensor into an intermediate sum over states. In Sec. VI.B we see that there are improved methods to identify the relevant states during truncation.

B. Optimized truncations

Section VI.A addressed the first work on a renormalization group procedure using a tensor formulation. Here we discuss refinements that occurred later. These refinements incorporate

[3]There are several numerical renormalization group methods that can be regarded as ancestors of the TRG; see Wilson (1975), White (1992, 1993), Nishino (1995), Nishino and Okunishi (1996), and Wang and Xiang (1997). See also the references at the end of Sec. IV.C and Ueda, Okunishi, and Nishino (2014).

[4]Coarse-graining approaches for tensor networks are generically referred to as TRG. Therefore, "TRG" does not necessarily identify a specific algorithm.

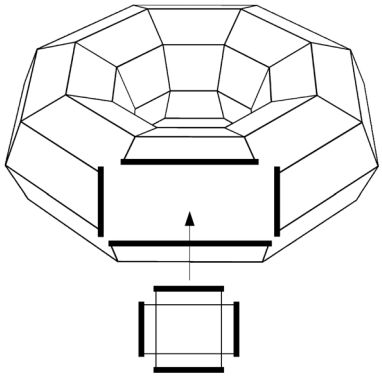

FIG. 14. A blocked tensor and its environment.

an environment tensor from which relevant states are determined and kept.

We begin by assuming that one has completed the contraction of a single block. Each tensor index of the blocked tensor now possesses D_{cut}^2 states. The next step is to find a way to determine which of the D_{cut}^2 states (or possibly a linear combination of them) corresponding to the tensor product associated with each index should be kept. Ideally, we want to address this question in terms of the environment of a single tensor. We can write

$$\mathrm{Tr}\prod_x T^{(x)} = \sum_{XX'YY'} E_{XX'YY'} T'^{(0)}_{XX'YY'}, \tag{95}$$

where $E_{XX'YY'}$ is obtained by tracing all the indices except for four pairs of indices associated with a single block that we have located at the origin, and $T'^{(0)}$ is the first block of four tensors. This is illustrated in Fig. 14. Constructing an environment from which important states are chosen is reminiscent of the finite-size density matrix renormalization group. The environment tensor $E_{XX'YY'}$ is close to what we are ultimately trying to calculate, so it is not immediately available. The only purpose of using $E_{XX'YY'}$ is to rank order the states of the tensor product, and its exact form does not appear in later calculations. Consequently, the exact form may not be too important, and as a first step we can attempt approximations.

A simple approximation is to ignore the details of the environment and use (Meurice, 2013)

$$E^{\text{app}}_{XX'YY} = C\delta_{XX'}\delta_{YY'} \tag{96}$$

for some positive constant C. We can then optimize the truncation by maximizing the approximate partition function expressed in terms of the trace of a matrix G such that

$$\mathrm{Tr}G = (1/C)\sum_{XX'YY'} E^{\text{app}}_{XX'YY'} T'^{(0)}_{XX'YY'}, \tag{97}$$

which can be achieved with

$$G_{XX'} = \sum_Y T'^{(0)}_{XX'YY}. \tag{98}$$

By looking at the expression in terms of the original tensors, one realizes that $G_{XX'}$ is in fact the square of another matrix (Meurice, 2013). If the eigenvalues of this matrix are real, then all the eigenvalues of G are positive and we can optimize the truncations by selecting the states corresponding to the largest eigenvalues of G.

A more refined approximation is to assume that the environment is a "mirror image" of the tensor itself (Xie *et al.*, 2012) as follows:

$$E^{\text{app}}_{XX'YY} = C' T'^{(0)\star}_{XX'YY'}. \tag{99}$$

The trace of G can then be identified using the following tensor norm:

$$\mathrm{Tr}\, G = \sum_{XX'YY'} T'^{(0)}_{XX'YY'} T'^{(0)\star}_{XX'YY'} = \|T'^{(0)}\|^2, \tag{100}$$

which is a sum of positive terms. This can be accomplished with the Hermitian matrix

$$G_{XX'} = \sum_{X''YY'} T'^{(0)}_{XX''YY'} T'^{(0)\star}_{X'X''YY'}. \tag{101}$$

The problem is then reduced to selecting the states that provide the best approximation of TrG, which is straightforward when all the eigenvalues are positive.

The procedure that we just described is isotropic. It is, however, possible to coarse grain in one direction at a time (Xie *et al.*, 2012) in order to reduce the size of the summed expressions. For instance, the summation over the tensor product indices Y and Y' in Eq. (101) can first be replaced by the following summations over single indices:

$$M_{X(x_1,x_2)X'(x'_1,x'_2)yy'} = \sum_a T_{x_1x'_1ya} T_{x_2x'_2ay'}. \tag{102}$$

The tensor M can then be used in Eq. (101) in place of $T^{(0)}$ as the blocked tensor to find the most relevant states for the X indices. This provides a coarse graining in the first direction. It is then necessary to coarse grain in the second direction using sums over single indices in the first direction. As our discussion focuses on $D = 2$, these two steps constitute a coarse graining that doubles the lattice spacing in all directions. Xie *et al.* (2012) conducted these calculations using higher-order generalizations of the SVD method called the higher-order tensor renormalization group (HOTRG).

A better description of the environment can be reached by following a local truncation procedure such as that described previously for a sufficiently large but finite number of times, at which point it is assumed that there is no environment and Eq. (96) can be used. In other words, by working with a finite lattice, the procedure is terminated by approximating the partition function as a trace of the last coarse-grained expression for the tensor. It is then possible to move backward (Xie *et al.*, 2009; Zhao *et al.*, 2010) and reconstitute the approximate environment of a single tensor coarse grained one fewer time. Explicit expressions based on the HOTRG construction were given by Xie *et al.* (2012). This can be

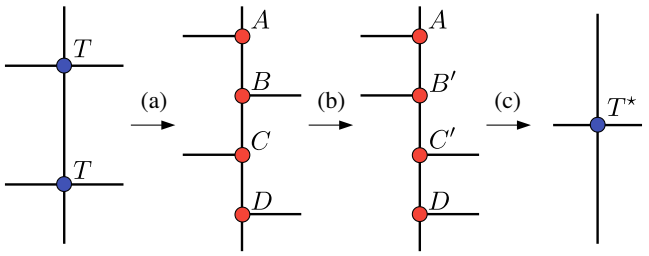

FIG. 15. Graphical description of the ATRG. (a) Decompose T into A and B and C and D using the SVD. (b) Swap the bonds of B and C. The swapping can also be done using the SVD: $\sum_i B_{xyi}C_{ix'y'} = (BC)_{xyx'y'} = \sum_i B'_{x'yi}S_iC'_{ixy}$. (c) Contract A, B', C', and D while truncating the dimensions of horizontal bonds.

pursued recursively until we reach the first coarse-graining level illustrated in Fig. 14.

An analogy with the backward propagation used in machine learning has recently been exploited to design new algorithms (Chen *et al.*, 2020). More generally, algorithmic improvement in the TRG context is a subject of active investigation (Bal *et al.*, 2017; Fishman *et al.*, 2018; Morita and Kawashima, 2021). The idea that the bound dimension can be regarded as a relevant direction that can be used to obtain data collapse was discussed by Vanhecke *et al.* (2019). For earlier developments see Tagliacozzo *et al.* (2008), Pollmann *et al.* (2009), and Pirvu *et al.* (2012). We would expect these considerations to provide a more systematic understanding of the truncation errors.

C. Higher-dimensional algorithms

While the Levin-Nave–type TRG can be applied to two-dimensional systems, higher-dimensional systems are dealt with using other algorithms. One such algorithm is the HOTRG (Xie *et al.*, 2012) mentioned in Sec. VI.B. Using the HOTRG, in principal, any dimensional tensor network can be coarse grained. When a D-dimensional tensor network is built using tensors with the bond dimension D_{cut}, the computational complexity of the HOTRG is $\mathcal{O}(D_{\mathrm{cut}}^{4D-1})$ and the memory complexity is $\mathcal{O}(D_{\mathrm{cut}}^{2D})$.

Recently cheaper algorithms were invented. The anisotropic tensor renormalization group (ATRG) (Adachi, Okubo, and Todo, 2020), whose graphical description is given in Fig. 15, achieved the time and memory complexities $\mathcal{O}(D_{\mathrm{cut}}^{2D+1})$ and $\mathcal{O}(D_{\mathrm{cut}}^{D+1})$, which are significant reductions from the HOTRG. The ATRG introduces an approximation of an approximation, and indeed, when the bond dimensions are the same, the ATRG is less accurate than the HOTRG. However, thanks to the cheaper complexity, the ATRG leads to better accuracy with a fixed CPU time. Using the ATRG, four-dimensional systems, where the HOTRG is much more expensive, have been under investigation (Akiyama, Kadoh *et al.*, 2020, Akiyama, Kuramashi *et al.*, 2020, Akiyama *et al.*, 2021).

Another approach, coarse graining on a triad tensor network representation, was taken by Kadoh and Nakayama (2019). They compared the triad tensor renormalization group approach to the original HOTRG and ATRG algorithms.

D. Observables with tensors

With the tensor formulation from Sec. V.A along with the coarse-graining algorithms from Sec. VI, it is possible to calculate derivatives of $\ln Z$, as well as to compute n-point correlation functions.

Because the tensor renormalization group process requires renormalizing the tensor during iterations, in order to compute the logarithm of the partition function these normalizations must be stored. For a coarse graining that is isotropic with $N_1, N_2, \ldots, N_D$ iterations in each direction and $N = \sum_{i=1}^{D} N_i$, note that the normalizations at each iteration are $\mathcal{N}^{(0)}$, $\mathcal{N}^{(1)}$, $\mathcal{N}^{(2)}$, etc., starting with the normalization of the initial tensor by $\mathcal{N}^{(0)}$. During the coarse-graining process, $\mathcal{N}^{(0)}$ appears $V = 2^N$ times, giving an overall factor of $\mathcal{N}^{(0)V}$. Likewise, each subsequent normalization appears to be 2^{N-n}, where n denotes the iteration number, i.e., $1, \ldots, N$. After the final step the total normalization on the effective tensor is given by

$$\mathcal{N}^{(0)V} \cdot \mathcal{N}^{(1)V/2} \cdot \mathcal{N}^{(2)V/4} \cdots \mathcal{N}^{(N)}. \tag{103}$$

The logarithm of the partition function is then given as the logarithm of this normalization added to the following logarithm of the trace of the final tensor:

$$\ln Z = \sum_{n=0}^{N} 2^{N-n} \ln \mathcal{N}^{(n)} + \ln \mathrm{Tr}[T], \tag{104}$$

where T is the final normalized effective tensor and the trace is the tensor trace.

Expectation values of N-point correlation functions (Gu, Levin, and Wen, 2008; Nakamoto and Takeda, 2016) are given by ratios of partition functions that are calculated separately using the tensor renormalization group as follows:

$$\langle \sigma^{(1)}\sigma^{(2)} \cdots \sigma^{(N)} \rangle = \frac{Z^{(N)}}{Z}, \tag{105}$$

with

$$Z^{(N)} = \sum_{\{\sigma\}} \sigma^{(1)}\sigma^{(2)} \cdots \sigma^{(N)} e^{-S} \tag{106}$$

and where the positions of the σ fields have been suppressed. In terms of tensors this amounts to N "impure" tensors, whose namesake comes from their altered local constraint. Since $Z^{(N)}$ contains additional spin fields located at specific sites, those spin fields alter the sum at that site over the field states and give

$$\sum_{\sigma_{x^*}} \sigma_{x^*}^{1+\sum_{\mu=1}^{D} n_{x^*-\hat{\mu},\mu} - n_{x^*,\mu}} = \begin{cases} 2 & \text{if } 1 + \sum_{\mu=1}^{D} n_{x^*-\hat{\mu},\mu} - n_{x^*,\mu} \text{ is even,} \\ 0 & \text{otherwise,} \end{cases} \tag{107}$$

where x^* is the location of the additional spin. These additional spins act as sources and sinks for the vector fields $n_{x,\mu}$ on the surrounding links, as can be seen with the new

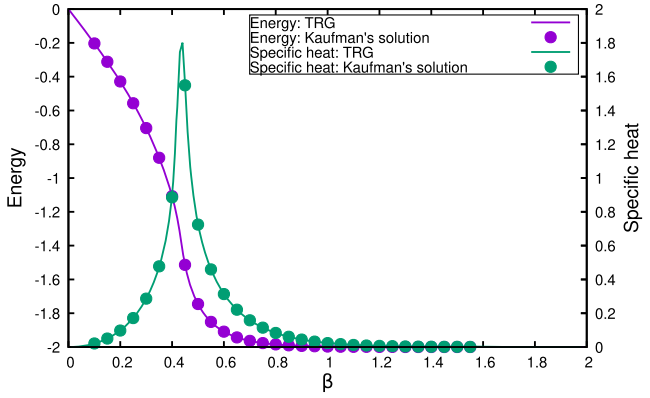

FIG. 16. Energy and specific heat of the two-dimensional Ising model on a 32×32 lattice with $D_{\text{cut}} = 32$.

constraint, where the divergence of the surrounding n fields must now be 1 modulo 2. To compute the ratio, if both $Z^{(N)}$ and Z are normalized identically throughout the calculation, only the ratio of the trace of the final effective tensors is necessary for the expectation value since the normalizations would cancel.

As illustrated in Fig. 16, the method can be used for the average energy and the specific heat, which are compared to the exact solutions using Kaufman's formula. The energy is calculated using the TRG with two neighboring impurity tensors, and the specific heat is given as the numerical β derivative of the energy. To show a graphical example of the contractions performed using impure tensors, four impurities on a plaquette are decomposed and contracted to form four impurities again, as illustrated in Fig. 17. Note that the energy can also be obtained using the numerical derivative of the logarithm of the partition function, and then the specific heat is the second numerical derivative. In general, the numerical derivatives cause a loss of significance, so obtaining the energy as a primary output of the TRG using the impurity tensor method helps one to improve the numerical accuracy. The impurity tensors destroy the translational invariance but the effect is local, so the computational complexity does not drastically increase.

E. Niemeijer–van Leeuwen equation

In Sec. V.D we constructed a coarse-grained tensor that can be used to give an exact expression for the partition function. Despite the fact that we integrated over microscopic degrees of freedom, the number of tensor indices needed for this exact representation grows exponentially with the size of the blocks. In Secs. VI.A and VI.B, we introduced truncations where a fixed number of indices D_{cut} was kept at each step. This procedure discards some information but allows us to compare the tensors before and after the coarse graining. Typically, the tensors tend to grow exponentially with the number of coarse-graining steps, and it is important to renormalize their absolute size or to consider only their ratios. After such a renormalization takes place, we obtain a RG transformation. The fixed points of this transformations are the central objects of the RG approach and it is useful to compare the TRG equations with standard RG equations due to Niemeijer and van Leeuwen (NvL) (Niemeijer and van Leeuwen, 1976).

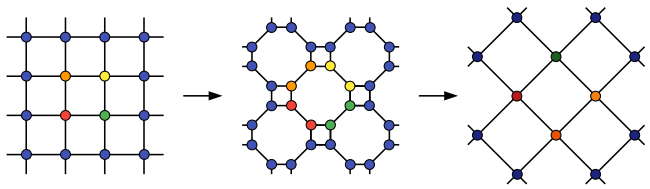

FIG. 17. TRG process for a tensor network with four impurities on a plaquette.

NvL were aware of the difficulty of controlling the new couplings generated by the blocking procedure, so they started immediately with the most general Ising interactions in a finite volume V. If no conditions are imposed, there are as many couplings as Ising configurations, so this is not suitable for numerical purposes. They then introduced 1 in the partition function as in Eq. (1) in order to define new Ising spins $\{\sigma'\}$ in a volume $V' = V/b^D$ with a new lattice spacing rescaled by the linear size of the blocks b. They were able to give a formal expression for the new couplings in terms of the original ones as $\mathbf{K}'(\mathbf{K})$. Strictly speaking, there are fewer couplings after the coarse graining because they considered the most general case involving the products of spins in arbitrary domains, but they assumed that only a certain number of quasilocal couplings were important and had the same form before and after the coarse graining. In addition, they assumed that the dependence of the free energy density $f(\mathbf{K})$ on these couplings is the same after the coarse graining. This led to the NvL equation

$$f(\mathbf{K}) = g(\mathbf{K}) + b^{-D} f(\mathbf{K}'). \tag{108}$$

The function $g = G/V$ comes from

$$G = \sum_{\{\sigma'\}} \ln\left(\sum_{\{\sigma\}} P(\{\sigma'\},\{\sigma\}) \exp[\mathcal{H}(\{\sigma\})]\right) \tag{109}$$

and is defined using the condition

$$\sum_{\{\sigma'\}} \mathcal{H}'(\{\sigma'\}) = 0, \tag{110}$$

where $\mathcal{H}$ and $\mathcal{H}'$ are the Hamiltonians before and after coarse graining.

Even though computing the new couplings and the functions may be difficult in practice (the new couplings are double partition functions), NvL succeeded in obtaining a formal relation that can be iterated and linearized near a fixed point. This allows us to identify the relevant directions, and it is often taken as the starting point for the introduction of the RG method in textbooks (Cardy, 1996).

For the TRG, we can factor out the increasing size of the tensors by imposing the normalization condition

$$T_{0000} = 1 \tag{111}$$

at each step. In other words, we divide all the tensors by one unnormalized tensor element. We now have the two steps

(coarse graining and renormalization) that define a RG transformation. We can write the exact identity as

$$\ln\left(\mathrm{Tr}\prod_{\text{sites}} T^{(\text{sites})}_{xx'yy'}\right)\Big/ V = (1/4)\ln(T'_{0000}) + (1/4)\ln\left(\mathrm{Tr}\prod_{\text{sites}'} T^{(\text{sites}')}_{XX'YY'}\right)\Big/ V', \quad (112)$$

where T'_{0000} is the unnormalized tensor element that we constructed in Sec. V.D. $T^{(\text{sites}')}_{XX'YY'}$ is the renormalized tensor, meaning the unnormalized tensor divided by T'_{0000}. Bearing in mind that $b^{-D} = 1/4$, we see an analogy with the NvL equation (108). $(1/4)\ln(T'_{0000})$ plays the role of $g(\mathbf{K})$. Note that $\mathrm{Tr}\prod_{\ldots}$ has different meanings on the two sides of the equation. However, if we assume that the coupling dependence of the densities is the same before and after as in NvL, we obtain a RG equation. In both cases, neglecting couplings can be justified by the fact the RG transformation has only a small number of important directions in the space of couplings. This will be illustrated with a simple example in Sec. VI.F. More details were given by Meurice (2020b).

F. A simple example of TRG fixed point

In the following we discuss the two-state truncation for the Ising model. In other words, we keep the same number of states for each index as for the initial tensor. With the indices taking two values, the rank-4 tensor has in principle 16 independent entries; however, because of the Ising selection rule, the sum of the indices must be even and thus eight of the tensor values are zero. In addition, if we preserve the symmetry under the rotation of the square lattice by $\pi/2$, this imposes

$$T_{1010} = T_{0110} = T_{1001} = T_{0101} \equiv t_1 \quad (113)$$

and

$$T_{1100} = T_{0011} \equiv t_2. \quad (114)$$

In addition, we define

$$T_{1111} \equiv t_3. \quad (115)$$

For the initial tensor, we have

$$t_1 = t_2 = \tanh(\beta), \qquad t_3 = t_1^2. \quad (116)$$

The property $t_1 = t_2$ is not preserved by the blocking procedure, which can be expressed as a mapping of the three-dimensional parameter space (t_1, t_2, t_3) into itself that we denote as $t'_i(t_1, t_2, t_3)$. Under this mapping, the elements of the tensor flow toward their fixed-point values based on the bare input value of β. The point of bifurcation in the fixed-point tensor elements can be used to determine the critical value of β.

As a numerical example, we use the method of Eq. (96) and the normalization from Eq. (111), which is discussed after Eq. (10) in the work of Meurice (2013). The results for t_1 as a function of the initial β for six iterations are shown in Fig. 18. We see that for values of β low enough, T_{1010} goes to zero at a faster rate as the number of iterations increases. On the other hand, for values of β large enough, T_{1010} goes to 1. As the number of iterations increases, the transition becomes sharper and sharper and singles out a critical value $\beta_c = 0.394\,867\,858\ldots$ where the curves for successive iterations intersect. This also singles out a fixed-point value for t_1 near 0.4. The graphs for t_2 and t_3 have similar features. Near β_c, the departure from the fixed-point value is approximately linear in $\beta - \beta_c$ with a slope of the form λ_1^{ℓ}, where ℓ is the number of iterations. It is possible to rescale $\beta - \beta_c$ by a factor λ_1 at each iteration to obtain the "data collapse" shown at the bottom of Fig. 18. Numerically, $t_1^\star = 0.422\,29$, $t_2^\star = 0.286\,37$, $t_3^\star = 0.274\,66$, and $\lambda_1 = 2.009\,310\,69$, which provides a critical exponent $\nu = \log b/\log\lambda_1 \simeq 0.993$ that is surprisingly close to the exact value 1 given that the truncation is drastic (Meurice, 2013). Similar results are obtained in a dual version of the map given by Aoki, Kobayashi, and Tomita (2009).

One would think that by adding a few more states we could get even better results; however, this is not the case (Efrati *et al.*, 2014). One of the reasons for this is explained in Sec. VI.G.

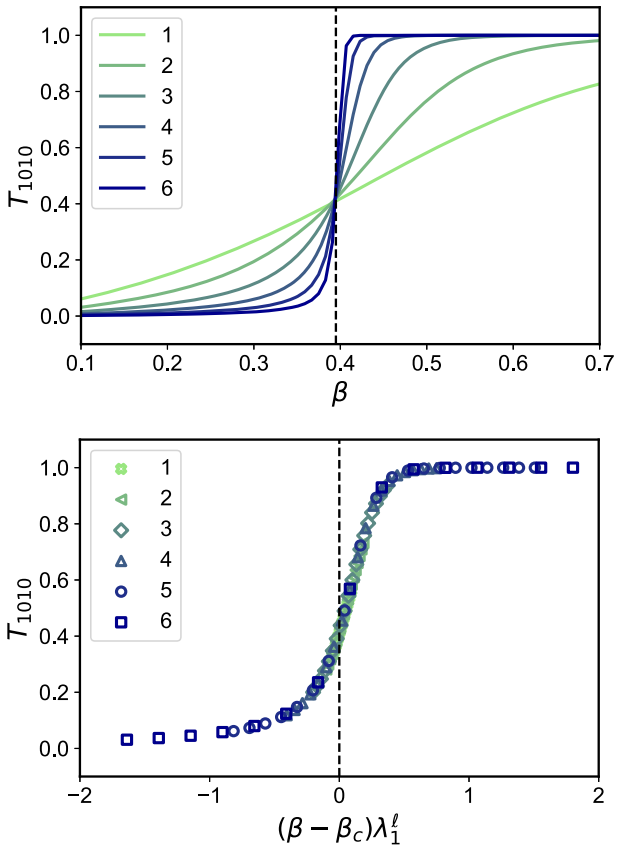

FIG. 18. $t_1 = T_{1010}$ vs β (top panel) and vs $(\beta - \beta_c)\lambda_1^{\ell}$ (bottom panel) for $\ell = 1, \ldots, 6$ iterations of the two-state approximation. The dotted line is at the critical value. As the iteration number increases, the curves sharpen (top panel) and the points spread more (bottom panel), and the color smoothly changes from light to dark (green to blue online).

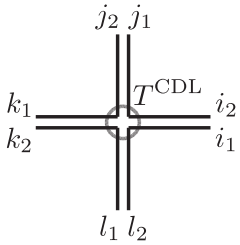

FIG. 19. CDL tensor.

G. Corner double line structure on tensor network

In this section we discuss a fixed point of the TRG (Levin and Nave, 2007) that is called the corner double line (CDL) tensor (Gu and Wen, 2009). Here we consider a toy model of short-range correlations that is expressed as a tensor network spanned by tensors with the following form:

$$T^{\mathrm{CDL}}_{kijl} = \delta_{i_1,l_2}\delta_{j_1,i_2}\delta_{k_1,j_2}\delta_{l_1,k_2}, \tag{117}$$

where each tensor index has two components [e.g., $i = (i_1, i_2)$]; see Fig. 19. We call T^{CDL} the CDL tensor, and it describes interactions on plaquettes as seen in Fig. 20. We now consider a TRG step for this tensor network.

The SVD of the CDL tensor is uniquely given by

$$T^{\mathrm{CDL}}_{kijl} = \sum_{m_1,m_2=1}^{\sqrt{D_{\mathrm{cut}}}} \delta_{i_1,m_2}\delta_{j_1,i_2}\delta_{m_1,j_2}\delta_{k_1,m_1}\delta_{l_1,k_2}\delta_{m_2,l_2}, \tag{118}$$

where we simply assume that all elementary components of the tensor indices run from 1 to $\sqrt{D_{\mathrm{cut}}}$ (e.g., $1 \le i_1, i_2 \le \sqrt{D_{\mathrm{cut}}}$). D_{cut} is assumed to be a square number. When the decomposed components are contracted, the coarse-grained tensor is then given by

$$\begin{aligned}(T^{\mathrm{CDL}})'_{kijl} = &\sum_{a,b,c,d=1}^{D_{\mathrm{cut}}} \delta_{i_1,c_1}\delta_{d_2,i_2}\delta_{j_1,d_2}\delta_{a_1,j_2}\delta_{k_1,a_1}\delta_{b_2,k_2} \\ &\times \delta_{l_1,b_2}\delta_{c_1,l_2}\delta_{a_2,b_1}\delta_{b_1,c_2}\delta_{c_2,d_1}\delta_{d_1,a_2} \\ &\propto T^{\mathrm{CDL}}_{kijl}.\end{aligned} \tag{119}$$

Each step is graphically displayed with the assignments of indices in Figs. 21 and 22. The CDL tensor turns out to be a fixed point of the TRG up to a constant factor. This is not a physical but rather an artificial fixed point, and this means that

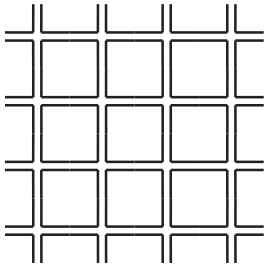

FIG. 20. CDL tensor network.

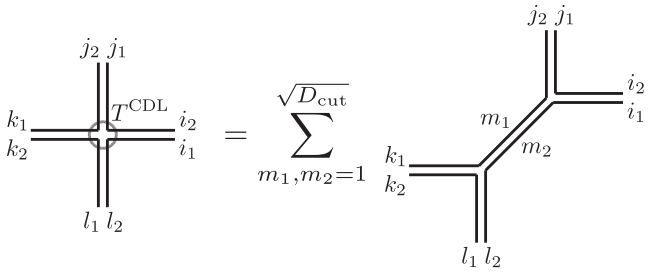

FIG. 21. SVD of a CDL tensor.

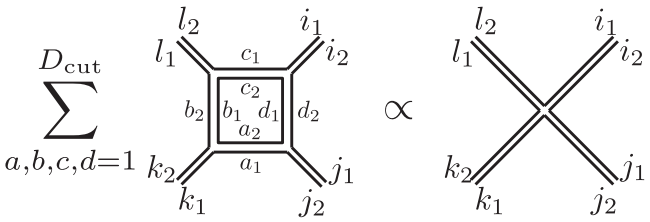

FIG. 22. Contraction step for a CDL tensor.

the TRG leaves short-range correlations on coarse-grained tensors. This is because the SVD is the best approximation of a tensor but is not the best for a network.

To avoid such an unexpected fixed point, one needs to consider more global blocking procedures. One ideal way is to insert unknown tensors [called "(dis)entangler"] on a network and variationally tune them to remove CDL structures. This method is called the tensor network renormalization (TNR) (Evenbly and Vidal, 2015) and leads to more precise computations. In principal, this can be extended to three or more dimensions, although the computational complexities would be extremely demanding. In two dimensions, more low-cost methods have been invented thus far (Yang, Gu, and Wen, 2017; Evenbly, 2018; Hauru, Delcamp, and Mizera, 2018), although we do not discuss them in detail here. The common concept in such approaches is to consider global cost functions and to remove the CDL structures on a network.

VII. TENSORS FOR SPIN MODELS WITH AN ABELIAN SYMMETRY

In this section, we discuss tensor formulations of generalizations of the Ising model. We first consider the case of the O(2) nonlinear sigma model introduced in Sec. II.B, where the spin variables form a two-dimensional unit vector varying continuously over a circle. We later show that the results extend easily to the clock models with a discrete $\mathbb{Z}_q$ symmetry.

A. O(2) nonlinear sigma model

The partition function for the O(2) model reads

$$Z_{\mathrm{O}(2)} = \prod_x \int_{-\pi}^{\pi} \frac{d\varphi_x}{2\pi} e^{-S_{\mathrm{O}(2)}}, \tag{120}$$

with

$$S_{\mathrm{O}(2)} = -\beta \sum_{x,\mu} \cos(\varphi_{x+\hat{\mu}} - \varphi_x). \tag{121}$$

We use the following Fourier expansion to expand the Boltzmann weights:

$$e^{\beta\cos(\varphi_{x+\hat{\mu}}-\varphi_x)} = \sum_{n_{x,\mu}=-\infty}^{\infty} e^{in_{x,\mu}\varphi_{x+\hat{\mu}}} I_{n_{x,\mu}}(\beta) e^{-in_{x,\mu}\varphi_x}. \tag{122}$$

This expansion factorizes the φ fields. We then integrate over all the φ fields using the orthogonality relations of the Fourier modes,

$$\begin{aligned}\int_{-\pi}^{\pi} \frac{d\varphi_x}{2\pi} \prod_{\mu=1}^{D} e^{i(n_{x-\hat{\mu},\mu}-n_{x,\mu})\varphi_x} \\ = \delta_{\sum_{\mu=1}^{D}(n_{x-\hat{\mu},\mu}-n_{x,\mu}),0} \\ = \delta_{n_{x,\mathrm{in}}-n_{x,\mathrm{out}},0},\end{aligned} \tag{123}$$

with $n_{x,\mathrm{in}}$ and $n_{x,\mathrm{out}}$ defined in the same way as in Sec. V. We can rewrite the partition function as the trace of a tensor product as follows:

$$Z = \mathrm{Tr} \prod_x T^{(x)}_{n_{x-\hat{1},1},n_{x,1},\ldots,n_{x,D}}. \tag{124}$$

The local tensor $T^{(x)}$ has $2D$ indices. The explicit form is

$$T^{(x)}_{n_{x-\hat{1},1},n_{x,1},\ldots,n_{x-\hat{D},D},n_{x,D}} = \sqrt{I_{n_{x-\hat{1},1}} I_{n_{x,1}}, \ldots, I_{n_{x-\hat{D},D}} I_{n_{x,D}}}\, \delta_{n_{x,\mathrm{out}},n_{x,\mathrm{in}}}. \tag{125}$$

The graphical representations of the tensors are similar to those of the Ising model. The only difference is that the indices attached to the legs are integers instead of integers modulo 2. The Kronecker delta in Eq. (125) enforces

$$\sum_{\mu=1}^{D} (n_{x,\mu} - n_{x-\hat{\mu},\mu}) = 0, \tag{126}$$

which is a discrete version of Noether current conservation if we interpret the $n_{x,j}$ with $j = 1, \ldots, D-1$ as spatial current densities and $n_{x,D}$ as a charge density. At sufficiently small β, the relative size of the higher-order Bessel functions compared to the zeroth-order Bessel function decays rapidly with their order, and it is justified to introduce a truncation.[5] If any of the indices of a tensor element are larger in magnitude than a certain value $n_{\max}$, we approximate the tensor element as zero. The compatibility of this type of truncation with the symmetries of the model is discussed in Sec. XIII.A.

The tensor formulation here can be seen from another perspective, i.e., by using the SVD on each nearest-neighbor factor and then calculating the φ integrals. The Fourier expansion of the nearest-neighbor interaction given by Eq. (122) can be understood as the spectral decomposition of the Boltzmann weight. Here the matrix $e^{in\varphi}$ is unitary, and is parametrized by the "indices" φ and n. To find the singular values, we multiply by the Hermitian conjugate and diagonalize (just as in the Ising case),

$$\begin{aligned}\int_0^{2\pi} \frac{d\varphi_j}{2\pi} e^{\beta\cos(\varphi_i-\varphi_j)} e^{\beta\cos(\varphi_j-\varphi_k)} \\ = \int_0^{2\pi} \frac{d\varphi_j}{2\pi} \sum_{n,m} e^{in\varphi_i} I_n e^{-in\varphi_j} e^{im\varphi_j} I_m e^{-im\varphi_k} \\ = \sum_{n,m} e^{in\varphi_i} I_n I_m e^{-im\varphi_k} \delta_{m,n} \\ = \sum_n e^{in\varphi_i} I_n^2 e^{-in\varphi_k},\end{aligned} \tag{127}$$

which gives the expected result that the singular values are the absolute value of the modified Bessel functions [$\lambda_n(\beta) = |I_n(\beta)|$]. We see from these examples that performing the character (or Fourier) expansion of the nearest-neighbor interaction during the tensor formulation is similar to the SVD of the same factor. In fact, when the coupling is positive, they are equivalent.

For convenience, when dealing with the group U(1) [or O(2) for that matter] we factorize all the $I_0(\beta)$ factors that dominate the small β regime and define the ratios

$$t_n(\beta) \equiv \frac{I_n(\beta)}{I_0(\beta)} \simeq \begin{cases} 1 - n^2/2\beta + \mathcal{O}(1/\beta^2) & \text{for } \beta \to \infty, \\ \beta^n/2^n n! + \mathcal{O}(\beta^{n+2}) & \text{for } \beta \to 0. \end{cases} \tag{128}$$

Equation (128) helps elucidate the role of the boundary conditions in the tensor formulation. As discussed in Sec. V.C, with open boundary conditions one sets the boundary tensor indices to 0, which in the previous definition reduces the weights on those links to a value of 1.

For a recent numerical investigation into the three-dimensional O(2) nonlinear sigma model comparing tensor methods, see Bloch *et al.* (2021).

B. *q*-state clock models

The results of this section hold for the $\mathbb{Z}_q$ restrictions. The infinite sums are replaced by finite sums with q values. The modified Bessel functions are replaced by their discrete counterparts,

$$I_n(\beta) \to I_n^{(q)}(\beta) \equiv (1/q) \sum_{\ell=0}^{q-1} e^{\beta\cos(2\pi/q\ell)} e^{-in(2\pi/q\ell)}, \tag{129}$$

which in the large-q limit turns into the usual integral formula. In the Ising case ($q = 2$), we have

$$I_0(\beta) \to \cosh(\beta), \qquad I_1(\beta) \to \sinh(\beta). \tag{130}$$

The selection rules in Eq. (126) remain valid modulo q.

For recent numerical TRG-inspired work on clock models and discussions of the second transition, see Chen *et al.* (2017), Chen, Xie, and Yu (2018), and Li *et al.* (2020). For an

[5] At large β, Bessel functions of all orders approach each other.

investigation into the critical behavior of the $\mathbb{Z}_q$ models when q is fractional, see Hostetler *et al.* (2021).

C. Dual reformulations with unconstrained variables

In Secs. III.D and V.B, we mentioned the possibility of expressing the closed paths of the expansion in powers of $\tanh(\beta)$ of the Ising model using dual variables. These ideas can be generalized for a large class of models with Abelian symmetries (Banks, Myerson, and Kogut, 1977; Savit, 1977, 1980; Einhorn and Savit, 1978, 1979; Kogut, 1979). In this section, we discuss the case of spin models with interactions on links. Models with interactions on plaquettes and higher-dimensional simplices are discussed in Sec. IX.A.2.

To maintain consistency with the rest of the article, in this section (unless otherwise specified) we use a Euclidean metric with all lower indices as well as implicit summations of repeated indices in order to make a stronger connection with the covariant formulation of Maxwell's equations. The discrete form of Noether current conservation given in Eq. (126), which also holds modulo q for q-state clock models can be written in a compact way as

$$\nabla_\mu n_\mu = 0, \tag{131}$$

where ∇_μ is a discrete derivative

$$\nabla_\mu f_x = f_{x-\hat{\mu}} - f_x. \tag{132}$$

Since more indices will appear, we keep the reference to the site x implicit. Following the example of Maxwell's equations written in a relativistically covariant way, we can express a conserved current as the gradient of an antisymmetric tensor of order 2 as follows:

$$n_\nu = \nabla_\mu C_{\mu\nu}. \tag{133}$$

Equation (133) holds in arbitrary dimensions D.

Because of the divergenceless condition Eq. (131), n_μ has $D-1$ degrees of freedom per link. On the other hand, $C_{\mu\nu}$ has $D(D-1)/2$ degrees of freedom, which is $(D-1)(D-2)/2$ more than $D-1$. The redundancy that appears for $D \geq 3$ can be made more obvious by introducing the following dual tensor with $D-2$ indices (Savit, 1977, 1980) and also $D(D-1)/2$ components:

$$C_{\mu\nu} = \frac{1}{(D-2)!}\epsilon_{\mu\nu\mu_1,\ldots,\mu_{D-2}}\tilde{C}_{\mu_1,\ldots,\mu_{D-2}}. \tag{134}$$

The $\tilde{C}$ field is precisely the dual field that lives on the dual lattice. If we plug this dual form into Eq. (133), we see that $\tilde{C}_{\mu_1,\ldots,\mu_{D-2}}$ can be shifted by antisymmetrized derivatives of lower rank tensors. For $D=3$, $\tilde{C}_\mu$ has three components and is defined up to a gradient such that we end up with the desired 2 independent degrees of freedom. For $D \geq 4$, the redundancy becomes nested: we need to count the redundancy of the redundancy, etc. For instance, for $D=4$, $\tilde{C}_{\mu\nu}$ has six components. The shift by the gradient of a four-vector naively subtracts 4 degrees of freedom, but this four-vector can itself be shifted by a gradient without affecting the initial shift, and we end up with $6-4+1=3$ degrees of freedom.

D. Chemical potential, complex temperature, and importance sampling

Since the tensor renormalization group (and tensor network methods generally) do not rely on sampling from probability measures, situations where sampling methods would falter or fail due to the loss of real, positive-definite weights never arise. Instead, only linear algebra is needed in the form of tensor contractions. This allows the method to address the "sign problem," which can occur during the inclusion of a chemical potential, and a complex coupling. Denbleyker *et al.* (2014) addressed this in the case of a complex temperature. They studied the zeros in the complex temperature plane, i.e., Fisher zeros, and found that the tensor renormalization group is able to out perform the reweighting method using in classical Monte Carlo studies that involve imaginary parts of the action.

Zou *et al.* (2014) and Yang *et al.* (2016) added a purely real chemical potential μ to the action of the two-dimensional O(2) nonlinear sigma model in the form

$$S_\mu = -\beta\sum_{x,\nu}\cos(\theta_{x+\hat{\nu}} - \theta_x - i\mu). \tag{135}$$

In Equation (135) the action has a complex sign problem. Zou *et al.* (2014) and Yang *et al.* (2016) studied the phase diagram of the model in the β-μ plane in both the discrete-time and continuous-time limits. Banerjee and Chandrasekharan (2010) studied this action while employing a sampling method known as the "worm algorithm" that uses a Fourier expanded form of the Boltzmann weight that eliminates the sign problem completely.

In fact, the worm algorithm (Prokof'ev and Svistunov, 2001) is intimately related to the tensor formulation. The beginning and the end of the worm correspond to the insertions of an impurity tensor and when the tensor elements are positive definite, it is possible to design a reformulation of the worm algorithm where tensor elements are weighted against each other in an "accept-reject," Metropolis style algorithm. In this way, a lattice configuration is populated with tensor indices at their respective locations (sites, links, etc.). These indices correspond to tensor elements, and hence weights. Moreover, the tensor interpretation [along with the exact blocking procedure (Liu *et al.*, 2013)] allows one to use the worm algorithm on exactly coarse-grained lattice models (when the coarse-grained tensor elements are again positive definite), and therefore use the renormalization group exactly with Monte Carlo studies. This procedure of "tensor sampling" is general for positive weights and is an interesting direction deserving of more attention.

VIII. TENSORS FOR SPIN MODELS WITH NON-ABELIAN SYMMETRIES

A. O(3) nonlinear sigma model

Consider the following action for the O(3) nonlinear sigma model in D dimensions:

$$
\begin{aligned}
S &= -\beta \sum_{x=1}^{N} \sum_{\mu=1}^{D} \sum_{a=1}^{3} \sigma_{x+\hat{\mu}}^{(a)} \sigma_{x}^{(a)} \\
&= -\beta \sum_{x=1}^{N} \sum_{\mu=1}^{D} \cos\theta_{x+\hat{\mu}} \cos\theta_{x} \\
&\quad + \sin\theta_{x+\hat{\mu}} \sin\theta_{x} \cos(\phi_{x+\hat{\mu}} - \phi_{x}) \\
&= -\beta \sum_{x=1}^{N} \sum_{\mu=1}^{D} \cos\gamma_{x+\hat{\mu},x}, \qquad (136)
\end{aligned}
$$

where θ is the polar angle, ϕ is the azimuthal angle, and γ is the angle in the plane created by the two vectors. $\sigma_x^{(a)}$ is a unit vector in three dimensions parametrized as $\sigma_x^{(1)} = \sin\theta_x \cos\phi_x$, $\sigma_x^{(2)} = \sin\theta_x \sin\phi_x$, and $\sigma_x^{(3)} = \cos\theta_x$.

We discuss two different possible ways to construct a tensor network here. The first tensor construction is based on the global symmetry group of the model. This construction was explored and used successfully by Liu *et al.* (2013), Unmuth-Yockey *et al.* (2015), and Bruckmann, Jansen, and Kühn (2019) for classical tensor network calculations and MPS calculations in the Hamiltonian formulation. Here we give the classical tensor formulation. Since each term in the action is a dot product between vectors of length 1, we can expand on basis functions for the sphere, i.e., the spherical harmonics. Consider the partition function

$$
\begin{aligned}
Z &= \int \mathcal{D}\Omega e^{-S} \\
&= \prod_{x} \int d\Omega_x \prod_{x,\mu} e^{\beta \cos\gamma_{x+\hat{\mu},x}}, \qquad (137)
\end{aligned}
$$

where $d\Omega$ is the normalized measure on S_2, i.e., $d\Omega = -d(\cos\theta)d\phi/4\pi$. Since each Boltzmann factor is a function of the cosine of the angle between the vectors, we can straightforwardly expand using Legendre polynomials as follows:

$$
e^{\beta \cos\gamma_{x+\hat{\mu},x}} = \sum_{l=0}^{\infty} \frac{2l+1}{4\pi} A_l(\beta) P_l(\cos\gamma_{x+\hat{\mu},x}). \qquad (138)
$$

This step is advantageous since it gives the A coefficients only l dependence. The A's can be solved for by inverting the previous expression,

$$
A_l(\beta) = 4\pi i^l j_l(-i\beta). \qquad (139)
$$

In Eq. (139) $j_n(z)$ represents the spherical Bessel function. The Legendre polynomials can then be rewritten as follows in terms of spherical harmonics using the addition theorem for spherical harmonics:

$$
P_l(\cos\gamma_{x+\hat{\mu},x}) = \frac{4\pi}{2l+1} \sum_{m=-l}^{l} Y_{lm}^{*}(\theta_{x+\hat{\mu}}, \phi_{x+\hat{\mu}}) Y_{lm}(\theta_x, \phi_x). \qquad (140)
$$

This step separates the dependencies on the coupled $x+\hat{\mu}$ and x sites and allows the factors to be treated individually. With the θ and ϕ dependence decoupled between neighboring sites, we can perform the angular integration for the field at each site. In D dimensions there are $2D$ nearest neighbors for each site, giving an integral of the form

$$
\int d\Omega_x \prod_{\mu=1}^{D} Y_{(lm)_{x,\mu}}(\theta_x, \phi_x) Y_{(lm)_{x-\hat{\mu},\mu}}^{*}(\theta_x, \phi_x). \qquad (141)
$$

Equation (141) can be evaluated as follows with the use of the Clebsch-Gordan series:

$$
\begin{aligned}
Y_{l_1 m_1}(\theta,\phi) Y_{l_2 m_2}(\theta,\phi) &= \sum_{L=|l_2-l_1|}^{l_1+l_2} \sum_{M=-L}^{L} C_{l_1 m_1 l_2 m_2}^{LM} C_{l_1 0 l_2 0}^{L0} \\
&\quad \times \sqrt{\frac{(2l_1+1)(2l_2+1)}{4\pi(2L+1)}} Y_{LM}(\theta,\phi), \qquad (142)
\end{aligned}
$$

along with the orthogonality of the spherical harmonics.

We now restrict to $D=2$ and continue explicitly. Equation (141) then takes the form

$$
\int d\Omega_x Y_{(lm)_{x,1}} Y_{(lm)_{x,2}} Y_{(lm)_{x-\hat{1},1}}^{*} Y_{(lm)_{x-\hat{2},2}}^{*}(\theta_x, \phi_x). \qquad (143)
$$

If we make the change of notation for $(lm)_{x,1}$ with $l_1 m_1$, $(lm)_{x,2}$ with $l_2 m_2$, etc., we find for Eq. (143)

$$
\begin{aligned}
\mathcal{C}_x &\equiv \int d\Omega_x Y_{l_1 m_1} Y_{l_2 m_2} Y_{l_3 m_3}^{*} Y_{l_4 m_4}^{*}(\theta_x, \phi_x) \\
&= \sqrt{(2l_1+1)(2l_2+1)(2l_3+1)(2l_4+1)} \\
&\quad \times \sum_{L,M} \frac{1}{(4\pi)^2(2L+1)} C_{l_1 m_1 l_2 m_2}^{LM} C_{l_1 0 l_2 0}^{L0} C_{l_3 m_3 l_4 m_4}^{LM} C_{l_3 0 l_4 0}^{L0}. \qquad (144)
\end{aligned}
$$

The Clebsch-Gordan coefficients constrain the surrounding l's around a site to satisfy the triangle inequalities and enforce a conservation law between the m's. This constraint must be imposed at every site. We formally define a composite index as $L \equiv \{l, m\}$, which has the dimension $(l_{\max}+1)^2$. This index contains all the states from $l=0$ up to some $l_{\max}$ given by $\sum_{l=0}^{l_{\max}}(2l+1) = (l_{\max}+1)^2$. We can write the local tensor as

$$
T_{L_{x-\hat{1},1} L_{x,1} L_{x,2} L_{x-\hat{2},2}}^{(x)} = \sqrt{A_{l_{x-\hat{1},1}} A_{l_{x,1}} A_{l_{x,2}} A_{l_{x-\hat{2},2}}}\, \mathcal{C}_x. \qquad (145)
$$

The constraint $\mathcal{C}$ in Eq. (144) is somewhat complicated, but the physical content is that it simply demands the four l's around a site to satisfy the triangle inequalities according to the typical addition of angular momenta while enforcing a conservation law on the O(2) subgroup m's. A positive feature of this formulation is that the weights (A's) depend only on l.

The second tensor formulation for the O(3) nonlinear sigma model uses the Taylor expansion of the Boltzmann weight to recast the model in terms of discrete fields. This formulation follows directly from Wolff (2010) and Bruckmann *et al.* (2015, 2016).

Starting with the partition function

$$Z = \int \mathcal{D}\Omega e^{-S} = \prod_{x=1}^{N} \frac{1}{4\pi} \int \sin\theta_x d\theta_x d\phi_x \prod_{x=1}^{N} \prod_{\mu=1}^{2} \prod_{a=1}^{3} e^{\beta \sigma_x^{(a)} \sigma_{x+\hat{\mu}}^{(a)}}. \quad (146)$$

We now expand the Boltzmann weight in a Taylor series as follows:

$$e^{\beta \sigma_x^{(a)} \sigma_{x+\hat{\mu}}^{(a)}} = \sum_{n_{x,\mu}^{(a)}=0}^{\infty} \frac{\beta^{n_{x,\mu}^{(a)}}}{n_{x,\mu}^{(a)}!} (\sigma_x^{(a)} \sigma_{x+\hat{\mu}}^{(a)})^{n_{x,\mu}^{(a)}}, \quad (147)$$

associating three natural numbers $n^{(a)}$ with each link. Reordering and collecting the same spin field at a site, we can write the partition function as

$$Z = \sum_{\{n\}} \left(\prod_x \prod_\mu \prod_a \frac{\beta^{n_{x,\mu}^{(a)}}}{n_{x,\mu}^{(a)}!} \right) \times \left(\prod_x \prod_\mu \prod_a \frac{1}{4\pi} \int (\sigma_x^{(a)})^{n_{x,\mu}^{(a)} + n_{x-\hat{\mu},\mu}^{(a)}} \sin\theta_x d\theta_x d\phi_x \right). \quad (148)$$

The first factors in parenthesis are the new weights associated with a configuration of n's. The integrals inside the second factor in parenthesis must be evaluated for each site. They are identical, so we focus on a single site and perform the integration. For one site the integral we must evaluate looks like

$$\frac{1}{4\pi} \int \prod_\mu (\sigma_x^{(1)})^{n_{x,\mu}^{(1)} + n_{x-\hat{\mu},\mu}^{(1)}} (\sigma_x^{(2)})^{n_{x,\mu}^{(2)} + n_{x-\hat{\mu},\mu}^{(2)}} \times (\sigma_x^{(3)})^{n_{x,\mu}^{(3)} + n_{x-\hat{\mu},\mu}^{(3)}} \sin\theta_x d\theta_x d\phi_x. \quad (149)$$

Using the explicit expressions for $\sigma^{(1)}$, $\sigma^{(2)}$, and $\sigma^{(3)}$ in terms of ϕ and θ, we can perform the ϕ and θ integrals separately. We find for θ that

$$\Theta_x \equiv \frac{1}{2} \int_0^{\pi} (\sin\theta_x)^{\sum_\mu \sum_{b=1}^{2} (n_{x,\mu}^{(b)} + n_{x-\hat{\mu},\mu}^{(b)}) + 1} \times (\cos\theta_x)^{\sum_\mu (n_{x,\mu}^{(3)} + n_{x-\hat{\mu},\mu}^{(3)})} d\theta_x, \quad (150)$$

and for ϕ

$$\Phi_x \equiv \frac{1}{2\pi} \int_0^{2\pi} (\sin\phi_x)^{\sum_\mu (n_{x,\mu}^{(2)} + n_{x-\hat{\mu},\mu}^{(2)})} \times (\cos\phi_x)^{\sum_\mu (n_{x,\mu}^{(1)} + n_{x-\hat{\mu},\mu}^{(1)})} d\phi_x. \quad (151)$$

Equation (150) can be computed exactly and gives

$$\Theta_x = \frac{1}{2} \int_0^{\pi} (\sin\theta_x)^{\sum_\mu \sum_{b=1}^{2} (n_{x,\mu}^{(b)} + n_{x-\hat{\mu},\mu}^{(b)}) + 1} \times (\cos\theta_x)^{\sum_\mu (n_{x,\mu}^{(3)} + n_{x-\hat{\mu},\mu}^{(3)})} d\theta_x = \frac{1}{2} \delta^{\mathrm{mod}2}_{\sum_\mu (n_{x,\mu}^{(3)} + n_{x-\hat{\mu},\mu}^{(3)}),0} B\left(\frac{1}{2} \left(1 + \sum_\mu (n_{x,\mu}^{(3)} + n_{x-\hat{\mu},\mu}^{(3)}) \right), 1 + \frac{1}{2} \sum_\mu \sum_{b=1}^{2} (n_{x,\mu}^{(b)} + n_{x-\hat{\mu},\mu}^{(b)}) \right), \quad (152)$$

where $B(p,q)$ is the beta function[6] and $\delta^{\mathrm{mod}2}$ is the Kronecker delta; however, the indices need only be equal modulo 2. Similarly, Eq. (151) can be computed as well, giving

$$\Phi_x = \frac{1}{2\pi} \int_0^{2\pi} (\sin\phi_x)^{\sum_\mu (n_{x,\mu}^{(2)} + n_{x-\hat{\mu},\mu}^{(2)})} \times (\cos\phi_x)^{\sum_\mu (n_{x,\mu}^{(1)} + n_{x-\hat{\mu},\mu}^{(1)})} d\phi_x = \frac{1}{\pi} \delta^{\mathrm{mod}2}_{\sum_\mu (n_{x,\mu}^{(1)} + n_{x-\hat{\mu},\mu}^{(1)}),0} \delta^{\mathrm{mod}2}_{\sum_\mu \sum_{b=1}^{2} (n_{x,\mu}^{(b)} + n_{x-\hat{\mu},\mu}^{(b)}),0} \times B\left(\frac{1}{2} \left(1 + \sum_\mu (n_{x,\mu}^{(1)} + n_{x-\hat{\mu},\mu}^{(1)}) \right), \frac{1}{2} \left(1 + \sum_\mu (n_{x,\mu}^{(2)} + n_{x-\hat{\mu},\mu}^{(2)}) \right) \right). \quad (153)$$

These are two constraints which need to be imposed at each site of the lattice. With these constraints and weights from the Taylor series expansion, we can now define a tensor at every lattice site.

Begin by defining a collective index given by $N_{x,\mu} \equiv n_{x,\mu}^{(1)} \otimes n_{x,\mu}^{(2)} \otimes n_{x,\mu}^{(3)}$, as well as the following weight associated with a link:

$$w_{x,\mu} \equiv \frac{\beta^{(1/2)\sum_a n_{x,\mu}^{(a)}}}{\sqrt{n_{x,\mu}^{(1)}! n_{x,\mu}^{(2)}! n_{x,\mu}^{(3)}!}}. \quad (154)$$

Now the tensor at site x in D dimensions is given by

$$T_{N_{x-\hat{1},1} N_{x,1}, \ldots, N_{x-\hat{D},D} N_{x,D}} = \left(\prod_{\mu=1}^{D} w_{x-\hat{\mu},\mu} w_{x,\mu} \right) \Theta_x \Phi_x. \quad (155)$$

This tensor has the useful property that (assuming $\beta > 0$) the tensor elements are positive. This follows from the positivity of β and the fact that the n's are non-negative. The constraints coming from the θ and ϕ integrals are positive as well since the beta functions are positive for positive arguments. This allows this formulation to be used in sampling methods, as it has been; see Wolff (2010) and Bruckmann *et al.* (2016). However, there are more indices necessary in this description, which increases the cost numerically in a tensor renormalization group algorithm.

B. SU(2) principal chiral model

The SU(2) principal chiral model consists of an SU(2) matrix associated with each site on the lattice that interacts with its nearest neighbors. The action on a D-dimensional square lattice with periodic boundary conditions is given by

$$S = -\frac{\beta}{2} \sum_{x=1}^{N} \sum_{\mu=1}^{D} \mathrm{Tr}[U_x U_{x+\hat{\mu}}^{\dagger}]. \quad (156)$$

[6] That is,

$$B(x,y) = \int_0^1 t^{x-1} (1-t)^{y-1} dt = \Gamma(x)\Gamma(y)/\Gamma(x+y).$$

The partition function for the model is given as the following Haar integration over each of the fields on the lattice:

$$Z = \int \mathcal{D}U e^{-S} = \prod_x \int dU_x e^{(\beta/2)\sum_{x,\mu}\mathrm{Tr}[U_x U^\dagger_{x+\hat{\mu}}]}. \tag{157}$$

Equation (157) depends only on the trace of group elements, which means that the characters of the group can be expanded on. We expand the Boltzmann weight as follows:

$$e^{(\beta/2)\mathrm{Tr}[U_x U^\dagger_{x+\hat{\mu}}]} = \sum_{r_{x,\mu}=0}^{\infty} F_{r_{x,\mu}}(\beta)\chi^{r_{x,\mu}}(U_x U^\dagger_{x+\hat{\mu}}), \tag{158}$$

where the sum runs over all half-integer irreducible representations of the group and the F's are as given in Appendix A.1. The expansion coefficients can be solved for by inverting Eq. (158) using the orthogonality of the characters. The characters are traces over matrix representations of the group; see Appendix A.2. This allows the group elements to be split and factorized [$\chi^r(U_x U^\dagger_{x+\hat{\mu}}) = \sum_{a,b} D^r_{ab}(U_x) D^{r\dagger}_{ba}(U_{x+\hat{\mu}})$], and subsequently integrated over. Collecting all the D matrices associated with the same site, we find an integral of the form

$$\int dU_x \prod_{\mu=1}^{D} D^{r_{x,\mu}} D^{r_{x-\hat{\mu},\mu}\,\dagger}(U_x), \tag{159}$$

where the matrix indices have been suppressed. We can perform this integral as follows with the help of the Clebsch-Gordan series:

$$D^{r_1}_{m_1 n_1}(U) D^{r_2}_{m_2 n_2}(U) = \sum_{R=|r_1-r_2|}^{r_1+r_2} \sum_{M=-R}^{R} \sum_{N=-R}^{R} C^{RM}_{r_1 m_1 r_2 m_2} C^{RN}_{r_1 n_1 r_2 n_2} D^R_{MN}(U), \tag{160}$$

along with the orthogonality of the D matrices; see Appendix A.2.

We now restrict to the case of $D = 2$. Equation (159) takes the form

$$\int dU_x D^{r_{x,1}}_{m_1 n_1} D^{r_{x-\hat{1},1}\,\dagger}_{m_2 n_2} D^{r_{x,2}}_{m_3 n_3} D^{r_{x-\hat{2},2}\,\dagger}_{m_4 n_4}(U_x), \tag{161}$$

and using the previously mentioned steps we find that

$$\mathcal{C}_x \equiv \int dU_x D^{r_{x,1}}_{m_1 n_1} D^{r_{x,2}}_{m_2 n_2} D^{r_{x-\hat{1},1}\,\dagger}_{m_3 n_3} D^{r_{x-\hat{2},2}\,\dagger}_{m_4 n_4}(U_x) = \sum_{R,M,N} d_R^{-1} C^{RM}_{r_{x,1} m_1 r_{x,2} m_2} C^{RN}_{r_{x,1} n_1 r_{x,2} n_2} \times C^{RN}_{r_{x-\hat{1},1} m_3 r_{x-\hat{2},2} m_4} C^{RM}_{r_{x-\hat{1},1} n_3 r_{x-\hat{2},2} n_4}, \tag{162}$$

where $d_r = 2r + 1$ is the dimension of the representation. This is the constraint associated with a site. As in the O(3) nonlinear sigma model, this constraint constrains the surrounding representation numbers on the links around a site through the triangle inequalities. If we formally define a composite index as $X_{x,1} \equiv \{r_{x,1}, m, n\}$, where m and n are the matrix indices naturally associated with an r on a link, we can then define a local tensor at each site by

$$T_{X_{x-\hat{1},1} X_{x,1} Y_{x,2} Y_{x-\hat{2},2}} = \sqrt{F_{r_{x,1}} F_{r_{x,2}} F_{r_{x-\hat{1},1}} F_{r_{x-\hat{2},2}}(\beta)}\,\mathcal{C}_x. \tag{163}$$

By contracting this tensor with itself recursively, one rebuilds the original partition function.

A possible alternative way to formulate a local tensor is to use the same discrete variables as used by Gattringer, Goschl, and Marchis (2018). This formulation is along the same lines as the second tensor formulation for the O(3) nonlinear sigma model in that it expands the Boltzmann weight in a Taylor series. Gattringer, Goschl, and Marchis (2018) used this formulation in sampling methods. We do not attempt to give the tensor formulation using these variables, but the required steps seem straightforward and mimic the steps in the second formulation of the O(3) tensor.

C. Truncations and asymptotic freedom

An important question is: How do the previous tensor formulations, and specifically the expansions beforehand that lead up to the tensor definitions, affect universality? When looking at Eq. (140) for the O(3) nonlinear sigma model, it is clear that this expansion does not affect the global O(3) invariance of the model, since one expands on the dot product between nearest-neighbor vectors. This interaction is O(3) invariant as long as each spin is rotated by the same rotation matrix, so a polynomial in this interaction remains O(3) invariant. Similarly, a truncation in the l variable to a finite $l_{\max}$ leaves the expansion O(3) invariant for the same reason. For this reason, after truncation but before integration the model consists of a local nearest-neighbor interaction that is O(3) invariant and in the same number of dimensions with which we started, indicating naively that this truncated model lies in the same universality class as the original O(3) nonlinear sigma model. Further evidence for this conclusion was provided by Bhattacharya *et al.* (2021). Likewise, the expansion in Eq. (147) is also globally O(3) invariant. Thus, any truncation on the n variables leaves the expansion dependent only on spins that interact with their neighbors in an O(3)-invariant fashion.

The O(3) nonlinear sigma model in two dimensions is known to be asymptotically free (Hasenfratz, Maggiore, and Niedermayer, 1990). On a two-dimensional lattice, the continuum limit is approached by taking the nearest-neighbor coupling β infinitely large. In this limit one expects the mass gap to obey the continuum perturbative result that predicts (Hasenfratz, Maggiore, and Niedermayer, 1990)

$$am = \frac{8}{e} a\Lambda_{\overline{\mathrm{MS}}} = 128\pi\beta \exp(-2\pi\beta). \tag{164}$$

The mass gap can be calculated by studying the exponential decay of the spin-spin correlation function (Wolff, 1990).

An initial study of the asymptotic scaling of the mass gap in this model was done by Unmuth-Yockey *et al.* (2015) using the tensor renormalization group. They compared tensor renormalization group calculations of the mass gap with results from Monte Carlo simulations. They found a slow convergence to the expected result as a function of $l_{\max}$. A more thorough study in the Hamiltonian formalism was conducted by Bruckmann, Jansen, and Kühn (2019) using MPSs at different truncations and different volumes. While they found relatively good convergence to the asymptotic result for $l_{\max} > 2$ and in the large volume limit, which supports this idea of universality, the lower $l_{\max}$ values did not converge as well.

For the action in Eq. (156), one has the freedom to rotate all group elements using the same global matrix, e.g., $U_x \to U'_x = VU_xV^\dagger$. This leaves the action invariant, as well as the measure. The expansion in Eq. (158) retains this freedom since the thing that is expanded on is the trace of group elements, which is the type of interaction that allows for this freedom. Furthermore, a truncation on the sum of representations in Eq. (158) does nothing to this symmetry. Again, a truncation then naively leaves the model with the same nearest-neighbor interaction with the same symmetries in the same number of dimensions, and one would expect this truncated model to lie in the same universality class as the original principal chiral model.

IX. TENSORS FOR LATTICE GAUGE THEORIES

In this section, we discuss gauge theories with Abelian symmetries. The gauge Ising model is the simplest model that we can consider. However, as for the spin models, we start with the continuous case and then obtain models with discrete symmetries such as the Ising and gauge clock models using the substitutions described in Sec. VII.B.

A. Pure gauge U(1)

The partition function for the pure gauge U(1) model introduced in Sec. II.B reads

$$Z_{\mathrm{PG}} = \prod_{x,\mu} \int_{-\pi}^{\pi} \frac{dA_{x,\mu}}{2\pi} e^{-S_{\mathrm{Wilson}}}, \tag{165}$$

with the action

$$S_{\mathrm{Wilson}} = -\beta_{\mathrm{pl}} \sum_{x,\mu<\nu} \cos(A_{x,\mu} + A_{x+\hat{\mu},\nu} - A_{x+\hat{\nu},\mu} - A_{x,\nu}). \tag{166}$$

Equation (166) possesses a local symmetry

$$A_{x,\mu}{}' = A_{x,\mu} - (\alpha_{x+\hat{\mu}} - \alpha_x). \tag{167}$$

Using the Fourier expansion

$$e^{\beta_{\mathrm{pl}} \cos(A_{x,\mu}+A_{x+\hat{\mu},\nu}-A_{x+\hat{\nu},\mu}-A_{x,\nu})} = \sum_{m_{x,\mu\nu}=-\infty}^{+\infty} e^{im_{x,\mu\nu}(A_{x,\mu}+A_{x+\hat{\mu},\nu}-A_{x+\hat{\nu},\mu}-A_{x,\nu})} I_{m_{x,\mu\nu}}(\beta_{\mathrm{pl}}) \tag{168}$$

to factorize the gauge fields and integrating over $A_{x,\mu}$ using the orthogonality of the U(1) elements, we obtain the following selection rule:

$$\sum_{\nu>\mu} [m_{x,\mu\nu} - m_{x-\hat{\nu},\mu\nu}] + \sum_{\nu<\mu} [-m_{x,\nu\mu} + m_{x-\hat{\nu},\nu\mu}] = 0. \tag{169}$$

In Eq. (169) the index $m_{x,\mu\nu}$ is associated with a plaquette starting at x, going in the direction of lower index μ, and then going in the direction ν. In D dimensions, there are $2(D-1)$ plaquettes attached to each link. This selection rule constrains the m values associated with those plaquettes. It is convenient to introduce a tensor that is associated with the plaquettes of the lattice. It has four indices that can be naturally associated with the four links bounding a plaquette. Since each plaquette has a single m value associated with it, the four tensor legs attached to a given plaquette $(x, \mu\nu)$ must carry the same index m. Following the terminology of Liu *et al.* (2013), we introduce a "B tensor" for each plaquette as follows:

$$B^{(x,\mu\nu)}_{m_1m_2m_3m_4} = \begin{cases} t_{m_1}(\beta_{\mathrm{pl}}) & \text{if all } m_i \text{ are the same,} \\ 0 & \text{otherwise,} \end{cases} \tag{170}$$

where t_m is as defined in Sec. VII.A. The B tensors are assembled (traced) together with "A tensors" attached to links with $2(D-1)$ legs orthogonal to the link (x, μ):

$$A^{(x,\mu)}_{m_1,\ldots,m_{2(D-1)}} = \delta_{m_{\mathrm{in}},m_{\mathrm{out}}}, \tag{171}$$

where $\delta_{m_{\mathrm{in}},m_{\mathrm{out}}}$ is shorthand notation for Eq. (169), $m_{\mathrm{in}} \equiv \sum_{\nu>\mu} m_{x-\hat{\nu},\mu\nu} - \sum_{\nu<\mu} m_{x-\hat{\nu},\nu\mu}$, and $m_{\mathrm{out}} \equiv \sum_{\nu>\mu} m_{x,\mu\nu} - \sum_{\nu<\mu} m_{x,\nu\mu}$. Notice that, in contrast to the conventions of Liu *et al.* (2013), the weight of the plaquettes is carried by the B tensor. The partition function with PBCs can now be written as

$$Z = [I_0(\beta_{\mathrm{pl}})]^{VD(D-1)/2} \mathrm{Tr} \prod_l A^{(l)}_{m_1,\ldots,m_{2(D-1)}} \prod_{\mathrm{pl}} B^{(\mathrm{pl})}_{m_1m_2m_3m_4}, \tag{172}$$

where the trace indicates index contraction following the previously described geometric procedure. The tensor assembly is illustrated in Fig. 23 for $D = 2$, and in Fig. 24 for $D = 3$.

1. Discrete Maxwell equations

The previously mentioned selection rule can be recast as a constraint on the m values that surround a link. Here we show that Eq. (169) represents a discrete version of Maxwell's equations: $\partial_\mu F^{\mu\nu} = 0$. For this purpose, we define the "electric integers"

$$e_{x,j} \equiv m_{x,jD}, \tag{173}$$

with $j = 1, \ldots, D-1$, which are associated with temporal plaquettes and which can be interpreted as electric fields. Equation (169) for $\mu = D$ reads

$$\sum_{j=1}^{D-1} (e_{x,j} - e_{x-\hat{j},j}) = 0. \tag{174}$$

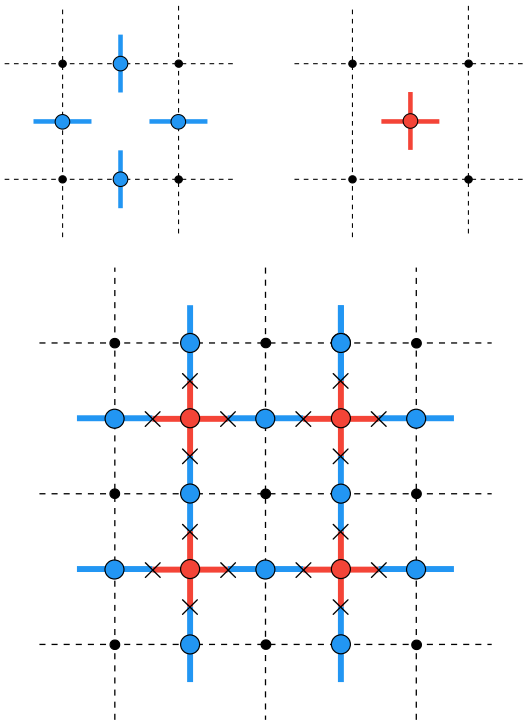

FIG. 23. Assemblies of the A and B tensors for $D = 2$.

Equation (174) is a discrete form of Gauss's law ($\boldsymbol{\nabla} \cdot \mathbf{E} = 0$) in the source-free model.

For $D \geq 3$, we can introduce magnetic fields in a dimension-dependent way. For $D = 3$, we define

$$b_x \equiv m_{x,12}. \tag{175}$$

Equation (169) for $\mu = 1, 2$ becomes

$$\begin{aligned} e_{x,1} - e_{x-\hat{\tau},1} &= -(b_x - b_{x-\hat{2}}), \\ e_{x,2} - e_{x-\hat{\tau},2} &= (b_x - b_{x-\hat{1}}). \end{aligned} \tag{176}$$

Equations (176) are a discrete version of the $D = 3$ Euclidean Maxwell equations

$$\partial_1 B = \partial_\tau E_2, \qquad \partial_2 B = -\partial_\tau E_1, \tag{177}$$

with $B = F^{12}$. However, there is no discrete equation corresponding to the Maxwell equation for the dual field-strength tensor

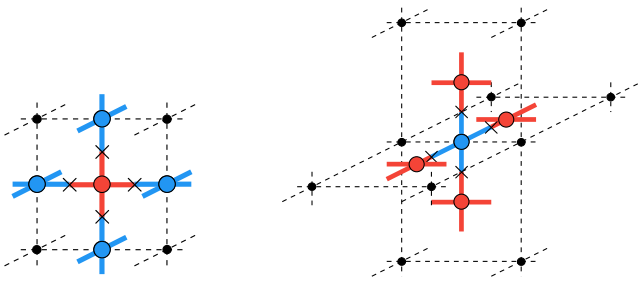

FIG. 24. Assemblies of the A and B tensors for $D = 3$.

$$\partial_\mu \epsilon^{\mu\nu\sigma} F_{\nu\sigma} = 0. \tag{178}$$

An example of a legal configuration violating the discrete version of Eq. (178), also written as $\partial_\tau B = -\boldsymbol{\nabla} \times \mathbf{E}$, can be constructed.

For $D = 4$, we define

$$b_{x,j} \equiv \epsilon_{jkl} m_{x,kl} \tag{179}$$

and obtain a discrete version of

$$\partial_\tau \mathbf{E} = -\boldsymbol{\nabla} \times \mathbf{B} \tag{180}$$

with the Euclidean magnetic field

$$F^{jk} = +\epsilon^{jkl} B^l. \tag{181}$$

Note that the sign in Eq. (180) is different in the Euclidean and Minkowskian spaces. Again there is no discrete version of the homogeneous equations for the dual field strength $\partial_\tau \mathbf{B} = -\boldsymbol{\nabla} \times \mathbf{E}$ and $\boldsymbol{\nabla} \cdot \mathbf{B} = 0$.

2. Abelian gauge duality

The dual construction of Sec. V.B for spin models can be extended to models with plaquettes and higher-dimensional simplex interactions (Savit, 1977), i.e., interactions over higher-dimensional geometric shapes, such as cubes and tetrahedra. If we first define $m_{\mu\nu} = -m_{\nu\mu}$ when $\mu > \nu$, the discrete Maxwell equations (169) take the form

$$\nabla_\nu m_{\mu\nu} = 0. \tag{182}$$

As explained in Sec. VII.C, Eq. (182) is divergenceless and represents $D - 1$ conditions. We can introduce the following dual tensor with $D - 3$ indices (Savit, 1977, 1980):

$$m_{\mu\nu} = \frac{1}{(D-3)!} \epsilon_{\mu\nu\rho\mu_1,\ldots,\mu_{D-3}} \nabla_\rho \tilde{C}_{\mu_1,\ldots,\mu_{D-3}}, \tag{183}$$

which provides an automatic solution of Eq. (182). After using the $D - 1$ conditions of Eq. (182), we are left with $(D-1)(D-2)/2$ independent components for $m_{\mu\nu}$. For $D = 3$, there is no redundancy and we have 1 degree of freedom. For $D = 4$, $\tilde{C}_\mu$ is defined up to a gradient and we recover the 3 degrees of freedom.

B. The compact Abelian-Higgs model

The compact Abelian Higgs model (CAHM) is a gauged version of the O(2) model where the global symmetry under a φ shift becomes local:

$$\varphi'_x = \varphi_x + \alpha_x. \tag{184}$$

Its partition function is

$$Z_{\mathrm{CAHM}} = \prod_x \int_{-\pi}^{\pi} \frac{d\varphi_x}{2\pi} \prod_{x,\mu} \int_{-\pi}^{\pi} \frac{dA_{x,\mu}}{2\pi} e^{-S_{\mathrm{Wilson}} - S_{\mathrm{U}(1)}}, \tag{185}$$

with

$$S_{\mathrm{U}(1)} = -\beta_l \sum_{x,\mu} \cos(\varphi_{x+\hat{\mu}} - \varphi_x + A_{x,\mu}) \tag{186}$$

and S_{Wilson} as in Eq. (166). Using the same U(1) Fourier expansions as before, the A-field integration can be carried out. The integration over $A_{x,\mu}$ yields the selection rule

$$\sum_{\nu>\mu}[m_{x,\mu\nu} - m_{x-\hat{\nu},\mu\nu}] + \sum_{\nu<\mu}[-m_{x,\nu\mu} + m_{x-\hat{\nu},\nu\mu}] + n_{x,\mu} = 0, \tag{187}$$

which simply inserts the $n_{x,\mu}$ in Eq. (169) and corresponds to the Maxwell equations with charges and currents

$$\partial_\mu F^{\mu\nu} = J^\nu. \tag{188}$$

Equation (169) indicates that the link indices $n_{x,\mu}$ can be seen as determined by unrestricted plaquette indices $m_{x,\mu\nu}$. We write this dependence as $n_{x,\mu}(\{m\})$ as a shorthand for Eq. (187).

Note that for $n_{x,\mu}(\{m\})$ the discrete current conservation equation (126) is automatically satisfied (Meurice, 2019) and, as long as the gauge fields are present, there is no need to enforce Eq. (126) independently. This is a discrete version of the fact that Maxwell's equations with charges and currents (187) imply that $\partial_\mu J^\mu = 0$.

With the introduction of the matter fields, we need to update the definition of the A tensors. We now have quantum numbers on the links ($n_{x,\mu}$) that are completely fixed by the plaquette quantum numbers, and they bring a weight $t_{n_{x,\mu}}(\beta_l)$. This translates into

$$A^{(x,\mu)}_{m_1,\ldots,m_{2(D-1)}} = t_{n_{x,\mu}(\{m\})}(\beta_l) \tag{189}$$

since Eq. (187) gives $n_{x,\mu}$ in terms of the surrounding m's. The partition function with PBCs can now be written as

$$Z_{\mathrm{CAHM}} = [I_0(\beta_{\mathrm{pl}})]^{VD(D-1)/2}[I_0(\beta_l)]^{VD} \times \mathrm{Tr}\prod_{x,\mu} A^{(x,\mu)}_{m_1,\ldots,m_{2(D-1)}} \prod_{x,\mu\nu} B^{(x,\mu\nu)}_{m_1 m_2 m_3 m_4}. \tag{190}$$

C. SU(2) gauge theory

SU(2) gauge theory in D dimensions is governed by an action of the form

$$S_{\mathrm{Wilson}} = -\frac{\beta_{\mathrm{pl}}}{2} \sum_{x=1}^{N} \sum_{\mu<\nu=1}^{D} \mathrm{ReTr}[U_{x,\mu} U_{x+\hat{\mu},\nu} U^\dagger_{x+\hat{\nu},\mu} U^\dagger_{x,\nu}]. \tag{191}$$

To construct a local tensor, we proceed as before and use the character expansion since the action depends only on the trace of group elements. The partition function for this model can be written as the following Haar integration over the group elements on the links of the lattice:

$$\begin{aligned} Z &= \int \mathcal{D}U e^{-S_{\mathrm{Wilson}}} \\ &= \int \mathcal{D}U_{x,\mu} \prod_x \prod_{\mu<\nu} e^{(\beta_{\mathrm{pl}}/2)\mathrm{ReTr}[U_{x,\mu} U_{x+\hat{\mu},\nu} U^\dagger_{x+\hat{\nu},\mu} U^\dagger_{x,\nu}]} \\ &= \int \mathcal{D}U_{x,\mu} \prod_x \prod_{\mu<\nu} e^{(\beta_{\mathrm{pl}}/2)\mathrm{ReTr}[U_{x,\mu\nu}]}, \end{aligned} \tag{192}$$

where $U_{x,\mu\nu}$ is the product of gauge fields around a plaquette. While this model is trivial in $D = 2$, there are currently no results using tensor methods in $D > 2$ for this model; however, there have been tensor studies of other gauge models (Zohar *et al.*, 2015, 2016; Kuramashi and Yoshimura, 2019; Unmuth-Yockey, 2019).

To proceed, we expand the Boltzmann weight (see Appendix A.1 for the F's) as

$$e^{(\beta_{\mathrm{pl}}/2)\mathrm{ReTr}[U_{x,\mu\nu}]} = \sum_{r_{x,\mu\nu}=0}^{\infty} F_{r_{x,\mu\nu}}(\beta_{\mathrm{pl}}) \chi^{r_{x,\mu\nu}}(U_{x,\mu\nu}). \tag{193}$$

Equation (193) associates an r with each plaquette on the lattice. The characters can be written as the following trace of the product of matrix representations of the group:

$$\chi^{r_{x,\mu\nu}}(U_{x,\mu\nu}) = \sum_{a,b,c,d} D^{r_{x,\mu\nu}}_{ab}(U_{x,\mu}) D^{r_{x,\mu\nu}}_{bc}(U_{x+\hat{\mu},\nu}) \times D^{r_{x,\mu\nu}\dagger}_{cd}(U_{x+\hat{\nu},\mu}) D^{r_{x,\mu\nu}\dagger}_{da}(U_{x,\nu}). \tag{194}$$

By factorizing the group elements in this way, we can perform the link integration link by link, reformulating the model in terms of the discrete representations and the matrix indices. In D dimensions, there are $2(D-1)$ plaquettes associated with each link. The integral over the group element associated with link (x,μ) then has the form

$$\int dU_{x,\mu} \prod_{\nu>\mu} D^{r_{x,\mu\nu}} D^{r_{x-\hat{\nu},\mu\nu}\dagger} \prod_{\nu<\mu} D^{r_{x,\nu\mu}\dagger} D^{r_{x-\hat{\nu},\nu\mu}}, \tag{195}$$

where the matrix indices have been suppressed and the D matrices all are the same $U_{x,\mu}$ rotation matrix or its Hermitian conjugate. Equation (195) is in general complicated but is simplified by using the Clebsch-Gordan series to systematically reduce it to an integral over only two D matrices. The Clebsch-Gordan series is given by

$$D^{r_1}_{m_1 n_1} D^{r_2}_{m_2 n_2} = \sum_{R=|r_1-r_2|}^{r_1+r_2} \sum_{M=-R}^{R} \sum_{N=-R}^{R} C^{RM}_{r_1 m_1 r_2 m_2} C^{RN}_{r_1 n_1 r_2 n_2} D^R_{MN}. \tag{196}$$

Using Eq. (196), we can collect the daggered and non-daggered D matrices in Eq. (195) and simplify them in pairs. The D matrices are orthogonal; see Appendix A.2.

The final expression is tedious to write, but there is nothing subtle about it. Here we write the final expression for $D = 3$ for a link in the $\mu = 2$ direction, and subsequently write the local tensors for $D = 3$ as well,

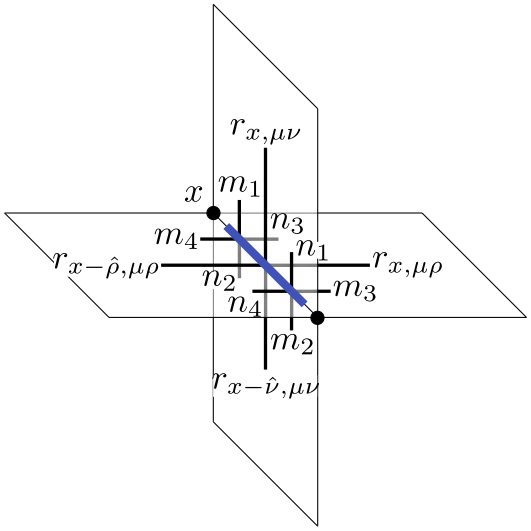

FIG. 25. Illustration of the three-dimensional tensor A tensor for SU(2) gauge theory in three dimensions.

$$\begin{aligned}\mathcal{C}^{(x,2)} &\equiv \int dU_{x,2} D^{r_{x,23}}_{m_1 n_1} D^{r_{x-\hat{3},23}\,\dagger}_{m_2 n_2} D^{r_{x,12}\,\dagger}_{m_3 n_3} D^{r_{x-\hat{1},12}}_{m_4 n_4} \\ &= \sum_{R,M,N} d_R^{-1} C^{RM}_{r_{x,23},m_1 r_{x-\hat{1},12} m_4} C^{RN}_{r_{x,23},n_1 r_{x-\hat{1},12} n_4} \\ &\quad \times C^{RN}_{r_{x,12},m_3 r_{x-\hat{3},23} m_2} C^{RM}_{r_{x,12},n_3 r_{x-\hat{3},23} n_2}. \end{aligned} \tag{197}$$

For each link in the lattice, there is a constraint $\mathcal{C}^{(x,\mu)}$ of this form. If we define a composite index formally as $R_{x,\mu\nu} = \{r_{x,\mu\nu}, m_1, n_1\}$, we can define a tensor associated with the links of the lattice whose indices are associated with the shared plaquettes as

$$A^{(x,\mu)}_{R_{x,\mu\nu} R_{x-\hat{\nu},\mu\nu} R_{x,\mu\rho} R_{x-\hat{\rho},\mu\rho}} = \mathcal{C}^{(x,\mu)}_{R_{x,\mu\nu} R_{x-\hat{\nu},\mu\nu} R_{x,\mu\rho} R_{x-\hat{\rho},\mu\rho}} \tag{198}$$

for $\nu \neq \rho \neq \mu$. The A tensor is defined as the constraint on a link. An illustration of the three-dimensional tensor is shown in Fig. 25.

This is not the entire story, though, since this tensor is not enough to reproduce the partition function of the original model. The weight factors $F_r(\beta_{\rm pl})$ still need to be accounted for. To include the weight factors, we define an additional tensor associated with the plaquettes of the lattice; however, there is a slightly subtle aspect with this tensor. That is the circulation of the D-matrix indices in Eq. (194) around the plaquette. These indices (which are now a part of the A tensor) are still required to be contracted in the pattern found in Eq. (194). To enforce this circulation, we assign Kronecker deltas to the new tensor in such a way that the contraction pattern of the matrix indices in Eq. (194) is reproduced. To be clear, consider Eq. (194) again, rewritten as

$$\begin{aligned}\chi^{r_{x,\mu\nu}}(U_{x,\mu\nu}) &= D^{r_{x,\mu\nu}}_{ab}(U_{x,\mu}) \delta_{bc} D^{r_{x,\mu\nu}}_{cd}(U_{x+\hat{\mu},\nu}) \delta_{de} \\ &\quad \times D^{r_{x,\mu\nu}\,\dagger}_{ef}(U_{x+\hat{\nu},\mu}) \delta_{fg} D^{r_{x,\mu\nu}\,\dagger}_{gh}(U_{x,\nu}) \delta_{ha}, \end{aligned} \tag{199}$$

with an implied sum over repeated indices here. These Kronecker deltas will be moved onto the new plaquette tensor as follows:

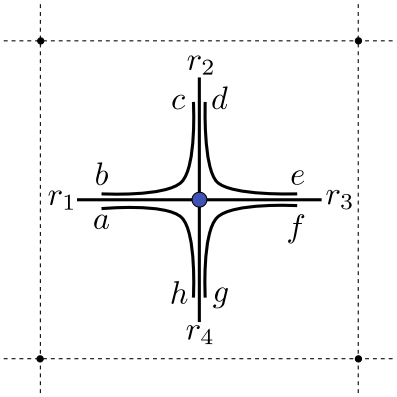

FIG. 26. Illustration of a B tensor.

$$\begin{aligned}B_{\{r_1 ab\}\{r_2 cd\}\{r_3 ef\}\{r_4 gh\}} &= \delta_{bc}\delta_{de}\delta_{fg}\delta_{ha} \\ &\quad \times \begin{cases} F_{r_1}(\beta_{\rm pl}) & \text{if all } r\text{'s are the same,} \\ 0 & \text{otherwise.} \end{cases} \end{aligned} \tag{200}$$

Each index of the B tensor is associated with one of the four links that border the plaquette. That makes this tensor identical for all dimensions. An illustration of this tensor can be seen in Fig. 26. By contracting this B tensor on the plaquettes with the A tensors on the links, the full partition function is constructed exactly. The contraction pattern between these indices is shown in Fig. 24.

D. The non-Abelian Higgs model

The lattice SU(2) gauge Higgs model in D dimensions consists of three main parts: the pure Yang-Mills lattice action, a gauge-matter interaction term, and a matter potential term. For the pure Yang-Mills term, we use the standard Wilson action

$$S_{\rm Wilson} = -\frac{\beta_{\rm pl}}{2} \sum_x \sum_{\mu<\nu} \mathrm{ReTr}[U_{x,\mu} U_{x+\hat{\mu},\nu} U^\dagger_{x+\hat{\nu},\mu} U^\dagger_{x,\nu}], \tag{201}$$

where one takes a product of the gauge fields associated with the links around an elementary square (plaquette) for each square of the lattice. For the gauge-matter coupling term, we have

$$S_{\rm U(2)} = -\frac{\kappa}{2} \sum_{x=1}^{N} \sum_{\mu=1}^{D} \Phi^\dagger_{x+\hat{\mu}} U_{x,\mu} \Phi_x. \tag{202}$$

The Φ field can be reexpressed in terms of a 2×2 matrix (Montvay and Münster, 1994), and the gauge-matter term becomes

$$S_{\rm U(2)} = -\frac{\kappa}{2} \sum_x \sum_\mu \mathrm{ReTr}[\phi^\dagger_{x+\hat{\mu}} U_{x,\mu} \phi_x], \tag{203}$$

where ϕ is now a 2×2 matrix. Since $\phi^\dagger_x \phi_x = \rho_x^2 \mathbb{1}$, ϕ_x can be written as $\phi_x = \rho_x \alpha_x$ with $\rho_x \in \mathbb{R}$, $\rho_x \geq 0$, and $\alpha_x \in \mathrm{SU}(2)$.

This expresses ϕ_x in terms of the Higgs (ρ_x) and Goldstone (α_x) modes, respectively. This allows the gauge-matter term to be again rewritten as

$$S_{\mathrm{U}(2)} = -\frac{\kappa}{2}\sum_x\sum_\mu \rho_{x+\hat{\mu}}\rho_x \mathrm{ReTr}[\alpha^\dagger_{x+\hat{\mu}}U_{x,\mu}\alpha_x]. \tag{204}$$

Finally, the Higgs potential

$$V = \sum_x [|\Phi_x|^2 + \lambda(|\Phi_x|^2 - 1)^2] \tag{205}$$

couples only same-site fields and therefore (in terms of the matrix ϕ_x) involves only the Higgs mode

$$V = \sum_x \rho_x^2 + \lambda(\rho_x^2 - 1)^2. \tag{206}$$

The partition function for this model is then

$$Z = \int \mathcal{D}U\mathcal{D}\rho\mathcal{D}\alpha e^{-S_{\mathrm{Wilson}}-S_{\mathrm{U}(2)}-V}, \tag{207}$$

where the integration over U and α is the SU(2) Haar measure, and the integration measure over ρ is given by $\rho_x^3 d\rho_x$ over $[0,\infty)$.

We consider only the limit in which $\lambda \to \infty$ and $\rho_x \to 1$, which is when the Higgs mass becomes infinitely large. In addition, we perform a change of variables on the gauge fields such that $U_{x,\mu} \to U'_{x,\mu} = \alpha^\dagger_{x+\hat{\mu}}U_{x,\mu}\alpha_x$. Up to an overall constant, this reduces the partition function to the form

$$\begin{aligned} Z &= \int \mathcal{D}U\mathcal{D}\alpha e^{-S_{\mathrm{Wilson}}-S_{\mathrm{U}(2)}} \\ &= \int \mathcal{D}U \exp\frac{\beta_{\mathrm{pl}}}{2}\sum_x\sum_{\mu<\nu}\mathrm{ReTr}[U_{x,\mu}U_{x+\hat{\mu},\nu}U^\dagger_{x+\hat{\nu},\mu}U^\dagger_{x,\nu}] \\ &\quad + \frac{\kappa}{2}\sum_x\sum_{\mu=1}^{D}\mathrm{ReTr}[U_{x,\mu}]. \end{aligned} \tag{208}$$

The tensor formulation for this model follows steps similar to those in Sec. IX.C. In fact, the expansion for the Yang-Mills term is identical to Eqs. (193) and (194). The expansion for the gauge-matter term is similar,

$$e^{(\kappa/2)\mathrm{ReTr}[U_{x,\mu}]} = \sum_{r_{x,\mu}=0}^{\infty} F_{r_{x\mu}}(\kappa)\chi^{r_{x,\mu}}(U_{x,\mu}), \tag{209}$$

and uses the same character expansion as in Sec. IX.C. Similarly, we know that

$$\chi^{r_{x,\mu}}(U_{x,\mu}) = \sum_a D^{r_{x,\mu}}_{aa}(U_{x,\mu}). \tag{210}$$

With these expansions for the gauge and gauge-matter Boltzmann weights, we find an integral for each link that is similar to Eq. (195); however, there is now an additional $\chi^r = \mathrm{Tr}[D^r]$ coming from the gauge-matter factor that gives

$$\int dU_{x,\mu}\chi^{r_{x,\mu}}\prod_{\nu>\mu}D^{r_{x,\mu\nu}}D^{r_{x-\hat{\nu},\mu\nu}\dagger}\prod_{\nu<\mu}D^{r_{x,\mu\nu}\dagger}D^{r_{x-\hat{\nu},\mu\nu}}. \tag{211}$$

Equation (211) can again be reduced to a manageable integral over only two D matrices using Eq. (196) and the form of χ^r given in Eq. (210).

We proceed by setting $D = 2$ and perform the computations explicitly for the local tensors. This was done in detail by Bazavov *et al.* (2019). Equation (211) for the $\mu = 1$ direction takes the form

$$\begin{aligned} &\sum_k \int dU_{x,1} D^{r_{x,1}}_{kk} D^{r_{x,12}}_{m_1n_1} D^{r_{x-\hat{2},12}\dagger}_{m_2n_2} \\ &\quad = \sum_k d^{-1}_{r_{x-\hat{2},12}} C^{r_{x-\hat{2},12}n_2}_{r_{x,1}kr_{x,12}m_1} C^{r_{x-\hat{2},12}m_2}_{r_{x,1}kr_{x,12}n_1} \end{aligned} \tag{212}$$

and, in the $\mu = 2$ direction,

$$\begin{aligned} &\sum_k \int dU_{x,2} D^{r_{x,2}}_{kk} D^{r_{x,12}\ \dagger}_{m_1n_1} D^{r_{x-\hat{1},12}}_{m_2n_2} \\ &\quad = \sum_k d^{-1}_{r_{x,12}} C^{r_{x,12}n_1}_{r_{x,2}kr_{x-\hat{1},12}m_2} C^{r_{x,12}m_1}_{r_{x,2}kr_{x-\hat{1},12}n_2}. \end{aligned} \tag{213}$$

With these constraints on the links we can define analogous A tensors on the links as well. We again formally define a composite index $R_{x,\mu\nu} = \{r_{x,\mu\nu}, m, n\}$ and define a tensor on a link from site x in the $\mu = 1$ direction as

$$A^{(x,1)}_{R_{x,12}R_{x-\hat{2},12}} = \sum_{r_{x,1}} F_{r_{x,1}}(\kappa)\sum_k d^{-1}_{r_{x-\hat{2},12}} C^{r_{x-\hat{2},12}n_2}_{r_{x,1}kr_{x,12}m_1} C^{r_{x-\hat{2},12}m_2}_{r_{x,1}kr_{x,12}n_1} \tag{214}$$

and, in the $\mu = 2$ direction, as

$$A^{(x,2)}_{R_{x,12}R_{x-\hat{1},12}} = \sum_{r_{x,2}} F_{r_{x,2}}(\kappa)\sum_k d^{-1}_{r_{x,12}} C^{r_{x,12}n_1}_{r_{x,2}kr_{x-\hat{1},12}m_2} C^{r_{x,12}m_1}_{r_{x,2}kr_{x-\hat{1},12}n_2}. \tag{215}$$

As previously mentioned, the tensor associated with the plaquettes from the pure Yang-Mills term is the same as in Eq. (200) and is the same regardless of dimension for the SU(2) gauge Higgs model as well. With the A and B tensors mentioned here, one can contract them in the appropriate pattern to construct the partition function exactly. This contraction pattern is shown in Fig. 23.

In fact, in $D = 2$ it is possible to go one step further and define a single tensor that can be contracted with itself to construct the partition function. Details of this construction were given by Bazavov *et al.* (2019).

Within this tensor reformulation it is also possible to straightforwardly define the Polyakov loop. For SU(2) in the fundamental representation the Polyakov loop at site x^* is given by

$$P_{x^*} = \mathrm{Tr}\left[\prod_{n=0}^{N_\tau-1} D^{1/2}(U_{x^*+n\hat{\tau},\tau})\right], \tag{216}$$

where τ indicates a direction chosen as the time. Here we assume periodic boundary conditions for both directions. The expectation value of this operator is

$$\langle P\rangle = \frac{1}{Z}\int \mathcal{D}U\, P e^{-S}. \tag{217}$$

One can recast this average in terms of local tensors by performing the same steps as before. The only difference in this case is that, for a particular spatial site x^*, all the temporal links have an additional D matrix associated with them, altering the integral found in, say, Eq. (213) using the inclusion of a fourth D matrix whose representation is $1/2$. However, one proceeds as before using Eq. (196) to make the integral manageable. The integral on the temporal links of the Polyakov loop has the form

$$\begin{aligned}
&\sum_k \int dU_{x,2} D^{r_{x,2}}_{kk} D^{r_{x,12}}_{m_1 n_1}{}^{\dagger} D^{r_{x-\hat{1},12}}_{m_2 n_2} D^{1/2}_{ij} \\
&= \sum_{k,R,M,N} C^{RM}_{r_{x,2} k r_{x-\hat{1},12} m_2} C^{RN}_{r_{x,2} k r_{x-\hat{1},12} n_2} \int dU_{x,2} D^{R}_{MN} D^{r_{x,12}}_{m_1 n_1}{}^{\dagger} D^{1/2}_{ij} \\
&= \sum_{k,R,M,N} d^{-1}_{r_{x,12}} C^{RM}_{r_{x,2} k r_{x-\hat{1},12} m_2} C^{RN}_{r_{x,2} k r_{x-\hat{1},12} n_2} C^{r_{x,12} n_1}_{RM\frac{1}{2} i} C^{r_{x,12} m_1}_{RN\frac{1}{2} j}.
\end{aligned} \tag{218}$$

If we define this constraint as $\tilde{\mathcal{C}}_{R_{x,12},R_{x-\hat{1},12}ij}$, then we can write the following tensor on the Polyakov loop links:

$$\tilde{A}_{R_{x^*,12},R_{x^*-\hat{1},12}ij} = \sum_{r_{x^*,2}} F_{r_{x^*,2}}(\kappa)\tilde{\mathcal{C}}_{R_{x^*,12},R_{x^*-\hat{1},12}ij}. \tag{219}$$

Equation (219) has two more indices than the typical A tensor. This is because of the additional D matrix from the Polyakov loop insertion. These additional matrix indices are contracted with each other and traced over as in the definition of Eq. (216).

With the local tensor of Bazavov *et al.* (2019) and Eq. (219), it is possible to use coarse-graining schemes to approximate the free energy and compute the expectation values. Using the higher-order tensor renormalization group for the case of $D = 2$, Bazavov *et al.* (2019) computed derivatives of the free energy along with the Polyakov loop and Polyakov loop correlator. Of the derivatives of the free energy, one of primary interest is the following average of the gauge-matter interaction and its fluctuations:

$$\langle L_\phi\rangle = \frac{1}{V}\frac{\partial \ln Z}{\partial \kappa}, \qquad \chi_{L_\phi} = \frac{1}{V}\frac{\partial^2 \ln Z}{\partial \kappa^2}. \tag{220}$$

Equations (220) were computed while the continuum limit was taken. The continuum limit in this model is controlled by the Yang-Mills coupling and the system volume since the Yang-Mills coupling is dimensionful in $D = 2$. By fixing the ratio at $\beta/V = c$, with c a constant, and increasing the system volume, one approaches the fixed-physical-volume continuum limit. An interesting result from this study was evidence for a crossover transition between a confining (pure Yang-Mills) regime and a Higgs regime. This can be seen in the expectation value of the squared fluctuations of the gauge-matter interaction in Fig. 27. In the figure one can see a gradual convergence as the continuum limit is approached, and the presence of a peak around $\kappa \approx 1.4$ separating the two regimes.

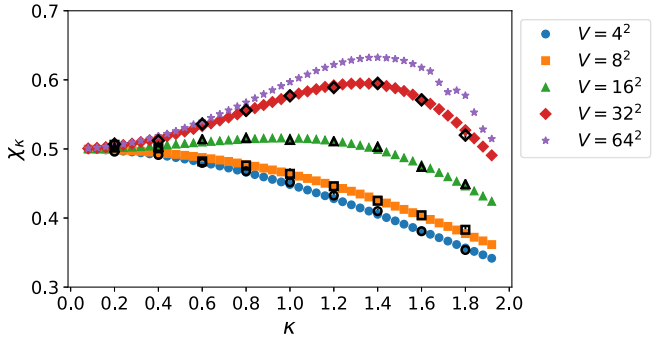

FIG. 27. The susceptibility in the gauge-matter interaction. There is a peak at around $\kappa \approx 1.4$ that seems to indicate a crossover between a confining regime characteristic of pure Yang-Mills theory and a Higgs regime where string breaking occurs. Here $\beta/V = 0.01$ was held fixed. HOTRG calculations for different volumes are represented by different symbols, while the hollow black markers are from Monte Carlo data as a check. The maximum representation used in the HOTRG calculation was $r = 1$, and the final number of states kept was 50. Adapted from Bazavov *et al.*, 2019.

This is further supported by the behavior of the Polyakov loop correlation function on either side of the peak value. Figures 28 and 29 show examples of the potential between static charges ($\mathcal{V}$) in the $\kappa < 1.4$ and $\kappa > 1.4$ regimes, respectively. The potential is found from the logarithm of the correlator. In Fig. 28 there is a linear confining potential that persists for long distances as the continuum limit is approached. In the Higgs-like regime seen in Fig. 29 there is a linear potential for short distances; however, after a certain distance the potential flattens and the force between the charges is zero (string breaking). The two regimes separated by a peak at around $\kappa \approx 1.4$ both appear to be confining, with only a crossover separating the two regimes.

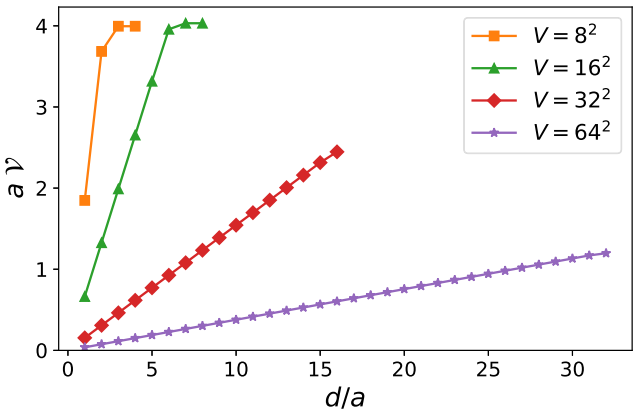

FIG. 28. The potential $\mathcal{V}$ between two static charges for $\kappa = 0.5$ as a function of distance, taking the continuum limit. For this value of κ we see string breaking at small systems, but as the large lattice volume limit is taken we find a linear potential across long distances. Here $\beta/V = 0.01$ was held fixed. The maximum representation used in the calculation was $r = 1$, and the final number of states kept in the calculation was 50. Adapted from Bazavov *et al.*, 2019.

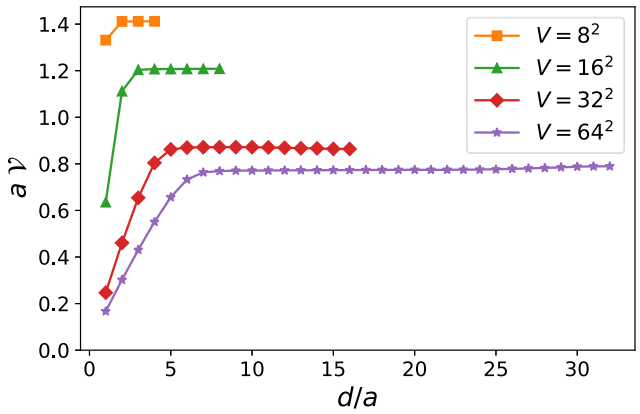

FIG. 29. The potential $\mathcal{V}$ between two static charges for $\kappa = 2$ as a function of distance, taking the continuum limit. Here we find the phenomenon of string breaking that persists even as we take the continuum limit after some distance. Here $\beta/V = 0.01$ was held fixed. The maximum representation used in the calculation was $r = 1$, and the final number of states kept in the calculation was 50. Adapted from Bazavov *et al.*, 2019.

X. TENSORS FOR MODELS WITH NONCOMPACT SCALARS

For tensor networks with discrete indices, scalar fields have to be discretized in a proper manner. There are several ways to apply simple discretization rules to scalar fields to make transfer matrices (Chung, 1999; Nishiyama, 2001a, 2001b; Lay and Rudnick, 2002; Iblisdir, Orus, and Latorre, 2007). In this section we discuss the cases of Lagrangian path integrals. Specifically, we consider a TRG study of the real ϕ^4 theory in two dimensions.

This section is organized as follows. We first present the definition of the real ϕ^4 model in Sec. X.A. In Sec. X.B, a tensor network representation of the real ϕ^4 model is made via the Gaussian quadrature rule.

A. Real ϕ^4 theory

The Euclidean action of the real ϕ^4 theory in two dimensions is

$$S_{\text{cont}} = \int d^2x \left\{ \frac{1}{2}(\partial_\nu \phi)^2 + \frac{\mu_0^2}{2}\phi^2 + \frac{\lambda}{4}\phi^4 \right\}, \tag{221}$$

where μ_0 and λ are the bare mass and the bare coupling, respectively. ϕ is a one-component real scalar field. This model possesses the spontaneous breaking of the Z_2 symmetry, where the expectation value of the field $\langle\phi\rangle$ is an order parameter.

From here on, we treat the model on a square lattice with periodic boundary conditions. The lattice action is given by

$$S_{\text{scalar}} = \sum_x \left\{ \frac{1}{2}\sum_{\nu=1}^{2} (\phi_{x+\hat{\nu}} - \phi_x)^2 + \frac{\mu_0^2}{2}\phi_x^2 + \frac{\lambda}{4}\phi_x^4 \right\}, \tag{222}$$

where x is the lattice coordinate and $\hat{\nu}$ denotes the unit vector along the $\hat{\nu}$ direction.

In two-dimensional scalar theories, one has to take care of the divergence of the one-loop self-energy. In this section the following renormalization condition for the squared mass,

$$\mu^2 = \mu_0^2 + 3\lambda A(\mu^2), \tag{223}$$

is used to define the renormalized squared mass $\mu A(\mu^2)$ denotes the one-loop self-energy on the lattice

$$A(\mu^2) = \frac{1}{V}\sum_{k_1,k_2=1}^{N} \frac{1}{\mu^2 + 4\sin^2(\pi k_1/N) + 4\sin^2(\pi k_2/N)} \tag{224}$$

with the lattice volume $V = N \times N$. To provide numerical results the nonlinear equation (223) is solved to translate the bare squared mass into the renormalized one. Note that the coupling constant is free of the renormalization; this is a common property in two-dimensional scalar theories. Renormalization in scalar field theories and especially in ϕ^4 theory was discussed by Coleman (1975) and Chang (1976).

B. Tensors from Gaussian quadrature

In this section a tensor network representation of the real ϕ^4 theory is derived using the Gaussian quadrature rule. This method was given and used in tensor network studies for Lagrangian path integrals by Kadoh *et al.* (2018, 2019, 2020) and, as they discussed, improves the accuracy of an earlier tensor network study of the real ϕ^4 model (Shimizu, 2012).

The partition function on the lattice is defined by

$$Z = \left(\prod_x \int_{-\infty}^{\infty} d\phi_x \right) e^{-S_{\text{scalar}} - S_h}, \tag{225}$$

where

$$S_h = \sum_x -h\phi_x. \tag{226}$$

For later use we introduce the external field h here. An important step to build a tensor network representation is to generate discrete degrees of freedom that are candidates for tensor indices.[7] In the following, we discuss mainly how to extract the discrete degrees of freedom from the continuous and noncompact scalar fields.

Since the action has only the nearest-neighbor interactions, the Boltzmann weight can be rewritten as a product of local factors as

$$e^{-S_{\text{scalar}} - S_h} = \prod_x \prod_{\nu=1}^{2} f(\phi_x, \phi_{x+\hat{\nu}}), \tag{227}$$

[7]See Campos, Sierra, and López (2019) and Vanhecke *et al.* (2019) and the more complete list of references given by Kadoh *et al.* (2019) for related approaches.

where the local factor is given by

$$f(\phi_1,\phi_2)=\exp\left\{-\frac{1}{2}(\phi_1-\phi_2)^2-\frac{\mu_0^2}{8}(\phi_1^2+\phi_2^2)\right.$$
$$\left.-\frac{\lambda}{16}(\phi_1^4+\phi_2^4)+\frac{h}{4}(\phi_1+\phi_2)\right\}. \tag{228}$$

To derive the discrete formula, we summarize the Gaussian quadrature rule for a weighted integral of a single variable function. We consider discretizing the well-defined target integral of a function g as

$$I=\int_{-\infty}^{\infty}dx\,W(x)g(x), \tag{229}$$

where W is a weight function. A successful way to discretize this type of integral is the Gaussian quadrature method. The quadrature rule gives a simple replacement of the integral with a discrete summation

$$I\approx\sum_{i=1}^{K}w_i g(y_i), \tag{230}$$

where y_i and w_i are the ith roots of the order of K orthonormal polynomial and the corresponding weight, respectively. Comprehensive definitions for the Gaussian quadrature rule (including the definition of weights) were given by Abramowitz and Stegun (1965). The species of the orthonormal polynomial is one's choice and corresponds to the form of the weight function W. Typical choices are the Legendre polynomials and the Hermite polynomials that correspond to $W(y)=1$ and $W(y)=e^{-y^2}$, respectively. If we consider the fact that the mass term in the action plays the role of the weight function, it seems to be natural to use the Hermite polynomials. Indeed, this choice was made by Kadoh *et al.* (2018, 2019, 2020), and we use the Hermite polynomials exclusively for the Gaussian quadrature rule in this section.[8] When g is a polynomial function of degree $2K-1$ or fewer, the Gaussian quadrature reproduces the exact value. Even if it is not, if g is well approximated by a polynomial function of degree $2K-1$ or fewer, the Gaussian quadrature would be accurate. We apply this quadrature rule to each integral of the scalar field in the path integral.

By applying the Gauss-Hermite quadrature to the partition function, a discrete form is introduced as

$$Z(K)=\sum_{\{\alpha\}}\prod_x w_{\alpha_x}e^{y_{\alpha_x}^2}\prod_{\nu=1}^{2}f(y_{\alpha_x},y_{\alpha_{x+\hat{\nu}}}), \tag{231}$$

where $\sum_{\{\alpha\}}$ denotes $\prod_x\sum_{\alpha_x=1}^{K}$. The discrete form depends on the order of the Hermite polynomial K, and this parameter is set large for accurate results. In practice, $K\geq 64$ could be regarded as sufficiently large (Kadoh *et al.*, 2018, 2019, 2020), though, in numerical results shown later in this section, $K=256$ is taken.

Note that the method is applied numerically and that thus far there has not been an analog of the previously given character expansions and orthogonality relations. In Sec. XII.F we show that for the Gauss-Hermite quadrature it is possible to interpret the construction in terms of a truncated version of the harmonic oscillator algebra of creation and annihilation operators.

In Eq. (231) the local Boltzmann factors can be regarded as $K\times K$ matrices, and one can perform the following SVD for them:

$$f(y_{\alpha_x},y_{\beta_{x+\hat{\nu}}})=\sum_{i_{x,\nu}=1}^{K}U_{\alpha_x i_{x,\nu}}\lambda_{i_{x,\nu}}V^{\dagger}_{i_{x,\nu}\beta_{x+\hat{\nu}}}, \tag{232}$$

where $\{\lambda\}$ is the singular values that are assumed to be in descending order ($\lambda_1\geq\lambda_2\geq\cdots\geq\lambda_K\geq 0$) and U and V are unitary matrices. Now a tensor network representation of $Z(K)$ is defined by

$$Z(K)=\sum_{\{X,T\}}\prod_x T(K)_{X_{x-\hat{1}}X_xT_xT_{x-\hat{2}}}, \tag{233}$$

where $\sum_{\{X,T\}}$ denotes $\prod_x\sum_{X_x=1}^{K}\sum_{T_x=1}^{K}$ and we have made the replacements $i_{x,1}\to X_x$ and $i_{x,2}\to T_x$. The tensor at any site is defined by

$$T(K)_{ijkl}=\sqrt{\lambda_i\lambda_j\lambda_k\lambda_l}\sum_{\alpha=1}^{K}w_\alpha e^{y_\alpha^2}V^{\dagger}_{i\alpha}U_{\alpha j}U_{\alpha k}V^{\dagger}_{\alpha l}. \tag{234}$$

At this stage the bond dimension of the tensors is K. To balance the computational cost and numerical accuracy, one may initially truncate the bond dimension to a certain value D_{cut} ($\leq K$). Kadoh *et al.* (2019) took $D_{\mathrm{cut}}\leq 64$ for actual computations, and the sufficiency of this choice is numerically shown.[9]

Physical quantities can also be expressed as tensor networks. A key point is to, respectively, treat the denominator and the numerator on the right-hand side of

$$\langle\phi\rangle=\frac{Z_1}{Z}, \tag{235}$$

where

$$Z_1=\left(\prod_x\int_{-\infty}^{\infty}d\phi_x\right)\phi_{\tilde{x}}e^{-S_h-S_{\mathrm{scalar}}}, \tag{236}$$

with $\tilde{x}\neq x$.[10] The presence of $\phi_{\tilde{x}}$ does not affect the tensor construction procedure, it merely alters which integral is being

[8] As mentioned, the choice does not matter for numerical accuracy as long as the degree of the orthonormal polynomial is sufficiently large.

[9] Note that a fast decay of the singular values guarantees the accuracy of such an approximation. Although the decay rate would be weak near the criticality, a notable accuracy of the critical coupling constant was achieved by Kadoh *et al.* (2019). This is reviewed later in this section.

[10] Because of the translation invariance, a subscript that denotes the coordinate in Eq. (235) is omitted.

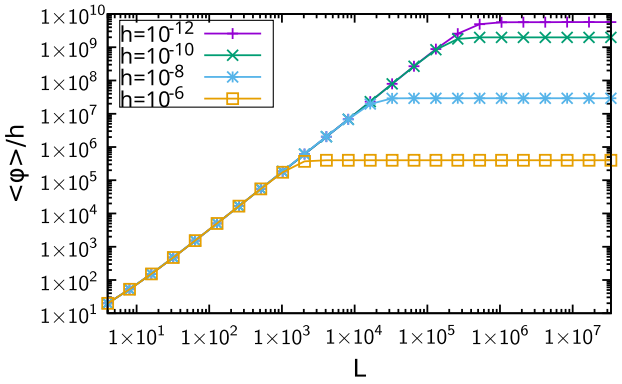

FIG. 30. Thermodynamic limit of $\langle\phi\rangle/h$ at $\mu_0^2 = -0.100\,617\,4$, $\lambda = 0.05$, and $D_{\text{cut}} = 32$ for $h \in [10^{-12}, 10^{-6}]$.

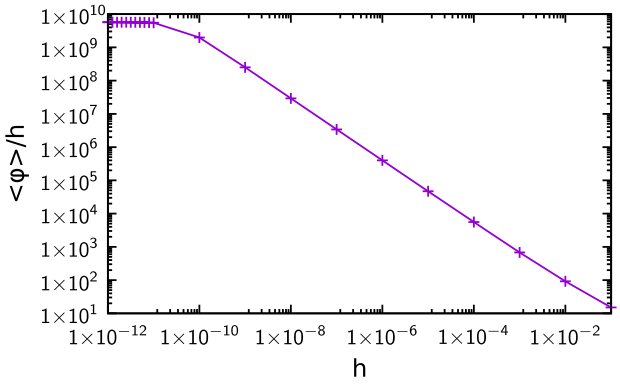

FIG. 31. Zero-external-field limit of $\langle\phi\rangle/h$ at $\mu_0^2 = -0.100\,617\,4$, $\lambda = 0.05$, and $D_{\text{cut}} = 32$ in the thermodynamic limit.

approximated, so the Gaussian quadrature rule and the SVD of the local factors work as before. However, the resultant tensor network representation contains an "impurity tensor" owing to $\phi_{\tilde{x}}$. To perform a coarse graining of a tensor network that contains impurities, one needs a little ingenuity; the details are discussed in Sec. VI.D. Finally, one can calculate Z and Z_1 separately, and using them the value of $\langle\phi\rangle$ is obtained using Eq. (235).

Here the numerical results for the real ϕ^4 theory are shown. The target quantities in this section are the critical coupling constant and its continuum limit value. Kadoh *et al.* (2019) proceeded with the continuum limit extrapolation as follows: (1) Take the thermodynamic and zero-external-field limits to get a susceptibility χ for given bare mass and bare coupling constants. (2) Find the critical mass where $\chi \to \infty$. (3) Extract the renormalized critical squared mass from Eq. (223). (4) Compute the dimensionless critical coupling constant λ/μ_c^2. (5) Vary λ from 0.1 to 0.005 and repeat the previous procedure to take the continuum limit.[11] (6) Take a linear extrapolation to find the critical coupling constant at $\lambda = 0$. As previously mentioned, the parameters for the tensor network analysis are set to $K = 256$ and $D \leq 64$. The legitimacy of this choice was confirmed numerically by Kadoh *et al.* (2019).

Figures 30 and 31 show the results of the thermodynamic limit and zero-external-field limit, respectively. In both cases, bare parameters and the bond dimension of the tensor are $\mu_0^2 = -0.100\,617\,4$, $\lambda = 0.05$, and $D_{\text{cut}} = 32$, as an example. In Fig. 30 the ratio $\langle\phi\rangle/h$ behaves as a constant in the extremely large spacetime volume where $L \geq 10^6$, so one can consider that the system reaches the thermodynamic limit for $L \geq 10^6$. In Fig. 31 the ratio also behaves as a constant for $h \leq 10^{-11}$, so $\langle\phi\rangle \approx \chi h$ holds. The susceptibility χ can then be obtained from the relation.[12]

From the susceptibilities for several masses, the critical mass where $\chi \to \infty$ is determined. Kadoh *et al.* (2019) used the following fitting formula:

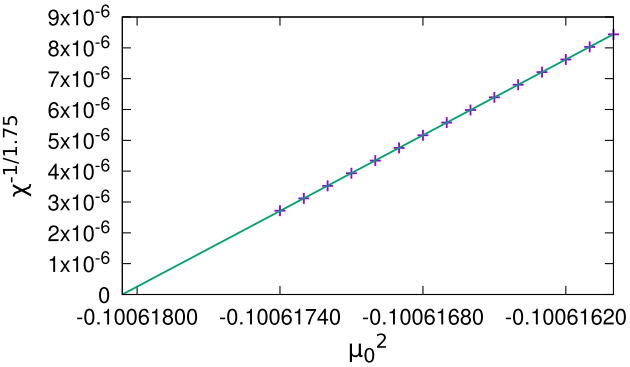

FIG. 32. Susceptibility as a function of μ_0^2 at $\lambda = 0.05$ and $D_{\text{cut}} = 32$.

$$\chi^{-1/1.75} = A|\mu_{0,c}^2 - \mu_0^2|^{\gamma/1.75}. \tag{237}$$

Figure 32 shows the susceptibility with the fit result with fixed $\gamma = \gamma_{\text{Ising}}$.[13] The critical bare squared mass $\mu_{0,c}^2$ is obtained as the μ_0^2 intercept of the line. The parameters are set to $\lambda = 0.05$ and $D_{\text{cut}} = 32$.

Taking the previous procedures for several values of λ, one can obtain the dimensionless critical coupling constant λ/μ_c^2 as a function of λ, and the remaining procedure is to take the continuum extrapolation. Kadoh *et al.* (2019) calculated the $\lambda = 0$ value of the dimensionless critical coupling using a linear extrapolation with a reasonable value $\chi^2 \approx 0.026$. The result was

$$\lim_{\lambda \to 0} \frac{\lambda}{\mu_c^2(\lambda)} = 10.913(56). \tag{238}$$

The error is due mainly to a fluctuation in the large D_{cut} region. Kadoh *et al.* (2019) showed that the D_{cut} dependence is the main source of the error.

Figure 33 shows a comparison of recent Monte Carlo work by Schaich and Loinaz (2009), Wozar and Wipf (2012), Bosetti, Palma, and Guagnelli (2015), and Bronzin, Palma,

[11] Note that if we do not omit showing the lattice spacing a, $a\lambda \to 0$ represents the continuum limit.

[12] Actually, the ratio shows a quadratic behavior for $h \leq 10^{-11}$, so it is proper to take the susceptibility using a more suitable fitting function. Kadoh *et al.* (2019) defined the susceptibility in such a way.

[13] Kadoh *et al.* (2019) supported the legitimacy of fixing γ to the exact value by reasonable reduced χ^2 values for fittings.

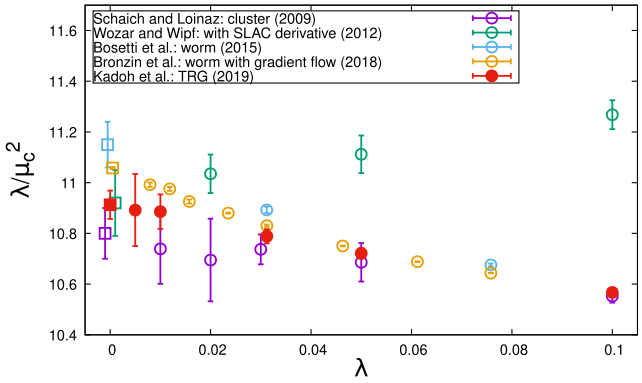

FIG. 33. Comparison of the continuum extrapolations of the critical coupling λ/μ_c^2 given in recent Monte Carlo work (Schaich and Loinaz, 2009; Wozar and Wipf, 2012; Bosetti, Palma, and Guagnelli, 2015; Bronzin, Palma, and Guagnelli, 2019), and in the TRG work (Kadoh *et al.*, 2019). At $\lambda = 0$, data points are horizontally shifted to ensure the visibility. Note that the work by Wozar and Wipf (2012) was conducted with the Stanford Linear Accelerator Center (SLAC) derivative for scalar fields, while the other work was done with a naive discretization.

and Guagnelli (2019) and the TRG work by Kadoh *et al.* (2019). The TRG result shows notable accuracy and has achieved the smallest λ value, which is essentially important for the continuum extrapolation. For a comprehensive list of references concerning the continuum limit value of the coupling constant, see Sakai (2019).

The two-dimensional complex ϕ^4 theory at finite density, a typical model that suffers from the sign problem, was studied by Kadoh *et al.* (2020). A complex scalar field is discretized using the Gaussian quadrature rule for both the real and the imaginary part of the fields. As in Eq. (231), a partition function of a multicomponent scalar field theory is discretized as

$$Z(K) = \sum_{\{\alpha,\beta,\ldots\}} \prod_x w_{\alpha_x} w_{\beta_x} \cdots e^{y_{\alpha_x}^2 + y_{\beta_x}^2 + \cdots} \prod_\nu h(y_{\alpha_x}, y_{\beta_x}, \ldots, y_{\alpha_{x+\hat{\nu}}}, y_{\beta_{x+\hat{\nu}}}, \ldots), \tag{239}$$

where h is the local Boltzmann factor of the model and the definitions of K, w, and y are the same as those used earlier in this section.[14]

Using the TRG, the silver blaze phenomenon[15] for thermodynamic quantities is observed. A point to note from the work is the ability of the TRG (in a model with a severe sign problem and a multicomponent scalar field) to produce robust and sustainable results. Note that Kadoh *et al.* (2020) measured the severeness of the sign problemusing the average phase factor $\langle e^{i\theta} \rangle = Z/Z_{\mathrm{pq}}$, where Z_{pq} is the phase quenched partition function.

[14]Here K is taken to be the same for each field component for simplicity; it can be taken differently for each field.

[15]This refers to the lack of change in the particle density when the chemical potential is varied below a certain critical value (Cohen, 2003).

C. Additional topics and references

For more precise works near criticality, it is natural to use improved coarse-graining algorithms such as loop TNR (Evenbly and Vidal, 2015; Yang, Gu, and Wen, 2017), graph-independent local truncations (GILTs) (Hauru, Delcamp, and Mizera, 2018), and full environment truncation (Evenbly, 2018). The element in common is that the CDL structure in the tensor networks must be properly dealt with; see Gu and Wen (2009) and Sec. VI.G. Recently GILTs were applied to the 2D real ϕ^4 model and a precise value of the critical coupling constant was reported (Delcamp and Tilloy, 2020). The results are comparable to those of Kadoh *et al.* (2019), recent Monte Carlo work, and other computational schemes. When one takes such a deterministic approach, the systematic error should be properly understood, and the definition of the error is important for more concrete discussions.

There could be a better scheme for generating tensor networks for scalar bosons, although the tensor network representation via the Gaussian quadrature rule seems to work quite well. One major concern is that the Gaussian quadrature rule effectively puts a cutoff on the scalar fields, so one cannot deal with models whose local Boltzmann factor $f(\phi_1, \phi_2)$ has a long (or perhaps infinite) tail in the $\phi_1 - \phi_2$ space; e.g., massless free scalar bosons could not be suitably treated with the Gaussian quadrature rule, which requires a fast damping of the local Boltzmann factor. Delcamp and Tilloy (2020) generated discrete degrees of freedom using a Taylor series expansion instead of the Gaussian quadrature rules, and their approach had the same issue.

XI. MODELS WITH FERMIONS

In this section we discuss tensor network representations and coarse-graining algorithms for fermion systems. An important point is that in fermion tensor networks additional Grassmann variables stemming from the original field variables are generated. Since there are not Grassmann valued data types on computers, one needs some special treatments for the Grassmann variables on tensor networks. The coarse-graining procedure for fermion tensor networks was given by Gu, Verstraete, and Wen (2010) and Gu (2013), and applications for relativistic fermion systems were given by Shimizu and Kuramashi (2014b) and Takeda and Yoshimura (2015).

A. Tensor representation for free Wilson fermions

In this section we construct a tensor network representation of a two-dimensional Wilson-Dirac fermion system. Interactions are not discussed here, but local interaction terms could be easily introduced, as they were by Shimizu and Kuramashi (2014b), Kadoh *et al.* (2018), and Yoshimura *et al.* (2018), who discussed U(1), four fermion, and Yukawa-type interactions, respectively. The Lagrangian density of the target system is given by

$$\mathcal{L}_x = \bar{\psi}_x (D\psi)_x, \tag{240}$$

where the Wilson-Dirac operator is defined by

$$D_{xx'} = (m+2)\delta_{x,x'} - \frac{1}{2}\sum_{\mu=1}^{2}\{(1+\gamma_\mu)\delta_{x,x'+\hat{\mu}} + (1-\gamma_\mu)\delta_{x,x'-\hat{\mu}}\}. \tag{241}$$

ψ and m are a two-component spinor field [$\psi_x = (\psi_x^{(1)}, \psi_x^{(2)})^T$] and the mass, respectively. The Grassmann variables satisfy anticommutation relations. We assume periodic boundary conditions in all directions in the remainder of this section.

The partition function of the system is given by

$$Z_F = \int \mathcal{D}\psi\mathcal{D}\bar{\psi} e^{-\sum_x \mathcal{L}_x}. \tag{242}$$

Under the following representations of gamma matrices,

$$\gamma_1 = \sigma_1 = \begin{pmatrix} 0 & 1 \\ 1 & 0 \end{pmatrix}, \qquad \gamma_2 = \sigma_3 = \begin{pmatrix} 1 & 0 \\ 0 & -1 \end{pmatrix}, \tag{243}$$

the hopping factors are expanded as

$$\begin{aligned} e^{-\sum_x \bar{\psi}_x (D\psi)_x} = \prod_x \Bigg\{ & e^{-(m+2)\bar{\psi}_x\psi_x} \\ & \times \sum_{X_{x,1}=0}^{1} (\bar{\chi}_{x+\hat{1}}^{(1)}\chi_x^{(1)})^{X_{x,1}} \sum_{X_{x,2}=0}^{1} (\bar{\chi}_x^{(2)}\chi_{x+\hat{1}}^{(2)})^{X_{x,2}} \\ & \times \sum_{T_{x,1}=0}^{1} (\bar{\psi}_{x+\hat{2}}^{(1)}\psi_x^{(1)})^{T_{x,1}} \sum_{T_{x,2}=0}^{1} (\bar{\psi}_x^{(2)}\psi_{x+\hat{2}}^{(2)})^{T_{x,2}} \Bigg\}, \end{aligned} \tag{244}$$

where χ and $\bar{\chi}$ are the following linear combinations of ψ and $\bar{\psi}$: $\chi_x = (1/\sqrt{2})(\psi_x^{(1)} + \psi_x^{(2)}, \psi_x^{(1)} - \psi_x^{(2)})$ and $\bar{\chi}_x = (1/\sqrt{2})(\bar{\psi}_x^{(1)} + \bar{\psi}_x^{(2)}, \bar{\psi}_x^{(1)} - \bar{\psi}_x^{(2)})$.[16] Each expansion is a binomial because of the nilpotency of Grassmann variables, and at this point discrete indices have arisen at each link.

Next we integrate out the old degrees of freedom. An important point here is to break the hopping factors into Grassmann-even structures to freely shuffle them one to another. To do that the following identities are useful:

$$(\bar{\Psi}_{x+\hat{\mu}}^{(1)}\Psi_x^{(1)}) = \int (\bar{\Psi}_{x+\hat{\mu}}^{(1)} d\bar{\Phi}_{x+\hat{\mu}}^{(1)})(\Psi_x^{(1)} d\Phi_x^{(1)})(\bar{\Phi}_{x+\hat{\mu}}^{(1)}\Phi_x^{(1)}), \tag{245}$$

$$(\bar{\Psi}_x^{(2)}\Psi_{x+\hat{\mu}}^{(2)}) = \int (\bar{\Psi}_x^{(2)} d\bar{\Phi}_x^{(2)})(\Psi_{x+\hat{\mu}}^{(2)} d\Phi_{x+\hat{\mu}}^{(2)})(\bar{\Phi}_x^{(2)}\Phi_{x+\hat{\mu}}^{(2)}). \tag{246}$$

Note that one has to introduce new Grassmann variables here. In addition, during the coarse-graining steps these variables are introduced and integrated out iteratively. This is a key point of the treatment of fermion tensor networks.

When the previously mentioned identities are used, each factor in Eq. (244) can be decomposed, and the partition function can then be deformed to

$$\begin{aligned} Z_F = \sum_{\{X,T\}} \int \mathcal{D}\psi\mathcal{D}\bar{\psi} \prod_x & e^{-(m+2)\bar{\psi}_x\psi_x} (\chi_x^{(1)} d\eta_x^{(1)})^{X_{x,1}} \\ & \times (\bar{\chi}_x^{(2)} d\bar{\eta}_x^{(2)})^{X_{x,2}} (\psi_x^{(1)} d\xi_x^{(1)})^{T_{x,1}} (\bar{\psi}_x^{(2)} d\bar{\xi}_x^{(2)})^{T_{x,2}} \\ & \times (\bar{\chi}_x^{(1)} d\bar{\eta}_x^{(1)})^{X_{x-\hat{1},1}} (\chi_x^{(2)} d\eta_x^{(2)})^{X_{x-\hat{1},2}} (\bar{\psi}_x^{(1)} d\bar{\xi}_x^{(1)})^{T_{x-\hat{2},1}} \\ & \times (\psi_x^{(2)} d\xi_x^{(2)})^{T_{x-\hat{2},2}} (\bar{\eta}_{x+\hat{1}}^{(1)}\eta_x^{(1)})^{X_{x,1}} (\bar{\eta}_x^{(2)}\eta_{x+\hat{1}}^{(2)})^{X_{x,2}} \\ & \times (\bar{\xi}_{x+\hat{2}}^{(1)}\xi_x^{(1)})^{T_{x,1}} (\bar{\xi}_x^{(2)}\xi_{x+\hat{2}}^{(2)})^{T_{x,2}}, \end{aligned} \tag{247}$$

where $\sum_{\{X,T\}}$ indicates that $\prod_x \sum_{X_{x,1},X_{x,2},T_{x,1}T_{x,2}=0}^{1}$. Here the new Grassmann degrees of freedom (η, $\bar{\eta}$, ξ, and $\bar{\xi}$) are introduced in the same manner as in Eqs. (245) and (246). Note that, thanks to the Grassmann-even decompositions, the old degrees of freedom ($\psi, \bar{\psi}, \chi$, and $\bar{\chi}$) that belong to the same coordinate are gathered up without involving sign factors. The tensor network representation of the partition function is then defined by

$$Z_F = \sum_{\{X,T\}} \int \prod_x T_{FX_{x-\hat{1}}X_xT_xT_{x-\hat{2}}} \mathcal{G}_{x,X_{x-\hat{1}}X_xT_xT_{x-\hat{2}}}, \tag{248}$$

where

$$\begin{aligned} T_{Fkijl} = \int & d\mathcal{A}^{(1)} d\bar{\mathcal{A}}^{(1)} d\mathcal{A}^{(2)} d\bar{\mathcal{A}}^{(2)} e^{-(m+2)\bar{\mathcal{A}}\mathcal{A}} \\ & \times \mathcal{A}^{(2)l_2} \bar{\mathcal{A}}^{(1)l_1} \mathcal{B}^{(2)k_2} \bar{\mathcal{B}}^{(1)k_1} \\ & \times \bar{\mathcal{A}}^{(2)j_2} \mathcal{A}^{(1)j_1} \bar{\mathcal{B}}^{(2)i_2} \mathcal{B}^{(1)i_1}, \end{aligned} \tag{249}$$

with dummy Grassmann variables

$$\mathcal{A} = (\mathcal{A}^{(1)}, \mathcal{A}^{(2)})^{\mathrm{T}}, \qquad \bar{\mathcal{A}} = (\bar{\mathcal{A}}^{(1)}, \bar{\mathcal{A}}^{(2)}), \tag{250}$$

$$\mathcal{B} = \frac{1}{\sqrt{2}}(\mathcal{A}^{(1)} + \mathcal{A}^{(2)}, \mathcal{A}^{(1)} - \mathcal{A}^{(2)})^{\mathrm{T}}, \tag{251}$$

$$\bar{\mathcal{B}} = \frac{1}{\sqrt{2}}(\bar{\mathcal{A}}^{(1)} + \bar{\mathcal{A}}^{(2)}, \bar{\mathcal{A}}^{(1)} - \bar{\mathcal{A}}^{(2)}), \tag{252}$$

and

$$\begin{aligned} \mathcal{G}_{x,kijl} = & d\eta_x^{(1)i_1} d\bar{\eta}_x^{(2)i_2} d\xi_x^{(1)j_1} d\bar{\xi}_x^{(2)j_2} \\ & \times d\bar{\eta}_x^{(1)k_1} d\eta_x^{(2)k_2} d\bar{\xi}_x^{(1)l_1} d\xi_x^{(2)l_2} \\ & \times (\bar{\eta}_{x+\hat{1}}^{(1)}\eta_x^{(1)})^{i_1} (\bar{\eta}_x^{(2)}\eta_{x+\hat{1}}^{(2)})^{i_2} \\ & \times (\bar{\xi}_{x+\hat{2}}^{(1)}\xi_x^{(1)})^{j_1} (\bar{\xi}_x^{(2)}\xi_{x+\hat{2}}^{(2)})^{j_2}. \end{aligned} \tag{253}$$

B. Grassmann tensor renormalization group

In this section, we describe the coarse-graining algorithm for tensor networks including Grassmann variables. The details were given by Takeda and Yoshimura (2015). We focus here on the treatment of Grassmann variables in the network. The coarse graining of the bosonic part of the tensor is assumed to be carried out as in Sec. VI.A, and it is helpful to consider this section alongside Sec. VI.A. The coarse graining

[16] Note that χ and $\bar{\chi}$ are introduced for notational simplicity, so the hopping terms are diagonal in spinor space.

of the Grassmann parts yields a phase factor that is to be incorporated into the bosonic part of the tensor.

The Grassmann part $\mathcal{G}$ is decomposed into the following two parts:

$$\mathcal{G}_{x,kijl} = \int (\Theta^{[1]}_{x,ij} d\bar{\eta}^{m_f}_{x^\star})(\Theta^{[3]}_{x,kl} d\eta^{m_f}_{x^\star-\hat{1}^\star})(\bar{\eta}_{x^\star}\eta_{x^\star-\hat{1}^\star})^{m_f}, \tag{254}$$

where

$$\begin{aligned}\Theta^{[1]}_{x,ij} = {} & d\eta^{(1)i_1}_x d\bar{\eta}^{(2)i_2}_x d\xi^{(1)j_1}_x d\bar{\xi}^{(2)j_2}_x \\ & \times (\bar{\eta}^{(1)}_{x+\hat{1}}\eta^{(1)}_x)^{i_1}(\bar{\eta}^{(2)}_x\eta^{(2)}_{x+\hat{1}})^{i_2} \\ & \times (\bar{\xi}^{(1)}_{x+\hat{2}}\xi^{(1)}_x)^{j_1}(\bar{\xi}^{(2)}_x\xi^{(2)}_{x+\hat{2}})^{j_2},\end{aligned} \tag{255}$$

$$\Theta^{[3]}_{x,kl} = d\bar{\eta}^{(1)k_1}_x d\eta^{(2)k_2}_x d\bar{\xi}^{(1)l_1}_x d\xi^{(2)l_2}_x, \tag{256}$$

with the new binary index $m_f = (i_1 + i_2 + j_1 + j_2) \bmod 2 = (k_1 + k_2 + l_1 + l_2) \bmod 2$. This decomposition is analogous to the decomposition that takes place in the original TRG. On the right-hand side of Eq. (254), each factor is Grassmann even thanks to the inclusion of the new Grassmann variables and the definition of the new binary index. This is similar to the construction of the fermion tensor network; see Eqs. (254)–(257). $x^\star$ denotes the new coordinate on the coarse-grained square lattice, and the unit vectors on the coarse-grained lattice are defined by $\hat{1}^\star = \hat{1} + \hat{2}$ and $\hat{2}^\star = \hat{1} - \hat{2}$; see also VI.A.

We have another way to decompose $\mathcal{G}$,

$$\mathcal{G}_{x,kijl} = (-1)^{l_1+l_2} \int (\Theta^{[2]}_{x,li} d\bar{\xi}^{m_f}_{x^\star})(\Theta^{[4]}_{x,jk} d\eta^{m_f}_{x^\star-\hat{2}^\star})(\bar{\eta}_{x^\star}\eta_{x^\star-\hat{2}^\star})^{m_f}, \tag{257}$$

where

$$\begin{aligned}\Theta^{[2]}_{x,li} = {} & d\bar{\xi}^{(1)l_1}_x d\xi^{(2)l_2}_x d\eta^{(1)i_1}_x d\bar{\eta}^{(2)i_2}_x \\ & \times (\bar{\eta}^{(1)}_{x+\hat{1}}\eta^{(1)}_x)^{i_1}(\bar{\eta}^{(2)}_x\eta^{(2)}_{x+\hat{1}})^{i_2},\end{aligned} \tag{258}$$

$$\begin{aligned}\Theta^{[4]}_{x,jk} = {} & d\xi^{(1)j_1}_x d\bar{\xi}^{(2)j_2}_x d\bar{\eta}^{(1)k_1}_x d\eta^{(2)k_2}_x \\ & \times (\bar{\xi}^{(1)}_{x+\hat{2}}\xi^{(1)}_x)^{j_1}(\bar{\xi}^{(2)}_x\xi^{(2)}_{x+\hat{2}})^{j_2}\end{aligned} \tag{259}$$

with the new binary index $m_f = (l_1 + l_2 + i_1 + i_2) \bmod 2 = (j_1 + j_2 + k_1 + k_2) \bmod 2$.

Using the previous two ways of decomposing $\mathcal{G}$, we can now integrate out the old Grassmann variables, yielding a phase factor

$$\begin{aligned}&\int \Theta^{[2]}_{x+\hat{2},T_x X_{x+\hat{2}}} \Theta^{[1]}_{x,X_x T_x} \Theta^{[4]}_{x+\hat{1},T_{x+\hat{1}} X_x} \Theta^{[3]}_{x+\hat{1}+\hat{2},X_{x+\hat{2}} T_{x+\hat{1}}} \\ &= (-1)^{\epsilon_{X_x T_x X_{x+\hat{2}} T_{x+\hat{1}}}},\end{aligned} \tag{260}$$

where

$$\begin{aligned}\epsilon_{X_x T_x X_{x+\hat{2}} T_{x+\hat{1}}} = {} & X_{x,2}(X_{x,1} + X_{x,2}) + T_{x,1}(T_{x,1} + T_{x,2}) \\ & + X_{x+\hat{2},2}(X_{x+\hat{2},1} + X_{x+\hat{2},2}) \\ & + T_{x+\hat{1},2}(T_{x+\hat{1},1} + T_{x+\hat{1},2}) \\ & + (X_{x,1} + X_{x,2} + X_{x+\hat{2},1} + X_{x+\hat{2},2}) \\ & \times (T_{x,1} + T_{x,2} + T_{x+\hat{1},1} + T_{x+\hat{1},2}).\end{aligned} \tag{261}$$

Note that the details of the phase factor depend on the ordering of the Θ's in Eq. (260) and that this ordering is not unique. Finally, the effect of the coarse graining of the Grassmann part is interpreted in terms of a non-Grassmann phase factor and constraints as follows:

$$\begin{aligned}&(-1)^{T_{x,1}+T_{x,2}+\epsilon_{X_x T_x X_{x+\hat{2}} T_{x+\hat{1}}}} \\ &\times \delta_{(X_{x+\hat{2},1}+X_{x+\hat{2},2}+T_{x+\hat{1},1}+T_{x+\hat{1},2}) \bmod 2, X_{x^\star,f}} \\ &\times \delta_{(T_{x+\hat{1},1}+T_{x+\hat{1},2}+X_{x,1}+X_{x,2}) \bmod 2, T_{x^\star,f}} \\ &\times \delta_{(X_{x,1}+X_{x,2}+T_{x,1}+T_{x,2}) \bmod 2, X_{x^\star-\hat{1}^\star,f}} \\ &\times \delta_{(T_{x,1}+T_{x,2}+X_{x+\hat{2},1}+X_{x+\hat{2},2}) \bmod 2, T_{x^\star-\hat{2}^\star,f}},\end{aligned} \tag{262}$$

where the indices labeled with f's are the previously introduced new binary indices. The phase and the Kronecker deltas are to be incorporated into the bosonic tensors, and the coarse-grained Grassmann part $\mathcal{G}^\star$ that consists of the new Grassmann variables is defined by

$$\mathcal{G}^\star_{x,kijl} = d\eta^{i_f}_x d\xi^{j_f}_x d\bar{\eta}^{k_f}_x d\bar{\xi}^{l_f}_x (\bar{\eta}_{x+\hat{1}^\star}\eta_x)^{i_f}(\bar{\xi}_{x+\hat{2}^\star}\xi_x)^{j_f}. \tag{263}$$

The previous procedure is iteratively executed along with the normal coarse-graining steps for the bosonic tensors.

C. Two-dimensional Schwinger model with Wilson fermions

Shimizu and Kuramashi (2014a) studied the critical behavior at $\theta = \pi$ of the two-dimensional Schwinger model with Wilson fermions. While studying the Fisher zeros, Shimizu and Kuramashi (2014a) confirmed that there is a critical point near $\kappa = 0.2415$ and that the phase transition belongs to the 2D Ising universality class, where κ is the inverse of the Wilson fermion mass m: $1/\kappa = 2(m + 2)$. In addition, they completed a Lee-Yang zero analysis to seriously study the phase structure. In the parameter space of a complex coupling, the Lee-Yang zeros of the partition function are found off of the real-coupling axis at finite volume. These zeros have their own critical behavior, and in the thermodynamic limit their approach and condensation along the real-coupling axis cause nonanalytic behavior on the real axis, thus indicating a phase transition.

Assuming that the gauge part of the lattice action is given by the usual Wilson action along with a topological term,

$$S_G = -\frac{1}{g^2}\sum_x \cos(A_{x,1} + A_{x+\hat{1},2} - A_{x+\hat{2},1} - A_{x,2}) - i\theta Q, \tag{264}$$

where $g^2 = 1/\beta_{pl}$ is the gauge coupling and Q is the following topological charge:

$$Q = \frac{1}{2\pi}\sum_x q_x, \tag{265}$$

where $q_x = (A_{x,1} + A_{x+\hat{1},2} - A_{x+\hat{2},1} - A_{x,2}) \bmod 2\pi$. The presence of this term incurs the sign problem in MC calculations. The scaling behavior of the partition function zeros in the complex θ plane is studied with a fixed $\mathrm{Re}\theta = \pi$. At the critical mass κ_c, the position of a partition function zero $\theta_0(L)$ would obey

$$\mathrm{Im}\theta_0(L) - \mathrm{Im}\theta_0(\infty) \propto L^{-(2\nu-\beta)/\nu} \tag{266}$$

with the critical exponents ν and β. If a first-order phase transition occurs (conjectured as being at $\kappa < \kappa_c$), it is expected that $\mathrm{Im}\theta_0(L) \propto L^{-2}$ with a vanishing $\mathrm{Im}\theta_0(\infty)$. On the other hand, if there are not phase transitions (conjectured as being at $\kappa > \kappa_c$), it is expected that $\mathrm{Im}\theta_0(\infty) \neq 0$.

Figure 34 shows the scaling behaviors of $\mathrm{Im}\theta_0(L)$, and the fitting results are summarized in Table I. The coupling is $1/g^2 = 10$. The bond dimension of the tensors is fixed at $D_{\mathrm{cut}} = 160$. These results show that (a) for $\kappa < \kappa_c$ $\mathrm{Im}\theta_0(\infty)$ vanishes and the exponent y is close to 2, (b) for $\kappa > \kappa_c$ $\mathrm{Im}(\infty)$ has a nonzero value, and (c) for $\kappa = 0.2415$ ($\approx\kappa_c$) $y = 1.869(10)$ is consistent with $y = 1.875$,which is the same result as for the 2D Ising universality class.

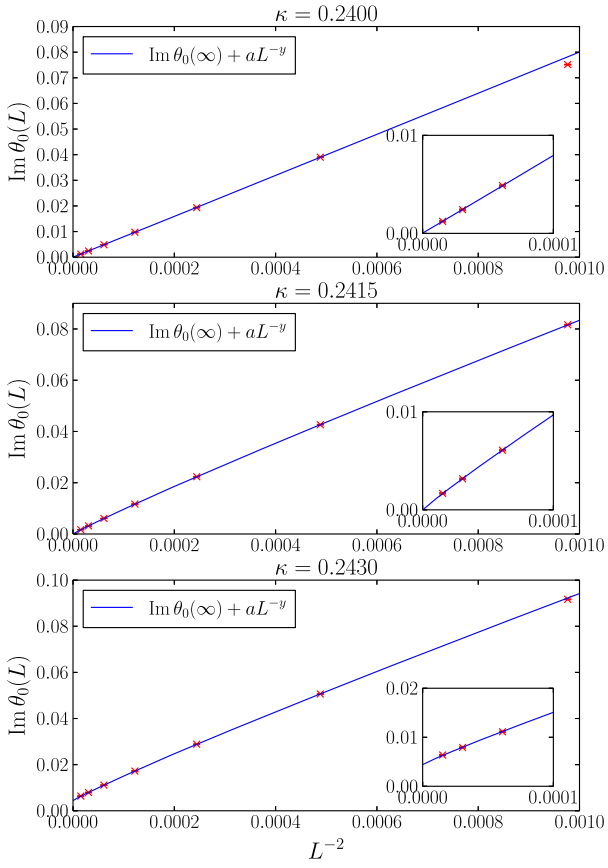

FIG. 34. Lee-Yang zeros for $\kappa = 0.24$ (top panel), 0.2415 (middle panel), and 0.243 (bottom panel). $1/g^2 = 10$. Solid lines are the fit results with a function $\mathrm{Im}\theta_0(L) = \mathrm{Im}\theta_0(\infty) + aL^{-y}$ via three parameters $\mathrm{Im}\theta_0(\infty)$, a, and y. Adapted from Shimizu and Kuramashi, 2014a.

TABLE I. Results of the fittings in Fig. 34. Adapted from Shimizu and Kuramashi, 2014a.

κ	y	$\mathrm{Im}\theta_0(\infty)$	Fit range	χ^2/d.o.f.
0.2400	2.009(12)	0.000 034(59)	$L \in [32\sqrt{2}, 256]$	0.65
0.2415	1.869(10)	−0.000 016(64)	$L \in [32\sqrt{2}, 256]$	0.41
0.2430	1.850(15)	0.004 42(12)	$L \in [32\sqrt{2}, 256]$	0.78

In summary, on the line $\theta = \pi$ there is no phase transition at $\kappa > \kappa_c$, there is the second-order phase transition belonging to the 2D Ising universality class at $\kappa = \kappa_c \approx 0.2415$, and there are first-order phase transitions at $\kappa < \kappa_c$. This is exactly the expected result.

There was a further study of the Berezinskii-Kosterlitz-Thouless transition in the (m, g) plane in the same model by the same authors (Shimizu and Kuramashi, 2018), but here we refer the interested reader only to the original paper.

This work is the first application of the Grassmann TRG to a relativistic fermion system. Following this study, an application to the two-dimensional Thirring model (Thirring, 1958), a pure fermion system, in the presence of a chemical potential was reported (Takeda and Yoshimura, 2015).

D. Three-dimensional free fermions

In three or more dimensions, the Grassmann parts of the tensors can be coarse grained in a similar manner as the higher-order TRG (Sakai, Takeda, and Yoshimura, 2017), and calculations of partition functions and Green's functions were given by Yoshimura *et al.* (2018) with relatively large bond dimensions.[17] Figure 35 shows the free energy density of the three-dimensional free fermion system, where the convergence in the number of states D_{cut} is extremely rapid, and one cannot see the difference between the Grassmann HOTRG results and the exact values in this resolution. The treatment of the Grassmann variables in the Grassmann HOTRG is straightforwardly applicable to ATRG (Adachi, Okubo, and Todo, 2020) and triad HOTRG (Kadoh and Nakayama, 2019); this fact will encourage researchers to approach higher-dimensional fermion models.

E. Two-dimensional $\mathcal{N} = 1$ Wess-Zumino model

The interacting two-dimensional $\mathcal{N} = 1$ Wess-Zumino model, a simple supersymmetric model, displays a vanishing partition function (Witten, 1982).[18] This fact indicates that the model suffers from a serious sign problem, as is the case in other generic supersymmetric models.[19]

[17]HOTRG in the presence of impurity tensors was discussed by Morita and Kawashima (2019). The technique that they used would also help to increase the accuracy of fermionic Green's functions.

[18]The partition function with periodic boundary conditions is equivalent to the trace of the fermion number operator $(-1)^F$.

[19]For a review on lattice supersymmetry see Catterall, Kaplan, and Unsal (2009).

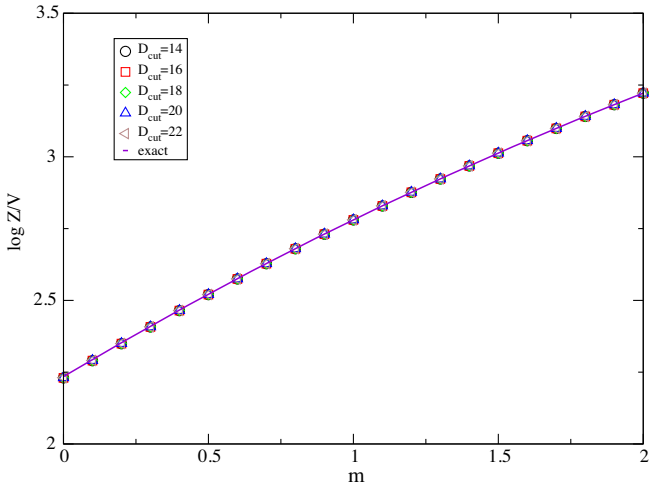

FIG. 35. Free energy density of three-dimensional free fermions for $V = 256^3$. Adapted from Yoshimura *et al.*, 2018.

The Euclidean continuum action of the model is given by

$$S_{\text{cont}} = \int d^2x \{\tfrac{1}{2}(\partial_\mu \phi)^2 + \tfrac{1}{2}W'(\phi)^2 + \tfrac{1}{2}\bar{\psi}(\gamma_\mu \partial_\mu + W''(\phi))\psi\}, \tag{267}$$

where ϕ and ψ are a one-component real scalar field and a two-component Majorana spinor field, respectively.[20] $W(\phi)$ is an arbitrary function of ϕ called the superpotential, which is the source of the Yukawa and ϕ^n interactions.

The spinor field ψ satisfies the Majorana condition

$$\bar{\psi} = -\psi^T C^{-1}, \tag{268}$$

with the charge conjugation matrix C:

$$C^T = -C, \qquad C^\dagger = C^{-1}, \qquad C^{-1}\gamma_\mu C = -\gamma_\mu^T. \tag{269}$$

The continuum action (267) is invariant under the supersymmetry transformation

$$\delta\phi = \bar{\epsilon}\psi, \tag{270}$$

$$\delta\psi = [\gamma_\mu \partial_\mu \phi - W'(\phi)]\epsilon, \tag{271}$$

where ϵ is a two-component Grassmann number and $\bar{\epsilon}$ is defined as in Eq. (268).

Using the symmetric difference operator $\partial_\mu^{\text{S}} = (\partial_\mu + \partial_\mu^*)/2$ with the forward difference ∂ and the backward difference ∂^*, the lattice action is given by

$$S = \sum_x \left\{ \frac{1}{2}(\partial_\mu^{\text{S}}\phi_x)^2 + \frac{1}{2}\left(W'(\phi_x) - \frac{r}{2}\partial_\mu\partial_\mu^*\phi_x\right)^2 + \frac{1}{2}\bar{\psi}_x(D\psi)_x \right\}. \tag{272}$$

[20]The numerical treatment of Majorana fermions on a discrete spacetime lattice was discussed by Wolff (2008).

Note that the lattice action also has the Wilson term in the scalar sector; this is required to retain equal footing for both the scalar and fermion sectors. It has been perturbatively proven that the broken supersymmetry on the lattice is restored in the continuum limit for this construction of the action (Golterman and Petcher, 1989). The Dirac operator on the lattice is defined by

$$D_{xx'} = \left(\gamma_\mu \partial_\mu^{\text{S}} - \frac{r}{2}\partial_\mu\partial_\mu^*\right)_{xx'} + W''(\phi_x)\delta_{xx'}, \tag{273}$$

where r is a nonzero real parameter called the Wilson parameter.

Tensor network representations of both the scalar and fermion parts are constructed in the manner as discussed in Secs. X.B and XI.A, respectively. An important feature of this model is the Wilson term of the scalar part whose square produces next-nearest-neighbor hopping terms in the lattice action. This fact prevents one from simply constructing a tensor network representation. Kadoh *et al.* (2018) introduced auxiliary scalar fields to make the nearest-neighbor form of the action[21]

$$\begin{aligned}\tilde{S}_{\text{B}} = \frac{1}{2}\sum_x \{&(\partial_\mu \phi_x)^2 + (W'(\phi_x))^2 + G_x^2 + H_x^2 \\ &- [rW'(\phi_x) + \alpha G_x + \beta H_x](\phi_{x+\hat{1}} + \phi_{x-\hat{1}} - 2\phi_x) \\ &- [rW'(\phi_x) + \alpha G_x - \beta H_x](\phi_{x+\hat{2}} + \phi_{x-\hat{2}} - 2\phi_x)\},\end{aligned} \tag{274}$$

with the auxiliary fields G and H and the constants $\alpha = \sqrt{(1-2r^2)/2}$ and $\beta = 1/\sqrt{2}$.

In Fig. 36, the partition function (called the Witten index in this model) of the free $\mathcal{N} = 1$ Wess-Zumino model, whose superpotential is given by $W(\phi) = (1/2)m\phi^2$ with the mass parameter m, is shown on the $V = 2 \times 2$ lattice.[22] In the free case, the partition function can be analytically obtained, and the exact solution is $Z = \text{sgn}\{m(m+4r)\}$. Thus, the exact solution is 1 for the $m > 0$ region shown in Fig. 36. The TRG results tend to converge to the exact value 1 with increasing D_{cut}, the number of singular values that are kept during the coarse-graining steps. The less accurate results in the small m region are due to the lack of a fast damping factor in the local Boltzmann weight that is required for the Gaussian quadrature rule to be effective, but such poor behavior is a special case for the noninteracting model.

When one deals with the interacting Wess-Zumino model that has ϕ^n-interaction terms, they guarantee the presence of fast damping. Since the tensor network representation given in the paper does not depend on the form of superpotential, the interacting $\mathcal{N} = 1$ Wess-Zumino model is within the scope of tensor analyses. In the interacting case, the restoration of the

[21]This prescription gives multicomponent scalar fields. For the treatment of multicomponent scalars, see also the study of 2D complex ϕ^4 theory by Kadoh *et al.* (2020).

[22]In order not to break the supersymmetry, the periodic boundary conditions are assumed in all directions for both fermions and bosons. The order of the Hermite polynomial used in the Gaussian quadrature is set to 64 in the paper.

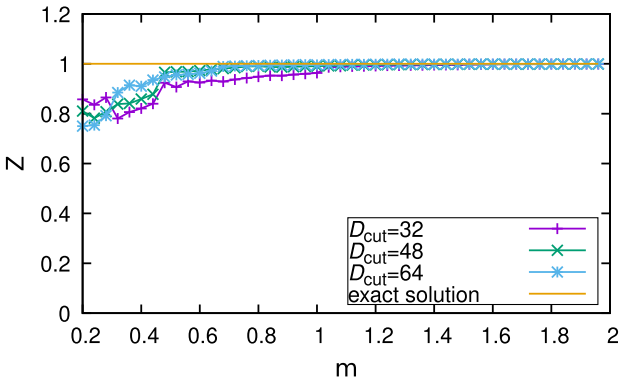

FIG. 36. Partition function as a function of m on a $V = 2 \times 2$ lattice.

broken supersymmetry on the lattice should first be confirmed numerically. However, from a technical point of view an explicit breaking of the Z_2 symmetry due to the Wilson term in the lattice action (Golterman and Petcher, 1989) causes singular behavior in the local Boltzmann factor. This fact makes numerical treatments difficult. In addition to the Wilson type discretization, other lattice regularizations are worth considering and, in such cases, tensor network analyses are helpful as long as the lattice model is written in a local way.

In addition, because complexities of the field contents do not affect the structure of tensor networks, more complicated models such as the $\mathcal{N} = (2, 2)$ Wess-Zumino model could be treated in the same way.

F. Two-dimensional Schwinger model with staggered fermions

In this section a tensor network representation of the Schwinger model with staggered fermions is discussed.[23] The one-flavor staggered action for the massless Schwinger model on a two-dimensional lattice has the action

$$S = S_F + S_g, \tag{275}$$

with

$$S_F = \frac{1}{2}\sum_{x=1}^{N}\sum_{\mu=1}^{2}\eta_{x,\mu}[\bar{\psi}_x U_{x,\mu}\psi_{x+\hat{\mu}} - \bar{\psi}_{x+\hat{\mu}}U^{\dagger}_{x,\mu}\psi_x], \tag{276}$$

and S_g is the usual Wilson action given by Eq. (21). Here $\eta_{x,\mu}$ is the staggered phase, which for $\eta_{x,1} = 1$ and for $\eta_{x,2} = (-1)^{x_1}$, with x_1 the 1-component of x. The partition function for this model is then given by

$$\begin{aligned} Z &= \int \mathcal{D}U\mathcal{D}\bar{\psi}\mathcal{D}\psi e^{-S} \\ &= \int \mathcal{D}U e^{\beta\sum_x \mathrm{Re}[U_{x,12}]} Z_F(U), \end{aligned} \tag{277}$$

with $\int \mathcal{D}U = \prod_x \int_{-\pi}^{\pi} dA_{x,\mu}/2\pi$, $\int \mathcal{D}\bar{\psi}\mathcal{D}\psi = \prod_x \int d\bar{\psi}_x d\psi_x$, and Z_F representing the part of the partition function that depends on the fermion fields.

Following Gattringer, Kloiber, and Sazonov (2015) in formulating the model in terms of discrete degrees of freedom, we first integrate out the fermions and generate an effective action depending only on the gauge fields. As a first step we redefine the link variables such that the staggered fermion phases $\eta_{x,\mu}$ can be absorbed into modified link variables $U_{x,\mu} \to \eta_{x,\mu}U_{x,\mu}$. Under this transformation the gauge action picks up an overall negative sign, but the measure is invariant. The Boltzmann factors associated with each bilinear fermion term can be Taylor expanded, yielding the partition function

$$\begin{aligned} Z_F = \int \mathcal{D}\bar{\psi}\mathcal{D}\psi \prod_x \prod_\mu \sum_{k_{x,\mu}=0}^{1} (-\tfrac{1}{2}\bar{\psi}_x U_{x,\mu}\psi_{x+\hat{\mu}})^{k_{x,\mu}} \\ \times \sum_{\bar{k}_{x,\mu}=0}^{1} (\tfrac{1}{2}\bar{\psi}_{x+\hat{\mu}}U^{\dagger}_{x,\mu}\psi_x)^{\bar{k}_{x,\mu}}. \end{aligned} \tag{278}$$

Notice that higher-order terms in the expansion of the Boltzmann factors vanish because of the Grassmannian nature of the fermions. The partition function is only nonzero when the Grassmann integration is saturated. This occurs only for closed fermionic loops and dimer configurations.

For a loop ℓ with length $L(\ell)$, one finds a contribution with an absolute value

$$\left(\frac{1}{2}\right)^{L(\ell)} \prod_{x,\mu\in\ell} (U_{x,\mu})^{k_{x,\mu}} (U^{\dagger}_{x,\mu})^{\bar{k}_{x,\mu}}, \tag{279}$$

where on a given link only a single k or $\bar{k}$ is nonzero. In addition, each loop carries a certain Z_2 phase that depends on the length of the loop and its winding along the temporal direction given by

$$-(-1)^{1/2L(\ell)}(-1)^{W(\ell)}. \tag{280}$$

In Eq. (280) the overall negative sign is the usual one for closed fermion loops, while the second factor keeps track of the number of forward hops, which is exactly half the total length of the loop for a closed loop. Finally, the factor $(-1)^{W(\ell)}$ of the loop is determined by the number of windings of the loop along the temporal direction assuming antiperiodic boundary conditions for the fermions. Using dimers and loops as basic constituents for nonzero contributions to the fermionic partition function, we can write

$$\begin{aligned} Z_F = \left(\frac{1}{2}\right)^V \sum_{\{\ell,d\}} (-1)^{N_L + (1/2)\sum_\ell L(\ell) + \sum_\ell W(\ell)} \\ \times \prod_\ell \left[\prod_{x,\mu\in\ell} (U_{x,\mu})^{k_{x,\mu}} (U^{\dagger}_{x,\mu})^{\bar{k}_{x,\mu}}\right], \end{aligned} \tag{281}$$

where $\sum_{\{\ell,d\}}$ indicates a sum over all valid loop and dimer configurations and N_L is the number of loops. We construct a

[23] While this section refers to the work of Gattringer, Kloiber, and Sazonov (2015), the elimination of fermion fields was also discussed by Zohar and Cirac (2018b, 2019).

local tensor that reproduces the nonzero configurations of this partition function.

We ignore the overall sign for now and deal simply with the magnitude. We allow two types of indices per link to capture separately the incoming and outgoing fermion lines, making the fermion site tensor a rank-8 object. To write a tensor, we first fix the coordinates so that right (1-direction) and up (2-direction) are positive (no overbar), and left and down are negative (overbar). Since each site either is the end point of a dimer or has a fermionic current incoming to it and outgoing from it, we can model this with the tensor structure (we omit the gauge link factors for now) as follows:

$$T^{(x)}_{k_{x-\hat{1},1}\bar{k}_{x-\hat{1},1}k_{x,1}\bar{k}_{x,1}k_{x,2}\bar{k}_{x,2}k_{x-\hat{2},2}\bar{k}_{x-\hat{2},2}} = \begin{cases} 1 \text{ if } k_{x-\hat{1},1}+k_{x-\hat{2},2}+\bar{k}_{x,1}+\bar{k}_{x,2}=1 \\ \quad \text{and } k_{x,1}+k_{x,2}+\bar{k}_{x-\hat{1},1}+\bar{k}_{x-\hat{2},2}=1, \\ 0 \text{ otherwise,} \end{cases} \tag{282}$$

where each $(k_i,\bar{k}_i)=0,1$. The pairs of indices are ordered (left, right, up, and down). A graphical representation of this tensor is shown in Fig. 37(a).

By repeatedly contracting this site tensor with copies of itself over the lattice, we can see that the full set of closed loops and dimers for the model at zero gauge coupling is generated, except for the overall factor of -1 for each closed fermion loop.

In order to include the gauge fields, we employ a character expansion of the Boltzmann factors associated with the gauge action:

$$e^{-\beta\cos[A_{x,1}+A_{x+\hat{1},2}-A_{x+\hat{2},1}-A_{x,2}]} = \sum_{m_{x,12}=-\infty}^{m_{x,12}=\infty} I_{m_{x,12}}(-\beta)e^{im_{x,12}[A_{x,1}+A_{x+\hat{1},2}-A_{x+\hat{2},1}-A_{x,2}]}. \tag{283}$$

Each plaquette is now labeled by an integer $m_{x,12}$ (which we shorten to m_x since there are temporal plaquettes in only two dimensions). Note that $I_{m_x}(-\beta)=(-1)^{m_x}I_{m_x}(\beta)$. In two dimensions each link is shared by two plaquettes. For a link in the $\mu=1$ direction, the two plaquettes give factors of $e^{im_xA_{x,1}}$ and $e^{-im_{x-\hat{2}}A_{x,1}}$. In the $\mu=2$ direction, $e^{-im_xA_{x,2}}$ and $e^{im_{x-\hat{1}}A_{x,2}}$. In addition, the link carries a factor of $e^{ik_{x,\mu}A_{x,\mu}}$ or $e^{-i\bar{k}_{x,\mu}A_{x,\mu}}$ coming from Z_F. Thus, in total, links carry two m indices inherited from their neighboring plaquettes together with a k and a $\bar{k}$ index associated with the fermionic hopping terms. The integral over a link variable is given by

$$\int_{-\pi}^{\pi}\frac{dA_{x,\mu}}{2\pi}e^{i(k_{x,\mu}-\bar{k}_{x,\mu})A_{x,\mu}}\prod_{\nu>\mu}e^{i(m_x-m_{x-\hat{\nu}})A_{x,\mu}}\prod_{\nu<\mu}e^{i(m_{x-\hat{\nu}}-m_x)A_{x,\mu}} = \delta^{(x,\mu)}_{\sum_{\nu>\mu}(m_x-m_{x-\hat{\nu}})+\sum_{\nu<\mu}(m_{x-\hat{\nu}}-m_x)+k_{x,\mu}-\bar{k}_{x,\mu},0}. \tag{284}$$

Equation (284) allows us to write the following partition function as a sum over m and $k,\bar{k}$ variables:

$$Z=\sum_{\{m\}}\sum_{\{k,\bar{k}\}}\left(\prod_x I_{m_x}(\beta)\right)\left(\prod_x T^{(x)}_{k_{x-\hat{1},1}\bar{k}_{x-\hat{1},1}k_{x,1}\bar{k}_{x,1}k_{x,2}\bar{k}_{x,2}k_{x-\hat{2},2}\bar{k}_{x-\hat{2},2}}\right) \times(-1)^{N_L+N_P+(1/2)\sum_\ell L(\ell)+\sum_\ell W(\ell)} \times\prod_{x,\mu}\delta^{(x,\mu)}_{\sum_{\nu>\mu}(m_x-m_{x-\hat{\nu}})+\sum_{\nu<\mu}(m_{x-\hat{\nu}}-m_x)+k_{x,\mu}-\bar{k}_{x,\mu},0}, \tag{285}$$

where $N_P=\sum_x m_x$. At this point we include all the minus signs for completeness. Gattringer, Kloiber, and Sazonov (2015) proved that every valid contribution to the partition function is positive in the case of periodic boundary conditions, so from now on we ignore the factor of $(-1)^{N_L+N_P+(1/2)\sum_\ell L(\ell)+\sum_\ell W(\ell)}$.

Associated with each link is a constraint between the k and $\bar{k}$ fields on the link and the adjacent m fields on the plaquettes given by Eq. (284). This is a natural object to use to form a tensor. We define a tensor on each link by

$$A^{(x,\mu)}_{m_xm_{x-\hat{\nu}}k^1_{x,\mu}\bar{k}^1_{x,\mu}k^2_{x,\mu}\bar{k}^2_{x,\mu}} \equiv \delta_{\sum_{\nu>\mu}(m_x-m_{x-\hat{\nu}})+\sum_{\nu<\mu}(m_{x-\hat{\nu}}-m_x)+k^1_{x,\mu}-\bar{k}^1_{x,\mu},0} \times\delta_{k^1_{x,\mu},k^2_{x,\mu}}\delta_{\bar{k}^1_{x,\mu},\bar{k}^2_{x,\mu}}. \tag{286}$$

In Eq. (286) the $k^i,\bar{k}^i$ indices are associated with the two ends of a link. These indices are diagonal, as indicated by the Kronecker deltas. A diagram showing the relative position of the fermion and plaquette indices is shown in Fig. 37(b).

Finally, we construct a tensor associated with the plaquettes of the lattice. This is the same tensor used in previous tensor formulations of Abelian gauge theories, the B tensor; see Eq. (170). A graphical representation of the B tensor is shown in Fig. 37(c). The contraction over these three (T, A, and B) unique tensor types can be represented as the tensor network shown in Fig. 38.

It is possible to include a topological term in the original action with the addition of

$$S_\Theta=\frac{i\Theta}{2\pi}\sum_x \mathrm{Im}[U_{x,12}]. \tag{287}$$

Taking the staggered phase into account and expanding the Wilson plaquette term and this term simultaneously as

$$e^{-\beta\mathrm{Re}[U_{x,12}]+(i\Theta/2\pi)\mathrm{Im}[U_{x,12}]} \tag{288}$$

$$=\sum_{m_x=-\infty}^{\infty}C_{m_x}(\beta,\Theta)e^{im_x(A_{x,1}+A_{x+\hat{1},2}-A_{x+\hat{2},1}-A_{x,2})}, \tag{289}$$

the previous steps in formulating a tensor network can be followed straightforwardly. One can solve for the C's numerically or analytically (Gattringer, Kloiber, and Sazonov, 2015). This amounts to the replacement

$$I_{m_x}(\beta)\to I_{m_x}(2\sqrt{\eta\bar{\eta}})(\eta/\bar{\eta})^{m_x/2} \tag{290}$$

in the definition of the B tensor, with $\eta=\beta/2-\Theta/4\pi$ and $\bar{\eta}=\beta/2+\Theta/4\pi$.

Using these tensors, one can perform numerical calculations using a coarse-graining scheme. Butt *et al.* (2020) used

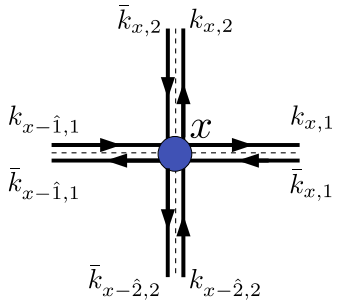

(a) T tensor on a site.

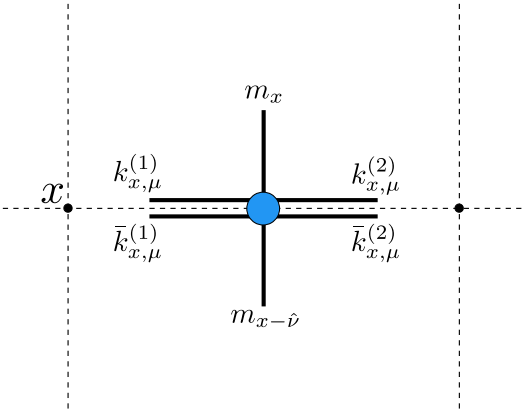

(b) A tensor on a link.

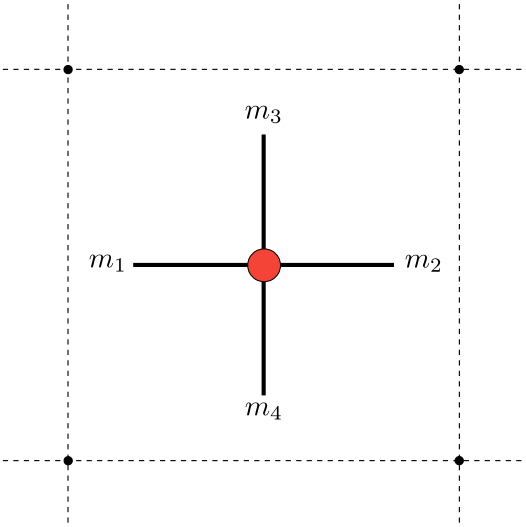

(c) B tensor on a plaquette.

FIG. 37. Graphical representations of tensors.

the higher-order tensor renormalization group to calculate the free energy for the massless Schwinger model with and without the presence of a topological term. From the free energy they calculated the average plaquette and the topological charge as functions of both the gauge coupling and the Θ parameter. The average plaquette and topological charge are given by

$$\langle U_p \rangle = \frac{1}{V}\frac{\partial \ln Z}{\partial \beta} \tag{291}$$

and

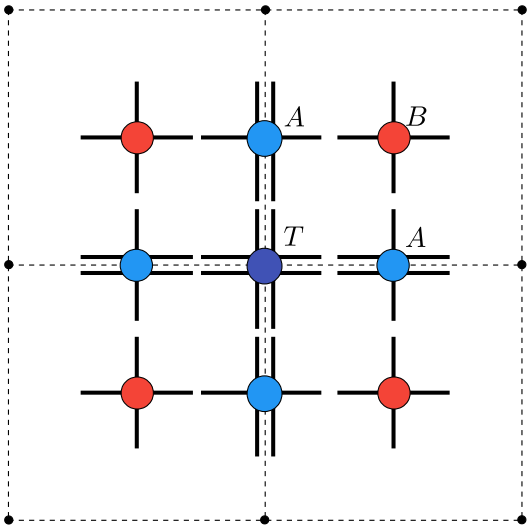

FIG. 38. Contraction pattern of basic tensors.

$$\langle Q \rangle = -\frac{1}{V}\frac{\partial \ln Z}{\partial \Theta}, \tag{292}$$

respectively. These results were compared to the Monte Carlo calculations of Göschl *et al.* (2017) when possible. A figure produced by Butt *et al.* (2020) showing the average plaquette as a function of the Θ parameter is depicted in Fig. 39 for a 4×4 lattice. In Fig. 40 we see a comparison between the tensor calculation and Monte Carlo simulation for a fixed volume on a 4×4 lattice of the topological charge. Butt *et al.* (2020) reported difficulty at larger volumes, perhaps owing to how the coarse-graining scheme determines which states are kept before knowing the boundary conditions on the lattice.

G. Additional topics and references

One of the primary goals in lattice gauge theory is the successful simulation of four-dimensional QCD at finite

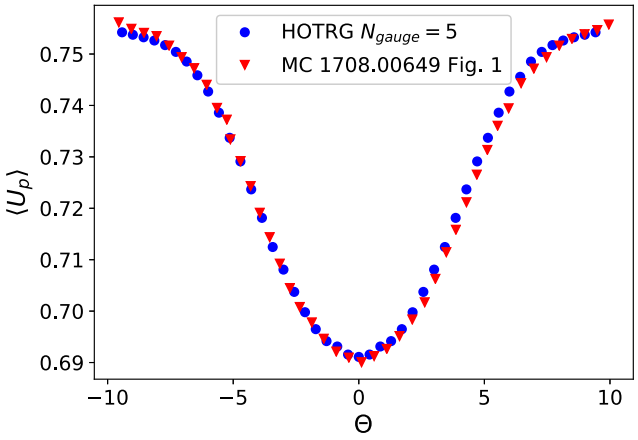

FIG. 39. The average plaquette as a function of the Θ parameter on a 4×4 lattice. Here $N_{\text{gauge}} = 5$ indicates a truncation on the m numbers such that m runs from −2 to 2. That is, $D_{\text{cut}} = 5$ initially on the B tensor. Adapted from Butt *et al.*, 2020.

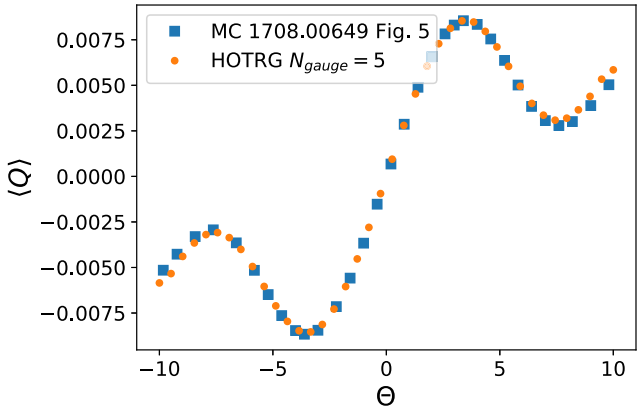

FIG. 40. The topological charge as a function of the Θ parameter on a 4×4 lattice. Here $N_{\text{gauge}} = 5$ indicates that five states where kept in the m numbers. The m values were allowed to run from -2 to 2 for each plaquette. That is, $D_{\text{cut}} = 5$ initially on the B tensor. Adapted from Butt *et al.*, 2020.

density. However, the computational time of the Grassmann HOTRG in four dimensions is extremely demanding: $\propto D_{\text{cut}}^{15}$ with the bond dimension D_{cut}. To achieve the goal, further improvements of the algorithm would be required, such as Monte Carlo approximation or sampling of the tensors and effective truncation of the bonds.

From an application point of view, nontrivial models in three dimensions would be within the range. The three-dimensional Thirring model that has a nontrivial phase structure and $(2+1)$-dimensional domain-wall fermion systems would be interesting targets.

In fermion systems, the spectra of tensors tend to have milder hierarchies than purely bosonic ones. Indeed, in their papers on the Schwinger model Shimizu and Kuramashi (2014a, 2014b, 2018) took the bond dimension of the tensors to be 160. This is large, so one cannot easily reproduce their results on standard, say, desktop or laptop, computers. Even in two dimensions serious calculations require improvements of the algorithms. In two dimensions, there are several improved schemes for bosonic tensor networks such as (loop) TNR (Evenbly and Vidal, 2015; Yang, Gu, and Wen, 2017), graph-independent local truncations (Hauru, Delcamp, and Mizera, 2018), and full environment truncation (Evenbly, 2018). Studies using these methods in the context of TLFT were completed by Kawauchi and Shinji (2018) and Delcamp and Tilloy (2020). Grassmannian versions of them would then all be possible directions.

Investigations of the Schwinger model with staggered fermions using the MPS formalism have also been conducted, with and without a topological term. Bañuls *et al.* (2013) studied the mass spectrum of the model and (Bañuls *et al.* (2017a) explored the phase diagram of the Schwinger model with two flavors of fermions in the presence of a chemical potential. They investigated the isospin as a function of the chemical potential and mappped the phase diagram in the chemical potential–mass plane. MPSs were also used to study the ground-state properties (Buyens *et al.*, 2014) and confinement and string breaking (Buyens *et al.*, 2016) of the one-flavor model. A more recent MPS study of the Schwinger model with the inclusion of a Θ term was done by Funcke, Jansen, and Kühn (2020). They looked at different thermodynamic quantities as a function of the Θ parameter, as well as the spectrum of the model. They also considered the continuum and chiral limits of the model where the Θ parameter becomes irrelevant.

XII. TRANSFER MATRIX AND HAMILTONIAN

We now move on from the topic of reformulating the partition function in terms of tensors to that of arranging their contractions so as to deduce a transfer matrix $\mathbb{T}$ that can be used to rewrite the partition function as in Eq. (33). Once the partition function has been written entirely in terms of local tensor contractions, it is possible to organize these index contractions into time layers. The natural choice is to use the indices attached to time links and/or spacetime plaquettes as the indices of the transfer matrices. Geometrically, the Hilbert space is located between two time slices, while the transfer matrix is centered on a time slice and connects two copies of the Hilbert space; see Fig. 43 for an illustration. To our knowledge, interchanging the role of these two types of layers is possible only by returning to configuration space.

In the rest of this section, we target models with continuous Abelian symmetries [the O(2) spin model and U(1) gauge theory] and describe their transfer matrices from a tensor perspective. However, it is not difficult to extend the discussion to other models.

A. Spin models

For spin models (Zou *et al.*, 2014), the transfer matrix can be constructed by taking all the tensors on a time slice and tracing over the spatial indices. This is illustrated for $D = 2$ and 3 in Fig. 41.

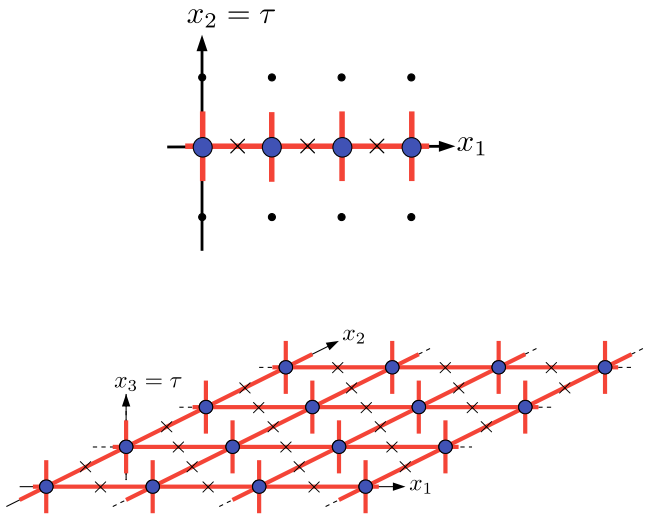

FIG. 41. Illustration of the transfer matrix for spin models in two and three dimensions. The black crosses indicate index contraction.

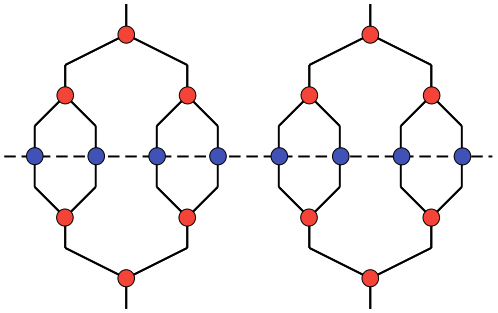

FIG. 42. Graphical representation of the coarse-graining truncation of the transfer matrix described in the text.

For the O(2) model, the following Hilbert space $\mathfrak{H}$ is the product of integer indices (see Sec. VII.A) attached to time links between two time slices:

$$\mathfrak{H} = |\{n\}\rangle = \bigotimes_{\mathbf{x},j} |n_{\mathbf{x},j}\rangle. \tag{293}$$

For $D = 2$ with N_s sites and periodic boundary conditions, the matrix elements of the transfer matrix $\mathbb{T}$ have the explicit form

$$\langle\{n'\}|\mathbb{T}|\{n\}\rangle = \sum_{\bar{n}_1\bar{n}_2,\ldots,\bar{n}_{N_s}} T^{(1,\tau)}_{\bar{n}_{N_s}\bar{n}_1 n_1 n'_1} T^{(2,\tau)}_{\bar{n}_1\bar{n}_2 n_2 n'_2} \cdots T^{(N_s,\tau)}_{\bar{n}_{N_s-1}\bar{n}_{N_s} n_{N_s} n'_{N_s}}, \tag{294}$$

with the individual tensors provided in Sec. VII. The transfer matrix can be coarse grained in the spatial dimension (Zou *et al.*, 2014; Yang *et al.*, 2016), as illustrated in Fig. 42. This method was used to perform numerical calculations by Zou *et al.* (2014), Yang *et al.* (2016), Unmuth-Yockey *et al.* (2018), and Zhang *et al.* (2018).

The symmetries of the model are completely encoded in Kronecker deltas appearing in the definition of the tensor (Meurice, 2019). This corresponds to a divergenceless condition and, with either periodic or open boundary conditions, the charges carried by the indices cannot flow out in the spatial directions. For the O(2) model, the sum of the time indices going into the time slice equals the sum of the indices going out of it. This conserved quantity can be identified as the charge of the initial and final states, and the transfer matrix commutes with the charge operator that counts the sum of the in or out indices. As we explain in Sec. XIII.A, setting some matrix elements to zero if some of the local indices exceed a value $n_{\max}$ in absolute value will not affect this property.

The transfer matrix can be used to define a Hamiltonian by taking an anisotropic limit where β becomes large on time links and small on space links (Fradkin and Susskind, 1978; Kogut, 1979). We define $\tilde{V} = 1/(\beta_\tau a_\tau)$, $\tilde{\mu} = \mu/a_\tau$, and $J = \beta_s/a_\tau$. The Hamiltonian is defined by

$$\mathbb{T} = \mathbb{1} - a_\tau \hat{\mathbb{H}} + \mathcal{O}(a_\tau^2). \tag{295}$$

Equation (295) will inherit the symmetry properties of the transfer matrix. Its explicit form is

$$\hat{\mathbb{H}} = \sum_{\mathbf{x}} \left[\frac{\tilde{V}}{2} \hat{L}_{\mathbf{x}}^2 - \tilde{\mu} \hat{L}_{\mathbf{x}} - \frac{J}{2} \sum_{\mathbf{x},\mu} (\hat{U}_{\mathbf{x}+\hat{\mu}} \hat{U}_{\mathbf{x}}^\dagger + \text{H.c.}) \right], \tag{296}$$

with the operator $\hat{L}|n\rangle = n|n\rangle$ and the operator $\hat{U} = e^{\hat{i}\hat{\varphi}}$, which corresponds to the insertion of $e^{i\varphi_x}$ in the path integral and raises the charge

$$\hat{U}|n\rangle = |n+1\rangle, \tag{297}$$

while its Hermitian conjugate lowers it,

$$(\hat{U})^\dagger |n\rangle = |n-1\rangle. \tag{298}$$

This implies the commutation relations

$$[\hat{L}, \hat{U}] = \hat{U}, \qquad [\hat{L}, \hat{U}^\dagger] = -\hat{U}^\dagger, \tag{299}$$

and

$$[\hat{U}, \hat{U}^\dagger] = 0. \tag{300}$$

B. Quantum simulations for the O(2) and O(3) model

For the O(2) nonlinear sigma model, Zou *et al.* (2014) used a mapping between the O(2) model and the Bose-Hubbard model. They related the two phase diagrams in the hopping–chemical potential plane and gave the explicit mapping between the variables in the two models. A similar approach can be seen as the limiting behavior of the Abelian Higgs model used by Bazavov *et al.* (2015) and Zhang *et al.* (2018) when the gauge coupling is taken to zero. Unmuth-Yockey *et al.* (2017) described a method to measure the second-order Rényi entropy for the O(2) model with a chemical potential in the limit, where it appears as the Bose-Hubbard model. They did this in the case of an ultracold atomic species trapped in an optical lattice at half filling. They also considered the experimental cost of extracting the central charge from measurements of the Rényi entropy.

There are a couple of results in progress toward quantum simulations of the O(3) nonlinear sigma model, but none currently on the principal chiral model. Schützhold and Mostame (2005) discussed a proposal for an analog quantum simulator for the O(3) nonlinear sigma model in two dimensions. The setup involves an idealized circuit of superconducting and insulating spheres and wires. The σ field is identified with the position of an electron living on the surface of an insulating sphere. The nearest-neighbor potential is discrete in space and identified with the difference in positions between adjacent electrons. This is mapped to the spatial gradient of the σ field. These two identifications are used to match couplings between the circuit model and the original nonlinear sigma model. Possible experimental parameters are discussed, as well as an analysis of noise contributions to the simulation.

Alexandru, Bedaque, Lamm, and Lawrence (2019) discussed an approach to quantum simulating the O(3) nonlinear sigma model using "digital" quantum computers implementing qubits. The original Hamiltonian is reexpressed in the angular momentum basis. In this basis (as previously

discussed) a truncation is made that preserves the O(3) symmetry of the model but reduces the local state space to four states. This is a natural truncation to the $l_{\max} = 1$ state, which possesses singlet and triplet states coming from the $l = 0$ and 1 states, respectively. This is precisely what one finds in the addition of angular momentum between the product of two spin-1/2 states. In this truncation and representation the model is cast in terms of two-qubit operators. Finally, Alexandru, Bedaque, Lamm, and Lawrence (2019) used a Suzuki-Trotter decomposition to write the Hamiltonian evolution in short, discrete steps. Each step is mapped to a quantum circuit over qubits. They simulated the Hamiltonian evolution on a classical computer and discussed results. They also performed runs on a quantum computer; however, at the time, they found "mostly noise."

C. Gauge models

The Hilbert space for the compact Abelian Higgs model, or its pure gauge U(1) limit (see Sec. IX.B), $\mathfrak{H}_G$ can be constructed as follows with the indices associated with spacetime plaquettes (see Sec. IX.A.1):

$$\mathfrak{H}_G = |\{\mathbf{e}\}\rangle = \bigotimes_{\mathbf{x},j} |e_{\mathbf{x},j}\rangle, \tag{301}$$

where the states $|e_{\mathbf{x},j}\rangle$ are eigenstates of $L_{\mathbf{x},j}$, which were defined following Eq. (296). Here we use $\hat{e}_{\mathbf{x},j}$ for the operator for clarity. The electric layer is a diagonal matrix $\mathbb{T}_E$ with matrix elements

$$\langle\{\mathbf{e}'\}|\mathbb{T}_E|\{\mathbf{e}\}\rangle = \delta_{\{\mathbf{e}\},\{\mathbf{e}'\}} T_E(\{\mathbf{e}\}), \tag{302}$$

where $T_E(\{\mathbf{e}\})$ are traced products of A tensors on time links with B tensors on spacetime plaquettes,

$$T_E(\{\mathbf{e}\}) = \mathrm{Tr} \prod_{\text{time } l} A^{(l)}_{m_1,\ldots,m_{2(D-1)}} \prod_{\text{sp time pl}} B^{(\mathrm{pl})}(\mathbf{e}). \tag{303}$$

The A tensor of the compact Abelian Higgs model is given in Eq. (189). It enforces Gauss's law in the pure gauge limit. The electric layer is illustrated in Fig. 43.

Similarly, we define as follows the magnetic matrix elements $\langle\{\mathbf{e}\}|\mathbb{T}_M|\{\mathbf{e}'\}\rangle$ with the indices $\mathbf{e}$ and $\mathbf{e}'$ carried by the time legs of the A tensors located on time links:

$$\langle\{\mathbf{e}'\}|\mathbb{T}_M|\{\mathbf{e}\}\rangle = \mathrm{Tr} \prod_{\text{space } l} A^{(l)}_{m_1,\ldots,m_{2(D-1)}}(\mathbf{e},\mathbf{e}') \prod_{\text{sp-sp pl}} B^{(\mathrm{pl})}. \tag{304}$$

The traces are taken over the spatial legs of the tensors, while the time legs are left open and carry the indices $\mathbf{e}$ and $\mathbf{e}'$. The magnetic layer is illustrated in Fig. 44.

We define the transfer matrix $\mathbb{T}$ as

$$\mathbb{T} \equiv [e^{-\beta_{\mathrm{pl}}} I_0(\beta_{\mathrm{pl}})]^{(V/N_\tau)D(D-1)/2} [e^{-\beta_l} I_0(\beta_l)]^{(V/N_\tau)D} \times \mathbb{T}_E^{1/2} \mathbb{T}_M \mathbb{T}_E^{1/2}, \tag{305}$$

with N_τ the number of sites in the temporal direction.

Proceeding as with the spin model (Fradkin and Susskind, 1978; Kogut, 1979), we define

$$\beta_{\tau\,\mathrm{pl}} = \frac{1}{a_\tau g_{\mathrm{pl}}^2}, \qquad \beta_{\tau l} = \frac{1}{a_\tau g_l^2} \tag{306}$$

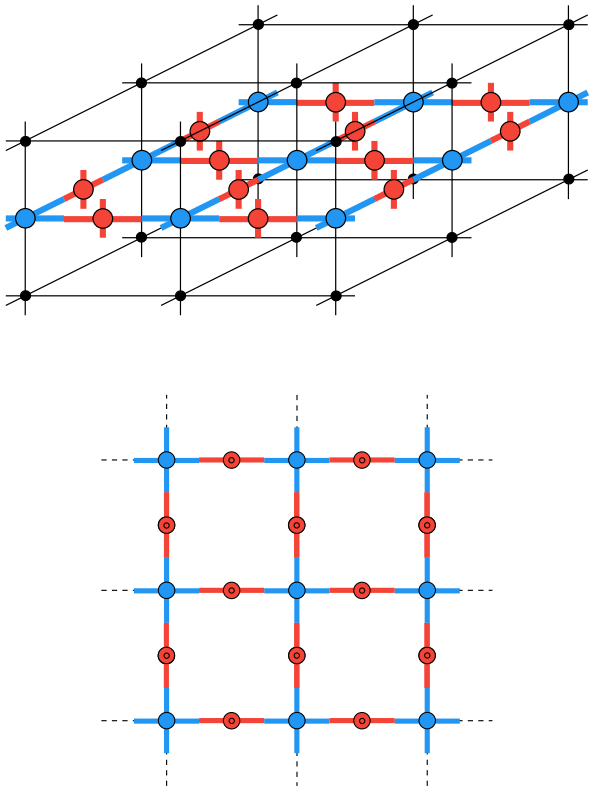

FIG. 43. Electric layer of the transfer matrix for $D = 3$ between two time slices (top graphic) and when viewed from above (bottom graphic).

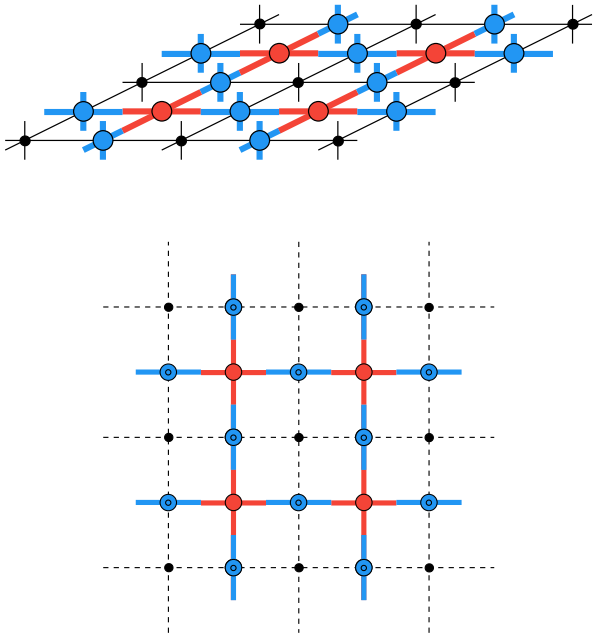

FIG. 44. Magnetic layer of the transfer matrix for $D = 3$ in a time slice (top graphic) and when viewed from above (bottom graphic).

for the couplings related to the time direction and

$$\beta_{s\,\mathrm{pl}} = a_\tau J_{\mathrm{pl}}, \qquad \beta_{sl} = a_\tau h_l \tag{307}$$

for the spatial couplings. We then obtain (Unmuth-Yockey, 2017; Meurice, 2020a)

$$\hat{\mathbb{H}} = \tfrac{1}{2} g_{\mathrm{pl}}^2 \sum_{\mathbf{x},j} (\hat{e}_{\mathbf{x},j})^2 + \tfrac{1}{2} g_l^2 \sum_{\mathbf{x}} \left(\sum_j (\hat{e}_{\mathbf{x},j} - \hat{e}_{\mathbf{x}-\hat{j},j}) \right)^2 - h_l \sum_{\mathbf{x},j} (\hat{U}_{\mathbf{x},j} + \mathrm{H.c.}) - J_{\mathrm{pl}} \sum_{\mathbf{x},j<k} (\hat{U}_{\mathbf{x},j} \hat{U}_{\mathbf{x}+\hat{j},k} \hat{U}^\dagger_{\mathbf{x}+\hat{k},j} \hat{U}^\dagger_{\mathbf{x},k} + \mathrm{H.c.}). \tag{308}$$

Notice that for the compact Abelian Higgs model the matter fields can absorb nonzero values in Eq. (174) (Gauss's law). However, in the limit where the link couplings are set to zero, we recover the pure gauge U(1) model where the A tensors for time links enforce Gauss's law. In Eq. (308), if the couplings h_l and g_l are set to zero, we recover the Hamiltonian for U(1) gauge theory in the Kogut-Susskind form.

Thus far everything we have done has been manifestly gauge invariant because the tensors resulted from a complete integration over the gauge fields. The partition function remains unchanged if we use a temporal gauge (Meurice, 2020a). If we gauge away the gauge fields on a time link instead of integrating over them, we lose the Gauss's law enforcement associated with that time link. However, the discrete Maxwell equations of Sec. IX.A.1 imply that if Gauss's law is satisfied on one electric layer, then it is also satisfied on all the other layers. With open boundary conditions in time, Gauss's law is trivially satisfied on the first and last layers. With periodic boundary conditions, we cannot gauge away the Polyakov loops, and we need to keep the integration over the temporal links for one layer. This is sufficient to enforce Gauss's law in that layer, and consequently everywhere.

If we prepare an initial state that satisfies Gauss's law, the exact time evolution will preserve this property. However, in the NISQ era various types of errors can introduce Gauss's law violations. For this reason, it has been argued (Unmuth-Yockey, 2019; Bender and Zohar, 2020; Kaplan and Stryker, 2020; Meurice, 2020a; Unmuth-Yockey, 2020) that it would be desirable to find a parametrization of Hilbert space where Gauss's law is automatically satisfied. One possibility discussed in Sec. XII.D is to use the unconstrained variables introduced in Sec. IX.A.2. A simple solution (Meurice, 2020a) for the Hilbert space $\mathfrak{H}_G$ introduced in Eq. (301) is to write $e_{\mathbf{x},i}$ as the discrete divergence of the antisymmetric tensors. For $D = 3$, we need only one field instead of two and obtain an optimal representation similar to that proposed by Unmuth-Yockey (2019) and Kaplan and Stryker (2020),

$$\begin{aligned} e_{\mathbf{x},1} &= -c_{\mathbf{x}} + c_{\mathbf{x}-\hat{2}}, \\ e_{\mathbf{x},2} &= +c_{\mathbf{x}} - c_{\mathbf{x}-\hat{1}}. \end{aligned} \tag{309}$$

For $D = 4$, we can write the electric field as the curl of a three-component vector (Meurice, 2020a). As this new vector is defined up to a gradient, we can attempt to use this freedom to remove, say, the first component. This would provide an expression of the form

$$\begin{aligned} e_{\mathbf{x},1} &= -c_{\mathbf{x},3} + c_{\mathbf{x}-\hat{2},3} + c_{\mathbf{x},2} - c_{\mathbf{x}-\hat{3},2}, \\ e_{\mathbf{x},2} &= +c_{\mathbf{x},3} - c_{\mathbf{x}-\hat{1},3}, \\ e_{\mathbf{x},3} &= -c_{\mathbf{x},2} + c_{\mathbf{x}-\hat{1},2}. \end{aligned} \tag{310}$$

However, the global implementation depends on the boundary conditions (Meurice, 2020a). A more recent discussion of Gauss's law for PBC and OBC was given by Bender and Zohar (2020). In summary, it is possible to enforce Gauss's law with no unphysical degrees of freedom that would waste computational resources. This can be done in any dimension and is better understood using the dual formulation discussed in Sec. XII.D.

D. Duality revisited and Gauss's law

The passage to the unconstrained variables discussed in the Lagrangian formalism (Sec. IX.A.2) solves Gauss's law in $D = 3$ and removes any gauge freedom from the model. In the continuous-time limit, when the transfer matrix is close to the identity and one can identify a Hamiltonian, there is no residual gauge freedom, and in fact the model is recast as a spin model.

In $D = 4$, the unconstrained variables that solve the divergenceless constraint in Abelian models are left with a redundancy themselves. That is, there is a local operation that leaves the new Hamiltonian unchanged, so the question of physical states remains. This arises from,

$$m_{x,\mu\nu} = \epsilon_{\mu\nu\rho\sigma} \Delta_\rho C_{x^*,\sigma}, \tag{311}$$

which introduces a new "gauge field" on the links of the dual lattice. The field-strength tensor for this gauge field possesses a redundancy similar to that of the original field; i.e., $C_{x,\mu} \to C'_{x,\mu} = C_{x,\mu} + \Delta_\mu \phi_x$ leaves the quantum Hamiltonian unchanged. In the electric basis (the L^z basis) this symmetry is manifested in an operator that raises and lowers all angular momentum numbers around a site by 1, $G_x = \prod_{\mu=1}^4 U^+_{x,\mu} U^-_{x-\hat{\mu},\mu}$. This operator commutes with the Hamiltonian. This identifies physical states as those that do not differ from others by arbitrary applications of G_x.

E. Quantum simulation of the Abelian Higgs model with cold atoms

There are a few concrete proposals for how to simulate the Abelian Higgs model using cold atoms trapped in an optical lattice. These methods either make use of the similarity between multispecies Bose-Hubbard models and the Abelian Higgs model or create an effective model only in terms of gauge degrees of freedom and construct the local Hilbert space of the model directly as a physical dimension and include operators for the new dimension.

Bazavov *et al.* (2015) proposed a two-species Bose-Hubbard model to simulate the Abelian Higgs model in a limit of infinite Higgs mass in $1 + 1$ dimensions. They used the Fourier expansion for the Abelian fields and rewrote the

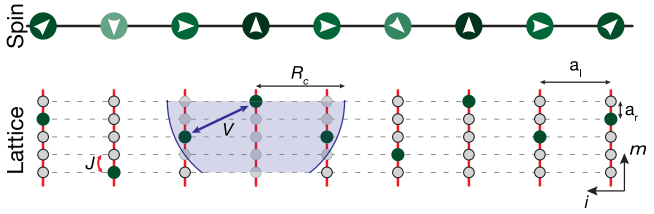

FIG. 45. Ladder setup in an optical lattice for the Abelian Higgs model in $1+1$ dimensions. Each vertical rung is a single spatial site and contains only a single atom, whose location along the rung indicates the angular momentum quantum number there. The nearest-neighbor interaction is mapped to the dressed Rydberg potential V between atoms. From Zhang *et al.*, 2018.

model in terms of discrete variables. The matter degrees of freedom were then integrated out, creating an effective theory only in terms of the discrete gauge-field degrees of freedom. Finally, they made use of the mapping between Schwinger bosons and SU(2) angular momentum operators to write the model in terms of bosonic creation-annihilation operators and number operators whose form matches that of a two-species Bose-Hubbard model. They compared the energy spectra between the original model and the Bose-Hubbard system and found good agreement.

González-Cuadra, Zohar, and Cirac (2017) proposed another multispecies Bose-Hubbard model to simulate the Abelian Higgs model in $2+1$ dimensions. They used a six-species Bose-Hubbard Hamiltonian and again found a mapping between their electric field and parallel transport operators and bosonic creation-annihilation and number operators. They created the plaquette interaction as a higher-order, perturbative, effective correction to the original Hamiltonian and reported on possible observables that could be seen in the laboratory experiment.

Zhang *et al.* (2018) took a different approach than the previous two researcher groups. Instead of attempting to capture the local Hilbert space with one from a composite multispecies Bose-Hubbard model, the discrete angular momentum quantum numbers associated with the electric field numbers are represented as new physical locations on a higher-dimensional lattice. For the $(1+1)$-dimensional Abelian Higgs model, a ladder is constructed where one of the lattice directions represents the spatial dimension and the other direction, the rungs of the ladder, represents the different possible angular momentum states. There is then much freedom regarding which atomic species to populate the lattice with. Zhang *et al.* (2018) used a dressed Rydberg potential to describe the two-body interactions. They proposed measuring the Polyakov loop and gave a prescription for how to do it. A figure of the lattice setup in the case of a five-state truncation is shown in Fig. 45.

F. Algebraic aspects of the Hamiltonian formulation

As practical implementations require a finite number of states, we now discuss the effect of a truncation on the algebra defined by Eqs. (299) and (300). By truncation, we mean that there is an $n_{\max}$ for which

$$\hat{U}|n_{\max}\rangle = 0, \qquad (\hat{U})^\dagger|-n_{\max}\rangle = 0. \tag{312}$$

These modifications contradict Eq. (300) since if $\hat{U}$ and $\hat{U}^\dagger$ commute, we can apply $\hat{U}^\dagger$ to the first of Eqs. (312) and obtain the result that $\hat{U}|n_{\max}-1\rangle$ is also zero, etc. If we consider the commutation relations with the restriction (312), we see that the only changes are

$$\begin{aligned}\langle n_{\max}|[\hat{U},\hat{U}^\dagger]|n_{\max}\rangle &= 1,\\ \langle -n_{\max}|[\hat{U},\hat{U}^\dagger]|-n_{\max}\rangle &= -1,\end{aligned} \tag{313}$$

instead of 0. The important point is that the truncation does not affect the basic expression of the symmetry in Eq. (300). It affects only matrix elements involving the $\hat{U}$ operators, and not in a way that contradicts charge conservation. For a related discussion of the algebra for the O(3) model, see Bruckmann, Jansen, and Kühn (2019).

Other deformations of the original Hamiltonian algebra defined by Eqs. (299) and (300) appear in the quantum link formulation of lattice gauge theories (Brower, Chandrasekharan, and Wiese, 1999). In this approach, one picks a representation of the SU(2) algebra and replace $\hat{U}$ with the raising operator S^+. Equation (312) is then satisfied if the dimension of the representation is $2n_{\max}+1$, but Eq. (300) becomes

$$[\hat{S}^+,\hat{S}^-] = 2\hat{S}^z. \tag{314}$$

Finally, we comment upon algebraic aspects of the Gaussian quadrature discussed in Sec. X.B. This numerical integration method averages over a finite number of sampling points which are the zeros of a Hermite polynomial of sufficiently large order $n_{\max}+1$. This can be related to a truncation of the standard harmonic oscillator algebra in the following way. If we use the standard raising and lowering operators on energy eigenstates $|n\rangle$ to calculate $\langle x|\hat{x}|n\rangle$, we recover the Hermite polynomial recursion formula. These relations still hold for the zeros of $H_{n_{\max}+1}$ until we reach the level $n_{\max}$. Iterating one more time provides a relation equivalent to

$$\hat{a}^\dagger|n_{\max}\rangle = 0. \tag{315}$$

The modified commutation relation becomes

$$[\hat{a},\hat{a}^\dagger] = \mathbb{1} - (n_{\max}+1)|n_{\max}\rangle\langle n_{\max}|. \tag{316}$$

A better algebraic understanding of the results of Sec. X.B would certainly be of great interest.

G. Additional topics and references

In Sec. IV.C tensor network studies of the Hamiltonian formalism in $1+1$ dimensions were reviewed. For $2+1$ and $3+1$ dimensions in the Hamiltonian formalism, there are relevant studies using projected entangled pair states and tree-tensor networks. Felser *et al.* (2020) considered $(2+1)$-dimensional electrodynamics at finite density. Electrodynamics in $3+1$ dimensions, again at finite density, was studied using tree-tensor networks by Magnifico *et al.* (2021). Conversely, $\mathbb{Z}_3$ gauge theory was studied using

PEPSs by Robaina, Bañuls, and Cirac (2021), and Abelian U(1) and non-Abelian SU(2) gauge theories were considered by Zohar *et al.* (2015, 2016). An entanglement renormalization group approach to $(2+1)$- and $(3+1)$-dimensional gauge theories was explored by Tagliacozzo and Vidal (2011). In the Hamiltonian formalism, the idea of a hybrid algorithm between tensor networks and the Monte Carlo method was discussed by Zohar and Cirac (2018a) and Emonts *et al.* (2020). Expansions in representations of continuous groups (Tagliacozzo, Celi, and Lewenstein, 2014; Zohar and Burrello, 2015) leading to figures related to Figs. 43 and 44 can be found in the tensor network literature. For recent work on SU(3), see Ciavarella, Klco, and Savage (2021).

An examination of the entanglement area law and how it appears in PEPS constructions, as well as the relationship between PEPSs and thermal states of local spin systems, was carried out by Verstraete *et al.* (2006). The inherent redundancy in a PEPS construction and its relationship to symmetry was discussed by Molnar *et al.* (2018). Furthermore, gauging a PEPS with a global symmetry to construct a PEPS with a local symmetry was studied by Haegeman *et al.* (2015) and Zohar and Burrello (2016).

XIII. ADDITIONAL ASPECTS

A. Symmetries and truncations

As explained in the Introduction, the implementation of field theory calculations with quantum computers requires discretizations and truncations of the problems considered. As symmetries play a crucial role in most of these calculations, we need to understand the effects of discretization on the realization of the original symmetries. The effects of the discretization of spacetime are well understood and the remaining discrete symmetries (discrete translations and rotations) are used consistently by lattice practitioners. On the other hand, the fate of internal continuous symmetries in reformulations involving discrete character expansions and truncations is a more complicated question. We report here recent progress on this question that has a great deal of generality and applies to global, local, continuous, and discrete symmetries (Meurice, 2019, 2020a).

We consider generic symmetries for a generic lattice model with action $S[\Phi]$, where Φ denotes a field configuration of fields ϕ_ℓ attached to locations ℓ that can be sites, links, or higher-dimensional objects. The partition function reads

$$Z = \int \mathcal{D}\Phi e^{-S[\Phi]}, \tag{317}$$

with $\mathcal{D}\Phi$ the measure of integration over the fields. We define expectation values of a function of the fields f as

$$\langle f(\Phi)\rangle = \frac{1}{Z}\int \mathcal{D}\Phi f(\Phi) e^{-S[\Phi]}. \tag{318}$$

A symmetry is defined as a field transformation

$$\phi_\ell \to \phi'_\ell = \phi_\ell + \delta\phi_\ell \tag{319}$$

such that the action and the integration measure are preserved. These invariances imply that

$$\langle f(\Phi)\rangle = \langle f(\Phi + \delta\Phi)\rangle. \tag{320}$$

If the action is not exactly invariant, $\exp(\delta S)$ is inserted in the expectation value on the right-hand side of the equation.

The O(2) model discussed in Sec. VII.A is invariant under the global shift

$$\varphi'_x = \varphi_x + \alpha. \tag{321}$$

Assuming that the function f is 2π periodic in its M variables, we expand in Fourier modes and, after using Eq. (320), obtain the following:

$$\text{If } \sum_{i=1}^{M} n_i \neq 0, \quad \text{then } \langle e^{i(n_1\varphi_{x_1}+\cdots+n_M\varphi_{x_M})}\rangle = 0. \tag{322}$$

This global selection rule can be explained (Meurice, 2019) in terms of the selection rule of the microscopic tensors at each site given in Eq. (126). It is a divergenceless condition that can be interpreted as a discrete version of Noether's theorem. If we enclose a site x in a small (compared to the lattice spacing) D-dimensional cube, the sum of indices corresponding to positive directions ($n_{x,\text{out}}$) is the same as the sum of indices corresponding to negative directions ($n_{x,\text{in}}$). For instance, in two dimensions the sum of the left and bottom indices equals the sum of the right and top indices. By assembling such elementary objects (tracing over indices corresponding to their interface), we can construct an arbitrary domain. Each tracing automatically cancels an in index with an out index and, consequently, at the boundary of the domain the sum of the in indices remains the same as the sum of the out indices. This discrete version of Gauss's theorem is illustrated for $D = 2$ in Fig. 46. We can pursue this process until we reach the boundary. For PBCs the in and out cancel, and for OBCs all the indices at the boundary are zero. In both cases, the system is "isolated," in the sense that no flux escapes to or comes from the environment. If we now remove one site from the entire domain, the pointwise conservation inside the rest of the domain implies that the indices connecting to the missing site satisfy the divergenceless condition independently.

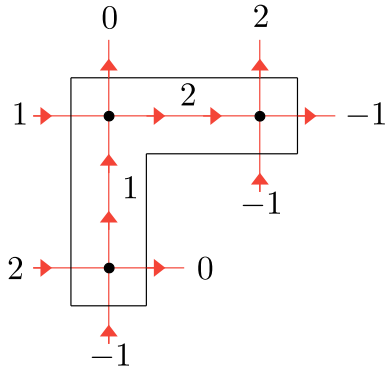

FIG. 46. Example of flux cancellations in $D = 2$. The total flux in and out of the upside-down L-shaped domain is $+1$.

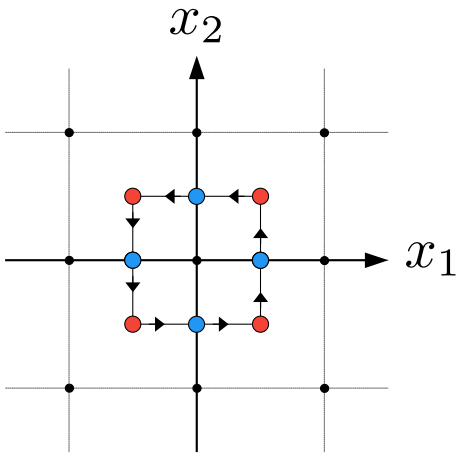

FIG. 47. Illustration of the fact that one divergenceless condition is redundant for $D = 2$.

This has a simple interpretation in terms of global symmetry of the model (Meurice, 2020a). We can use the symmetry to fix the value of ϕ at the missing site instead of integrating over the possible values because, as just explained, the divergenceless condition resulting from this integration is redundant.

We can now understand the global selection rule of Eq. (322). The insertion of various $e^{in_Q\varphi_x}$ is equivalent to inserting an impure tensor which differs from the pure tensor by the Kronecker symbol replacement $\delta_{n_{x,\text{out}},n_{x,\text{in}}} \to \delta_{n_{x,\text{out}},n_{x,\text{in}}+n_Q}$. Proceeding as before for PBCs or OBCs, this implies that the sum of the charges should be zero.

To summarize, the global selection rule is a consequence of the selection rule at each site that is the Kronecker delta in the expression of the tensors. It is independent of the particular values taken by the tensors (like Bessel functions). Thus, if we set some of the tensor elements to zero, as we do in a truncation, this does not affect the global selection rule and truncations are compatible with symmetries (Meurice, 2019).

The reasoning can be extended to local symmetries (Meurice, 2020a). For the CAHM, the divergenceless condition for the $n_{x,\mu}$ is redundant with the selection rule coming from the integration over the gauge fields, as expressed in Eq. (187). This means that we can eliminate the φ field with the unitary gauge. It was shown (Meurice, 2019) that in the pure gauge limit the set of equations (169) are not independent. If we pick a site, we can construct an in-out partition for the legs attached to links coming out of this site. The sum of in indices is the same as the sum of the out indices, and if we assemble them on the boundary of a D-dimensional cube, one of the divergenceless conditions follows from the other $2D-1$ conditions. This is illustrated for $D = 2$ in Fig. 47, where three of the delta functions on the A tensors attached to the links imply the fourth one.

The redundancy argument extends to discrete $\mathbb{Z}_q$ subgroups of U(1), where the divergenceless condition is expressed modulo q and the infinite set of Bessel functions are replaced by the q discrete ones. We conclude that Noether's theorem can be expressed in the tensor formulation context in this way: for each symmetry, there is a corresponding tensor redundancy. This applies to global, local, continuous, and discrete Abelian symmetries (Meurice, 2020a).

B. Topological considerations

In classical field theory, the boundary conditions play an important role in the investigation of topological solutions. As a simple example, if an angle variable φ satisfies the Laplace equation in $D = 1$, then PBCs allow the existence of solutions with any winding number. On the other hand, for arbitrary Dirichlet boundary conditions, the concept of winding number is not applicable because the one-dimensional interval does not have the topology of a circle.

In the $D = 1$ O(2) model, we observe features that are reminiscent of this observation. For PBCs, we can assemble the following tensors with any index n:

$$T_{nn'} = \delta_{nn'}\sqrt{I_n(\beta)I_{n'}(\beta)} \tag{323}$$

and

$$Z_{\text{PBC}} = \text{Tr}[T^{N_\tau}] = \sum_{n=-\infty}^{\infty} I_n(\beta)^{N_\tau}. \tag{324}$$

On the other hand, for OBCs we have a zero index at the ends and

$$Z_{\text{OBC}} = I_0(\beta)^{N_\tau - 1}. \tag{325}$$

It is often believed that the contributions for various n in Z_{PBC} correspond to the topological sectors of the classical equations of motion that become Laplace's equation in the continuum limit (so for large β). This is not correct because the $I_n(\beta)$ differ from I_0 by corrections of $-n^2/(2\beta)$, as shown in Eq. (128), while in the semiclassical solution one expects suppression of the form $\exp(-\beta n^2 C)$ for some calculable constant C. However, the two types of behaviors are swapped after the Poisson summation

$$\sum_{\ell=-\infty}^{\infty} e^{-B/2\ell^2} = \sqrt{\frac{2\pi}{B}} \sum_{n=-\infty}^{\infty} e^{[-(2\pi)^2/2B]n^2}. \tag{326}$$

A detailed analysis of the classical solutions (Meurice, 2020a) showed that $B = \beta(2\pi)^2/N_\tau$, and that summations over the winding numbers using Poisson summation and the calculation of the quadratic fluctuations precisely reproduce the leading behavior of Eq. (324) in the large-β limit. Similar observations were made by Akerlund and Forcrand (2015) for a version of the O(2) model where the fluctuations are limited.

Similar results were obtained for the $D = 2$ pure gauge U(1) model. In these calculations, the possibility of fixing the values of variables that lead to redundant selection rules to arbitrary values (as discussed in Sec. XIII.A) removes the zero modes from the quadratic fluctuation calculations. Note also that it is possible to construct models where the large-β approximations are exact. Questions pertaining to topological configurations and duality were discussed for Abelian gauge models of this type in various dimensions by Banks, Myerson, and Kogut (1977), Savit (1977), Gattringer, Goschl, and Marchis (2018), and Sulejmanpasic and Gattringer (2019).

C. Quantum gravity

Tensor networks have also found use in the study of quantum gravity. One of the directions where tensor networks have appeared is in the "spin-foam" formulation of quantum gravity (Perez, 2013). Dittrich, Mizera, and Steinhaus (2016) developed a tensor network formulation along with a coarse-graining scheme where the intention was to use it on a spin-foam partition function, although it is applicable in other situations. The algorithm was sketched out, and some numerical results for the two- and three-dimensional Ising models were presented. Asaduzzaman, Catterall, and Unmuth-Yockey (2020) started with the partition function for two-dimensional gravity, where the gauge symmetry was extended to unify the tetrad and spin-connection variables into a single connection. They presented a tensor formulation and studied the zeros of the partition function (Fisher's zeros) in the complex-coupling plane.

XIV. CONCLUSIONS

In summary, TLFT provides new ways to approach models studied by lattice gauge theorists. For models with compact field variables, character expansions and orthogonality relations provide ways to calculate the difficult integrals exactly and replace them with discrete sums. For continuous field variables, the sums are infinite and need to be truncated for practical implementations. These truncations preserve global and local symmetries.

We showed that, by combining tensor blocking and truncations, we can obtain coarse-grained versions of the original model where the new "effective" tensors are assembled in the same way as the original tensors while different values are taken. The TRG flows in the space of tensors replace the RG flows in the space of effective interactions. The effective tensors remain local in the coarse-grained system of coordinates. When the Euclidean action is real, TRG calculations can be compared with accurate results obtained using importance sampling in the original Lagrangian formulation. Tensor sampling could also be conducted by generalizations of the worm algorithm. TRG calculations can be extended to the case of complex actions and evade sign problems.

Note that if a reasonable control of the truncations can be reached for values of D_{cut} that are achievable with current computers, the computation cost scales logarithmically with the volume of the system, which is exceptionally efficient. The scaling of the cost with the dimension can be seen as an obstacle; however, recent progress in three and four dimensions provides an optimistic outlook.

The continuum limits of lattice models can be constructed in the vicinity of RG fixed points. Universal quantities such as the critical exponents can be extracted by linearizing the RG transformation near the fixed point. The naive approach for this program has to be amended due to the existence of unphysical fixed points. This requires a detailed understanding of the UV and IR entanglement.

TLFT allows for the construction of transfer matrices and smoothly connects the classical Lagrangian approach at Euclidean time to the Hamiltonian approach. The discreteness of the reformulation combined with truncations provides approximate Hamiltonians that are suitable for quantum simulation experiments and quantum computations. TLFT is a natural tool for designing quantum circuits. In the NISQ era, benchmarking is crucial for assessing the progress in this direction. Hybrid formalisms combining real and imaginary time can be accommodated easily by TLFT and may play an important role in the near future.

The TLFT program is making good progress toward the long-term goal of performing QCD calculations. We expect that it will play an important role in developing practical methods to approach nuclear matter, jet physics, and fragmentation. Active collaborations between the lattice gauge theory and condensed matter communities seem essential to achieving these goals and will hopefully provide benefits in both areas.

ACKNOWLEDGMENTS

Y. M. thanks the late C. Itzykson, D. Speiser, and J. Weyers for their teaching on group theory, Pontryagin duality, the Peter-Weyl theorem, and strong coupling expansions. We thank M. C. Bañuls, J. Bloch, S. Catterall, E. Gustafson, Z. Hang, M. Hite, R. Maxton, D. Simons, Z. Y. Xie, J. Zeiher, J. Zhang, H. Zou, and members of the QuLAT Collaboration, for useful discussions and comments. This work was supported in part by the U.S. Department of Energy (DOE) under Awards No. DE-SC0010113 and No. DE-SC0019139. This work is supported by the DOE QuantISED program through the theory consortium "Intersections of QIS and Theoretical Particle Physics" at Fermilab. This manuscript has been co-authored by employees of Fermi Research Alliance, LLC, under Contract No. DE-AC02-07CH11359 for the U.S. Department of Energy, Office of Science, Office of High Energy Physics.

APPENDIX: REVIEW OF MATHEMATICAL RESULTS

1. Character expansions

One of the most important relations that we use in this review is the change of basis called the character expansion. In the cases considered here, this relates a compact variable (discrete and bounded or continuous and bounded) to their Pontryagin dual. The relevant relation can be written as

$$f(x_\alpha) = \sum_{k_\alpha} \lambda_{k_\alpha} \chi^{k_\alpha}(x_\alpha). \tag{A1}$$

In Eq. (A1) x_α is the compact variable under consideration (it can be a matrix or a spin, for example), and f is a "class function," a function that depends only on the trace of the compact variables. k_α is the dual variable, which takes on the values of the irreducible representations of the group to which x_α belongs. Finally, χ^{k_α} are the characters of the group, which are complete and orthogonal. In practice, we use the following,

$$e^{\beta\sigma} = \sum_{n=0}^{1} \lambda_n(\beta)\sigma^n, \tag{A2}$$

$$e^{\beta\cos\theta} = \sum_{n=-\infty}^{\infty} I_n(\beta) e^{in\theta}, \tag{A3}$$

$$e^{\beta \mathrm{Tr}[U]} = \sum_{r=0}^{\infty} F_r(\beta)\chi^r(U), \tag{A4}$$

for the groups $\mathbb{Z}_2$, U(1), and SU(2), where λ_n, I_n, and F_r are the expansion coefficients and σ^n, $e^{in\theta}$, and $\chi^r(U)$ are the characters of the respective groups. For $\mathbb{Z}_2$ the expansion coefficients are given by $\lambda_0 = \cosh\beta$ and $\lambda_1 = \sinh\beta$. For U(1) the coefficients are given by the modified Bessel functions. For SU(2) the coefficients are given by (Itzykson and Drouffe, 1991)

$$F_r(\beta) = I_{2r}(\beta) - I_{2r+2}(\beta), \tag{A5}$$

where I_n is again the modified Bessel function of the order of n.

2. Orthogonality and completeness

As previously mentioned, the expansions in Eq. (A2) are examples of the completeness and orthogonality of the characters. In each of those cases we have

$$\frac{1}{2}\sum_{\sigma} \sigma^n \sigma^m = \delta^{(2)}_{n,m}, \tag{A6}$$

$$\int_{-\pi}^{\pi} \frac{d\theta}{2\pi} e^{in\theta} e^{-im\theta} = \delta_{n,m}, \tag{A7}$$

$$\int dU \chi^r(U)\chi^{r'}(U) = (2r+1)^{-1}\delta_{r,r'}, \tag{A8}$$

where $\delta^{(2)}$ is a Kronecker delta with the equivalency taken modulo 2. We also use the following orthogonality of the matrix representations of group elements under the Haar measure:

$$\int dU D^r_{mn}(U) D^{*r'}_{m'n'}(U) = (2r+1)^{-1}\delta_{r,r'}\delta_{m,m'}\delta_{n,n'}, \tag{A9}$$

with the asterisk indicating complex conjugation without transposition. The D matrices are related to the characters through the trace $\chi^r(U) = \mathrm{Tr}[D^r(U)]$.

On the other hand, these characters obey a completeness relation. This is given by the sum over the representations rather than the original group variables,

$$\frac{1}{2}\sum_{n=0}^{1} \sigma^n \sigma'^n = \delta_{\sigma,\sigma'}, \tag{A10}$$

$$\sum_{n=-\infty}^{\infty} e^{in(\theta-\theta')} = \delta(\theta-\theta'), \tag{A11}$$

$$\sum_{r=0}^{\infty}(2r+1)\mathrm{Tr}[D^r(U)D^{r\dagger}(U')] = \delta(U,U'), \tag{A12}$$

$$\sum_{r=0}^{\infty}(2r+1)\chi^r(UU'^{-1}) = \delta(U,U'). \tag{A13}$$

3. Singular value decomposition

The SVD plays a central role in many different parts of this review, and when dealing with compact variables it is completely determined by the character expansion. Here we give a bare working knowledge of how it will be used. One of the basic ideas is to regard Boltzmann factors $f(x_\alpha, x_\beta)$, which appear in the partition function, as $K \times K$ matrices when x_α and x_β take K values, and with that interpretation perform the following SVD:

$$f(x_\alpha, x_\beta) = \sum_{j=1}^{K} U_{x_\alpha j}\lambda_j V^\dagger_{jx_\beta}, \tag{A14}$$

where $\{\lambda\}$ are the singular values that are assumed to be in descending order ($\lambda_1 \geq \lambda_2 \geq \cdots \geq \lambda_K \geq 0$) and U and V are unitary matrices. This decomposition can be done for any matrix, and they need not immediately have the interpretation of a Boltzmann factor.

When the x_α can be identified with the elements of an additive group and if the matrix elements depend only on $x_\alpha - x_\beta$, the U and V matrices are square matrices that can be expressed in terms of the characters discussed in Sec. III.D. For the $\mathbb{Z}_q$ group, we have $K = q$,

$$U_{x_\alpha j} = \exp\left(i\frac{2\pi}{q} j x_\alpha\right) \tag{A15}$$

and

$$V_{x_\beta j} = \exp\left(i\frac{2\pi}{q} j x_\beta\right). \tag{A16}$$

Another case that occurs often is to use the SVD to split a higher-dimensional array in two. Consider a generic tensor A_{ijkl} with dimensions $(D_{\mathrm{cut}}, D_{\mathrm{cut}}, D_{\mathrm{cut}}, D_{\mathrm{cut}})$. Suppose that one wanted to somehow factorize this tensor into two smaller rank tensors, one with indices i and j, and the other with indices k and l. One can then do the following:

$$A_{ijkl} \to A_{(i\otimes j)(k\otimes l)} \tag{A17}$$

$$= A_{IJ} = \sum_{M,M'=1}^{D^2_{\mathrm{cut}}} U_{IM}\lambda_M \delta_{MM'} V^\dagger_{M'J} \tag{A18}$$

$$= \sum_{M=1}^{D^2_{\mathrm{cut}}} (U_{IM}\sqrt{\lambda}_M)(\sqrt{\lambda}_M V^\dagger_{MJ}) \tag{A19}$$

$$= \sum_{M=1}^{D^2_{\mathrm{cut}}} B_{ijM} C_{Mkl}, \tag{A20}$$

which is the split that we were looking for. This allows any tensor to be split exactly into smaller rank tensors, with the sum over intermediate states as the price.

REFERENCES

Abramowitz, Milton, and Irene A. Stegun, 1965, *Handbook of Mathematical Functions: With Formulas, Graphs, and Mathematical Tables*, Vol. 55 (Courier Corporation, North Chelmsford, MA).

Adachi, Daiki, Tsuyoshi Okubo, and Synge Todo, 2020, "Anisotropic tensor renormalization group," Phys. Rev. B **102**, 054432.

Akerlund, Oscar, and Philippe de Forcrand, **2015**, "U(1) lattice gauge theory with a topological action," J. High Energy Phys. 06, 183.

Akiyama, Shinichiro, Daisuke Kadoh, Yoshinobu Kuramashi, Takumi Yamashita, and Yusuke Yoshimura, 2020, "Tensor renormalization group approach to four-dimensional complex ϕ^4 theory at finite density," J. High Energy Phys. 09, 177.

Akiyama, Shinichiro, Yoshinobu Kuramashi, Takumi Yamashita, and Yusuke Yoshimura, 2020, "Phase transition of four-dimensional Ising model with tensor network scheme," Proc. Sci. LATTICE2019, 138 [arXiv:1911.12954].

Akiyama, Shinichiro, Yoshinobu Kuramashi, Takumi Yamashita, and Yusuke Yoshimura, **2021**, "Restoration of chiral symmetry in cold and dense Nambu–Jona-Lasinio model with tensor renormalization group," J. High Energy Phys. 01, 121.

Alexandru, Andrei, Paulo F. Bedaque, Siddhartha Harmalkar, Henry Lamm, Scott Lawrence, and Neill C. Warrington (NuQS Collaboration), 2019, "Gluon field digitization for quantum computers," Phys. Rev. D **100**, 114501.

Alexandru, Andrei, Paulo F. Bedaque, Henry Lamm, and Scott Lawrence (NuQS Collaboration), 2019, "σ Models on Quantum Computers," Phys. Rev. Lett. **123**, 090501.

Anderson, P. W., 1973, "Resonating valence bonds: A new kind of insulator?," Mater. Res. Bull. **8**, 153–160.

Aoki, Ken-Ichi, Tamao Kobayashi, and Hiroshi Tomita, 2009, "Domain wall renormalization group analysis of two-dimensional Ising model," Int. J. Mod. Phys. B **23**, 3739–3751.

Aoki, S., *et al.* (Flavour Lattice Averaging Group), 2020, "FLAG Review 2019: Flavour Lattice Averaging Group (FLAG)," Eur. Phys. J. C **80**, 113.

Asaduzzaman, Muhammad, Simon Catterall, and Judah Unmuth-Yockey, 2020, "Tensor network formulation of two-dimensional gravity," Phys. Rev. D **102**, 054510.

Atiyah, M. F., 2007, "Duality in mathematics and physics" (unpublished), https://fme.upc.edu/ca/arxius/butlleti-digital/riemann/071218_conferencia_atiyah-d_article.pdf.

Bailey, Jon A., *et al.* (Fermilab Lattice and MILC Collaborations), 2015, "$|V_{ub}|$ from $b \to \pi \ell \nu$ decays and $(2+1)$-flavor lattice QCD," Phys. Rev. D **92**, 014024.

Baker, George A., 1972, "Ising model with a scaling interaction," Phys. Rev. B **5**, 2622–2633.

Bal, M., M. Mariën, J. Haegeman, and F. Verstraete, 2017, "Renormalization Group Flows of Hamiltonians Using Tensor Networks," Phys. Rev. Lett. **118**, 250602.

Balian, R., J. M. Drouffe, and C. Itzykson, 1975, "Gauge fields on a lattice. III. Strong-coupling expansions and transition points," Phys. Rev. D **11**, 2104–2119.

Banerjee, D., M. Bögli, M. Dalmonte, E. Rico, P. Stebler, U.-J. Wiese, and P. Zoller, 2013, "Atomic Quantum Simulation of U(N) and SU(N) Non-Abelian Lattice Gauge Theories," Phys. Rev. Lett. **110**, 125303.

Banerjee, D., M. Dalmonte, M. Muller, E. Rico, P. Stebler, U. J. Wiese, and P. Zoller, 2012, "Atomic Quantum Simulation of Dynamical Gauge Fields Coupled to Fermionic Matter: From String Breaking to Evolution after a Quench," Phys. Rev. Lett. **109**, 175302.

Banerjee, Debasish, and Shailesh Chandrasekharan, 2010, "Finite size effects in the presence of a chemical potential: A study in the classical nonlinear O(2) sigma model," Phys. Rev. D **81**, 125007.

Banks, Tom, R. Myerson, and John B. Kogut, 1977, "Phase Transitions in Abelian Lattice Gauge Theories," Nucl. Phys. **B129**, 493–510.

Bañuls, M. C., K. Cichy, K. Jansen, and J. I. Cirac, **2013**, "The mass spectrum of the Schwinger model with matrix product states," J. High Energy Phys. 11, 158.

Bañuls, Mari Carmen, and Krzysztof Cichy, 2020, "Review on novel methods for lattice gauge theories," Rep. Prog. Phys. **83**, 024401.

Bañuls, Mari Carmen, Krzysztof Cichy, J. Ignacio Cirac, Karl Jansen, and Stefan Kühn, 2017a, "Density Induced Phase Transitions in the Schwinger Model: A Study with Matrix Product States," Phys. Rev. Lett. **118**, 071601.

Bañuls, Mari Carmen, Krzysztof Cichy, J. Ignacio Cirac, Karl Jansen, and Stefan Kühn, 2017b, "Efficient Basis Formulation for $(1+1)$-Dimensional SU(2) Lattice Gauge Theory: Spectral Calculations with Matrix Product States," Phys. Rev. X **7**, 041046.

Bañuls, Mari Carmen, Krzysztof Cichy, J. Ignacio Cirac, Karl Jansen, and Stefan Kühn, **2018**, "Tensor networks and their use for lattice gauge theories," Proc. Sci. LATTICE2018, 022 [arXiv:1810.12838].

Bañuls, Mari Carmen, *et al.*, 2020, "Simulating lattice gauge theories within quantum technologies," Eur. Phys. J. D **74**, 165.

Barthel, Thomas, Carlos Pineda, and Jens Eisert, 2009, "Contraction of fermionic operator circuits and the simulation of strongly correlated fermions," Phys. Rev. A **80**, 042333.

Baxter, R. J., 1968, "Dimers on a rectangular lattice," J. Math. Phys. (N.Y.) **9**, 650–654.

Bazavov, Alexei, Simon Catterall, Raghav G. Jha, and Judah Unmuth-Yockey, 2019, "Tensor renormalization group study of the non-Abelian Higgs model in two dimensions," Phys. Rev. D **99**, 114507.

Bazavov, Alexei, Yannick Meurice, Shan-Wen Tsai, Judah Unmuth-Yockey, and Jin Zhang, 2015, "Gauge-invariant implementation of the Abelian Higgs model on optical lattices," Phys. Rev. D **92**, 076003.

Bender, Julian, and Erez Zohar, 2020, "Gauge redundancy-free formulation of compact QED with dynamical matter for quantum and classical computations," Phys. Rev. D **102**, 114517.

Berges, Juergen, Nikolaos Tetradis, and Christof Wetterich, 2002, "Nonperturbative renormalization flow in quantum field theory and statistical physics," Phys. Rep. **363**, 223–386.

Bernien, Hannes, *et al.*, 2017, "Probing many-body dynamics on a 51-atom quantum simulator," Nature (London) **551**, 579–584.

Bervillier, C., 2013, "Revisiting the local potential approximation of the exact renormalization group equation," Nucl. Phys. **B876**, 587–604.

Bervillier, Claude, Andreas Juttner, and Daniel F. Litim, 2007, "High-accuracy scaling exponents in the local potential approximation," Nucl. Phys. **B783**, 213–226.

Bhattacharya, Tanmoy, Alexander J. Buser, Shailesh Chandrasekharan, Rajan Gupta, and Hersh Singh, 2021, "Qubit Regularization of Asymptotic Freedom," Phys. Rev. Lett. **126**, 172001.

Bloch, Immanuel, Jean Dalibard, and Wilhelm Zwerger, 2008, "Many-body physics with ultracold gases," Rev. Mod. Phys. **80**, 885–964.

Bloch, Jacques, Raghav G. Jha, Robert Lohmayer, and Maximilian Meister, 2021, "Tensor renormalization group study of the 3D O(2) model," Phys. Rev. D **104**, 094517.

Bonnes, Lars, Daniel Charrier, and Andreas M. Läuchli, 2014, "Dynamical and steady-state properties of a Bose-Hubbard chain

with bond dissipation: A study based on matrix product operators," Phys. Rev. A **90**, 033612.
Bosetti, Paolo, Barbara De Palma, and Marco Guagnelli, 2015, "Monte Carlo determination of the critical coupling in ϕ_2^4 theory," Phys. Rev. D **92**, 034509.
Bowers, R. G., and G. S. Joyce, 1967, "Lattice Model for the λ Transition in a Bose Fluid," Phys. Rev. Lett. **19**, 630–632.
Bronzin, Simone, Barbara De Palma, and Marco Guagnelli, 2019, "New Monte Carlo determination of the critical coupling in ϕ_2^4 theory," Phys. Rev. D **99**, 034508.
Browaeys, Antoine, and Thierry Lahaye, 2020, "Many-body physics with individually controlled Rydberg atoms," Nat. Phys. **16**, 132–142.
Brower, R., S. Chandrasekharan, and U.-J. Wiese, 1999, "QCD as a quantum link model," Phys. Rev. D **60**, 094502.
Bruckmann, Falk, Christof Gattringer, Thomas Kloiber, and Tin Sulejmanpasic, 2016, "Two-dimensional O(3) model at nonzero density: From dual lattice simulations to repulsive bosons," Phys. Rev. D **94**, 114503.
Bruckmann, Falk, Christof Gattringer, Thomas Kloiber, and Tin Sulejmanpašić, 2015, "Dual lattice representations for O(N) and CP($N-1$) models with a chemical potential," Phys. Lett. B **749**, 495–501.
Bruckmann, Falk, Karl Jansen, and Stefan Kühn, 2019, "O(3) nonlinear sigma model in $1+1$ dimensions with matrix product states," Phys. Rev. D **99**, 074501.
Butt, Nouman, Simon Catterall, Yannick Meurice, Ryo Sakai, and Judah Unmuth-Yockey, 2020, "Tensor network formulation of the massless Schwinger model with staggered fermions," Phys. Rev. D **101**, 094509.
Buyens, Boye, Jutho Haegeman, Karel Van Acoleyen, Henri Verschelde, and Frank Verstraete, 2014, "Matrix Product States for Gauge Field Theories," Phys. Rev. Lett. **113**, 091601.
Buyens, Boye, Jutho Haegeman, Henri Verschelde, Frank Verstraete, and Karel Van Acoleyen, 2016, "Confinement and String Breaking for QED_2 in the Hamiltonian Picture," Phys. Rev. X **6**, 041040.
Byrnes, T. M. R., P. Sriganesh, R. J. Bursill, and C. J. Hamer, 2002, "Density matrix renormalization group approach to the massive Schwinger model," Phys. Rev. D **66**, 013002.
Byrnes, Tim, and Yoshihisa Yamamoto, 2006, "Simulating lattice gauge theories on a quantum computer," Phys. Rev. A **73**, 022328.
Campos, Manuel, Germán Sierra, and Esperanza López, 2019, "Tensor renormalization group in bosonic field theory," Phys. Rev. B **100**, 195106.
Campostrini, Massimo, Paolo Rossi, and Ettore Vicari, 1995, "Strong-coupling expansion of chiral models," Phys. Rev. D **52**, 358–385.
Cardy, J., 1996, *Scaling and Renormalization in Statistical Physics*, Cambridge Lecture Notes in Physics (Cambridge University Press, Cambridge, England).
Castro Neto, A. H., F. Guinea, N. M. R. Peres, K. S. Novoselov, and A. K. Geim, 2009, "The electronic properties of graphene," Rev. Mod. Phys. **81**, 109–162.
Catterall, Simon, David B. Kaplan, and Mithat Unsal, 2009, "Exact lattice supersymmetry," Phys. Rep. **484**, 71–130.
Celi, A., B. Vermersch, O. Viyuela, H. Pichler, M. D. Lukin, and P. Zoller, 2020, "Emerging Two-Dimensional Gauge Theories in Rydberg Configurable Arrays," Phys. Rev. X **10**, 021057.
Cervera-Lierta, Alba, 2018, "Exact Ising model simulation on a quantum computer," Quantum **2**, 114.
Chang, Shau-Jin, 1976, "The existence of a second-order phase transition in the two-dimensional ϕ^4 field theory," Phys. Rev. D **13**, 2778.
Chen, Bin-Bin, Yuan Gao, Yi-Bin Guo, Yuzhi Liu, Hui-Hai Zhao, Hai-Jun Liao, Lei Wang, Tao Xiang, Wei Li, and Z. Y. Xie, 2020, "Automatic differentiation for second renormalization of tensor networks," Phys. Rev. B **101**, 220409.
Chen, Jing, Hai-Jun Liao, Hai-Dong Xie, Xing-Jie Han, Rui-Zhen Huang, Song Cheng, Zhong-Chao Wei, Zhi-Yuan Xie, and Tao Xiang, 2017, "Phase transition of the q-state clock model: Duality and tensor renormalization," Chin. Phys. Lett. **34**, 050503.
Chen, Ming-Cheng, *et al.*, 2020, "Demonstration of Adiabatic Variational Quantum Computing with a Superconducting Quantum Coprocessor," Phys. Rev. Lett. **125**, 180501.
Chen, Yong, Zhi-Yuan Xie, and Ji-Feng Yu, 2018, "Phase transitions of the five-state clock model on the square lattice," Chin. Phys. B**27**, 080503.
Chung, S. G., 1999, "Essential finite-size effect in the two-dimensional XY model," Phys. Rev. B **60**, 11761–11764.
Ciavarella, Anthony, Natalie Klco, and Martin J. Savage, 2021, "Trailhead for quantum simulation of SU(3) Yang-Mills lattice gauge theory in the local multiplet basis," Phys. Rev. D **103**, 094501.
Cirac, Ignacio, David Perez-Garcia, Norbert Schuch, and Frank Verstraete, 2021, "Matrix product states and projected entangled pair states: Concepts, symmetries, theorems," Rev. Mod. Phys. **93**, 045003.
Cirac, J. Ignacio, and Frank Verstraete, 2009, "Renormalization and tensor product states in spin chains and lattices," J. Phys. A **42**, 504004.
Clark, Logan W., Brandon M. Anderson, Lei Feng, Anita Gaj, K. Levin, and Cheng Chin, 2018, "Observation of Density-Dependent Gauge Fields in a Bose-Einstein Condensate Based on Micromotion Control in a Shaken Two-Dimensional Lattice," Phys. Rev. Lett. **121**, 030402.
Cohen, Thomas D., 2003, "Functional Integrals for QCD at Nonzero Chemical Potential and Zero Density," Phys. Rev. Lett. **91**, 222001.
Coleman, Sidney, R. Jackiw, and H. D. Politzer, 1974, "Spontaneous symmetry breaking in the O(N) model for large N," Phys. Rev. D **10**, 2491–2499.
Coleman, Sidney R., 1975, "The quantum Sine-Gordon equation as the massive Thirring model," Phys. Rev. D **11**, 2088.
Corboz, Philippe, Glen Evenbly, Frank Verstraete, and Guifré Vidal, 2010, "Simulation of interacting fermions with entanglement renormalization," Phys. Rev. A **81**, 010303.
Creutz, Michael, 1977, "Gauge fixing, the transfer matrix, and confinement on a lattice," Phys. Rev. D **15**, 1128–1136.
Creutz, Michael, 2001, "Lattice gauge theory: A retrospective," Nucl. Phys. B, Proc. Suppl. **94**, 219–226.
Creutz, Michael, Laurence Jacobs, and Claudio Rebbi, 1979, "Monte Carlo study of Abelian lattice gauge theories," Phys. Rev. D **20**, 1915.
Dasgupta, Raka, and Indrakshi Raychowdhury, 2022, "Cold-atom quantum simulator for string and hadron dynamics in non-Abelian lattice gauge theory," Phys. Rev. A **105**, 023322.
Davoudi, Zohreh, Mohammad Hafezi, Christopher Monroe, Guido Pagano, Alireza Seif, and Andrew Shaw, 2020, "Towards analog quantum simulations of lattice gauge theories with trapped ions," Phys. Rev. Research **2**, 023015.
Davoudi, Zohreh, Indrakshi Raychowdhury, and Andrew Shaw, 2021, "Search for efficient formulations for Hamiltonian simulation of non-Abelian lattice gauge theories," Phys. Rev. D **104**, 074505.

Debnath, S., N. M. Linke, C. Figgatt, K. A. Landsman, K. Wright, and C. Monroe, 2016, "Demonstration of a small programmable quantum computer with atomic qubits," Nature (London) **536**, 63–66.

de Forcrand, Philippe, **2010**, "Simulating QCD at finite density," Proc. Sci. LATTICE2009, 010 [arXiv:1005.0539].

Delcamp, Clement, and Antoine Tilloy, 2020, "Computing the renormalization group flow of two-dimensional ϕ^4 theory with tensor networks," Phys. Rev. Research **2**, 033278.

Denbleyker, Alan, Yuzhi Liu, Y. Meurice, M. P. Qin, T. Xiang, Z. Y. Xie, J. F. Yu, and Haiyuan Zou, 2014, "Controlling sign problems in spin models using tensor renormalization," Phys. Rev. D **89**, 016008.

Detmold, William, and Kostas Orginos, 2013, "Nuclear correlation functions in lattice QCD," Phys. Rev. D **87**, 114512.

Devoret, M. H., and R. J. Schoelkopf, 2013, "Superconducting circuits for quantum information: An outlook," Science **339**, 1169–1174.

Dittrich, Bianca, Sebastian Mizera, and Sebastian Steinhaus, 2016, "Decorated tensor network renormalization for lattice gauge theories and spin foam models," New J. Phys. **18**, 053009.

Dyson, Freeman J., 1969, "Existence of a phase transition in a one-dimensional Ising ferromagnet," Commun. Math. Phys. **12**, 91–107.

Edwards, E. E., S. Korenblit, K. Kim, R. Islam, M.-S. Chang, J. K. Freericks, G.-D. Lin, L.-M. Duan, and C. Monroe, 2010, "Quantum simulation and phase diagram of the transverse-field Ising model with three atomic spins," Phys. Rev. B **82**, 060412.

Efrati, Efi, Zhe Wang, Amy Kolan, and Leo P. Kadanoff, 2014, "Real-space renormalization in statistical mechanics," Rev. Mod. Phys. **86**, 647–667.

Einhorn, Martin B., and Robert Savit, 1978, "Topological excitations in the Abelian Higgs model," Phys. Rev. D **17**, 2583.

Einhorn, Martin B., and Robert Savit, 1979, "Phase transitions in the Abelian Higgs model," Phys. Rev. D **19**, 1198.

Emonts, Patrick, Mari Carmen Bañuls, Ignacio Cirac, and Erez Zohar, 2020, "Variational Monte Carlo simulation with tensor networks of a pure $\mathbb{Z}_3$ gauge theory in $(2+1)$D," Phys. Rev. D **102**, 074501.

Evenbly, G., 2018, "Gauge fixing, canonical forms, and optimal truncations in tensor networks with closed loops," Phys. Rev. B **98**, 085155.

Evenbly, G., and G. Vidal, 2015, "Tensor Network Renormalization," Phys. Rev. Lett. **115**, 180405.

Fannes, Mark, Bruno Nachtergaele, and Reinhard F. Werner, 1992, "Finitely correlated states on quantum spin chains," Commun. Math. Phys. **144**, 443–490.

Felser, Timo, Pietro Silvi, Mario Collura, and Simone Montangero, 2020, "Two-Dimensional Quantum-Link Lattice Quantum Electrodynamics at Finite Density," Phys. Rev. X **10**, 041040.

Fetter, A. L., and J. D. Walecka, 2003, *Quantum Theory of Many-Particle Systems*, Dover Books on Physics (Dover Publications, New York).

Feynman, R. P, 1982, "Simulating physics with computers," Int. J. Theor. Phys. **21**, 467–488.

Fishman, M. T., L. Vanderstraeten, V. Zauner-Stauber, J. Haegeman, and F. Verstraete, 2018, "Faster methods for contracting infinite two-dimensional tensor networks," Phys. Rev. B **98**, 235148.

Fradkin, Eduardo H., and Leonard Susskind, 1978, "Order and disorder in gauge systems and magnets," Phys. Rev. D **17**, 2637.

Friedenauer, A., H. Schmitz, J. T. Glueckert, D. Porras, and T. Schaetz, 2008, "Simulating a quantum magnet with trapped ions," Nat. Phys. **4**, 757–761.

Friedenauer, Axel, 2010, "Simulation of the quantum Ising model in an ion trap," Ph.D. thesis (Ludwig Maximilian University of Munich).

Funcke, Lena, Tobias Hartung, Karl Jansen, Stefan Kühn, Manuel Schneider, Paolo Stornati, and Xiaoyang Wang, 2022, "Towards quantum simulations in particle physics and beyond on noisy intermediate-scale quantum devices," Phil. Trans. R. Soc. A **380**, 20210062.

Funcke, Lena, Karl Jansen, and Stefan Kühn, 2020, "Topological vacuum structure of the Schwinger model with matrix product states," Phys. Rev. D **101**, 054507.

Gattringer, Christof, Daniel Goschl, and Carlotta Marchis, 2018, "Kramers-Wannier duality and worldline representation for the SU(2) principal chiral model," Phys. Lett. B **778**, 435–441.

Gattringer, Christof, Daniel Göschl, and Tin Sulejmanpašić, 2018, "Dual simulation of the 2D U(1) gauge Higgs model at topological angle $\theta = \pi$: Critical endpoint behavior," Nucl. Phys. **B935**, 344–364.

Gattringer, Christof, Thomas Kloiber, and Michael Müller-Preussker, 2015, "Dual simulation of the two-dimensional lattice U(1) Gauge-Higgs model with a topological term," Phys. Rev. D **92**, 114508.

Gattringer, Christof, Thomas Kloiber, and Vasily Sazonov, 2015, "Solving the sign problems of the massless lattice Schwinger model with a dual formulation," Nucl. Phys. **B897**, 732–748.

Georgescu, I. M., S. Ashhab, and Franco Nori, 2014, "Quantum simulation," Rev. Mod. Phys. **86**, 153–185.

Goldstone, J., 1961, "Field theories with 'superconductor' solutions," Nuovo Cimento **19**, 154–164.

Goldstone, Jeffrey, Abdus Salam, and Steven Weinberg, 1962, "Broken symmetries," Phys. Rev. **127**, 965–970.

Golterman, Maarten F. L., and Donald N. Petcher, 1989, "A local interactive lattice model with supersymmetry," Nucl. Phys. **B319**, 307–341.

González-Cuadra, Daniel, Erez Zohar, and J Ignacio Cirac, 2017, "Quantum simulation of the Abelian-Higgs lattice gauge theory with ultracold atoms," New J. Phys. **19**, 063038.

Göschl, Daniel, Christof Gattringer, Alexander Lehmann, and Christoph Weis, 2017, "Simulation strategies for the massless lattice Schwinger model in the dual formulation," Nucl. Phys. **B924**, 63–85.

Green, Frederic, and Stuart Samuel, 1981, "The large-N phase transition in the U(N) chiral models," Phys. Lett. **103B**, 110–112.

Gross, David J., and Frank Wilczek, 1973, "Ultraviolet Behavior of Non-Abelian Gauge Theories," Phys. Rev. Lett. **30**, 1343–1346.

Gu, Z.-C, M. Levin, and X.-G. Wen, 2008, "Tensor-entanglement renormalization group approach as a unified method for symmetry breaking and topological phase transitions," Phys. Rev. B **78**, 205116.

Gu, Zheng-Cheng, 2013, "Efficient simulation of Grassmann tensor product states," Phys. Rev. B **88**, 115139.

Gu, Zheng-Cheng, Frank Verstraete, and Xiao-Gang Wen, 2010, "Grassmann tensor network states and its renormalization for strongly correlated fermionic and bosonic states," arXiv:1004.2563.

Gu, Zheng-Cheng, and Xiao-Gang Wen, 2009, "Tensor-entanglement-filtering renormalization approach and symmetry protected topological order," Phys. Rev. B **80**, 155131.

Guardado-Sanchez, Elmer, Peter T. Brown, Debayan Mitra, Trithep Devakul, David A. Huse, Peter Schauß, and Waseem S. Bakr, 2018, "Probing the Quench Dynamics of Antiferromagnetic Correlations in a 2D Quantum Ising Spin System," Phys. Rev. X **8**, 021069.

Gürsey, F., 1960, "On the symmetries of strong and weak interactions," Nuovo Cimento **16**, 230–240.

Gustafson, Erik, 2020, "Projective cooling for the transverse Ising model," Phys. Rev. D **101**, 071504.

Gustafson, Erik, Patrick Dreher, Zheyue Hang, and Yannick Meurice, 2021, "Indexed improvements for real-time Trotter evolution of a $(1+1)$ field theory using NISQ quantum computers," Quantum Sci. Technol. **6**, 045020.

Gustafson, Erik, Yannick Meurice, and Judah Unmuth-Yockey, 2019, "Quantum simulation of scattering in the quantum Ising model," Phys. Rev. D **99**, 094503.

Gustafson, Erik, Yingyue Zhu, Patrick Dreher, Norbert M. Linke, and Yannick Meurice, 2021, "Real-time quantum calculations of phase shifts using wave packet time delays," Phys. Rev. D **104**, 054507.

Gustafson, Erik, *et al.*, 2021, "Large scale multi-node simulations of $\mathbb{Z}_2$ gauge theory quantum circuits using Google Cloud Platform," arXiv:2110.07482.

Gustafson, Erik J., and Henry Lamm, 2021, "Toward quantum simulations of $\mathbb{Z}_2$ gauge theory without state preparation," Phys. Rev. D **103**, 054507.

Hackett, Daniel, C., Kiel Howe, Ciaran Hughes, William Jay, Ethan T. Neil, and James N. Simone, 2019, "Digitizing gauge fields: Lattice Monte Carlo results for future quantum computers," Phys. Rev. A **99**, 062341.

Haegeman, Jutho, Karel Van Acoleyen, Norbert Schuch, J. Ignacio Cirac, and Frank Verstraete, 2015, "Gauging Quantum States: From Global to Local Symmetries in Many-Body Systems," Phys. Rev. X **5**, 011024.

Haegeman, Jutho, J. Ignacio Cirac, Tobias J. Osborne, and Frank Verstraete, 2013, "Calculus of continuous matrix product states," Phys. Rev. B **88**, 085118.

Haegeman, Jutho, and Frank Verstraete, 2017, "Diagonalizing transfer matrices and matrix product operators: A medley of exact and computational methods," Annu. Rev. Condens. Matter Phys. **8**, 355–406.

Hasenfratz, P., M. Maggiore, and F. Niedermayer, 1990, "The exact mass gap of the O(3) and O(4) non-linear σ-models in $d=2$," Phys. Lett. B **245**, 522–528.

Hauru, Markus, Clement Delcamp, and Sebastian Mizera, 2018, "Renormalization of tensor networks using graph independent local truncations," Phys. Rev. B **97**, 045111.

Hebenstreit, M., D. Alsina, J. I. Latorre, and B. Kraus, 2017, "Compressed quantum computation using a remote five-qubit quantum computer," Phys. Rev. A **95**, 052339.

Herbut, I., 2007, *A Modern Approach to Critical Phenomena* (Cambridge University Press, Cambridge, England).

Honda, Masazumi, Etsuko Itou, Yuta Kikuchi, Lento Nagano, and Takuya Okuda, 2022, "Classically emulated digital quantum simulation for screening and confinement in the Schwinger model with a topological term," Phys. Rev. D **105**, 014504.

Horn, D., 1981, "Finite matrix models with continuous local gauge invariance," Phys. Lett. **100B**, 149–151.

Hostetler, Leon, Jin Zhang, Ryo Sakai, Judah Unmuth-Yockey, Alexei Bazavov, and Yannick Meurice, 2021, "Clock model interpolation and symmetry breaking in O(2) models," Phys. Rev. D **104**, 054505.

Iblisdir, S., R. Orus, and J. I. Latorre, 2007, "Matrix product states algorithms and continuous systems," Phys. Rev. B **75**, 104305.

Ising, Ernst, 1925, "Contribution to the theory of ferromagnetism," Z. Phys. **31**, 253–258.

Islam, R., *et al.*, 2011, "Onset of a quantum phase transition with a trapped ion quantum simulator," Nat. Commun. **2**, 377.

Islam, Rajibul, Ruichao Ma, Philipp M. Preiss, M. Eric Tai, Alexander Lukin, Matthew Rispoli, and Markus Greiner, 2015, "Measuring entanglement entropy in a quantum many-body system," Nature (London) **528**, 77–83.

Itzykson, C., and J. M. Drouffe, 1991, *Statistical Field Theory: Volume 1—From Brownian Motion to Renormalization and Lattice Gauge Theory*, Cambridge Monographs on Mathematical Physics (Cambridge University Press, Cambridge, England).

Jaksch, D., C. Bruder, J. I. Cirac, C. W. Gardiner, and P. Zoller, 1998, "Cold Bosonic Atoms in Optical Lattices," Phys. Rev. Lett. **81**, 3108–3111.

Johri, Sonika, Damian S. Steiger, and Matthias Troyer, 2017, "Entanglement spectroscopy on a quantum computer," Phys. Rev. B **96**, 195136.

Jordan, Stephen P., Keith S. M. Lee, and John Preskill, 2014, "Quantum computation of scattering in scalar quantum field theories," Quantum Inf. Comput. **14**, 1014–1080.

Kadanoff, L. P., 1976, "Notes on Migdal's recursion formulas," Ann. Phys. (N.Y.) **100**, 359–394.

Kadanoff, Leo P., 1966, "Scaling laws for Ising models near T_c," Phys. Phys. Fiz. **2**, 263–272.

Kadanoff, Leo P., 1975, "Variational Principles and Approximate Renormalization Group Calculations," Phys. Rev. Lett. **34**, 1005–1008.

Kadanoff, Leo P., and Anthony Houghton, 1975, "Numerical evaluations of the critical properties of the two-dimensional Ising model," Phys. Rev. B **11**, 377–386.

Kadoh, Daisuke, Yoshinobu Kuramashi, Yoshifumi Nakamura, Ryo Sakai, Shinji Takeda, and Yusuke Yoshimura, **2018**, "Tensor network formulation for two-dimensional lattice $\mathcal{N}=1$ Wess-Zumino model," J. High Energy Phys. 03, 141.

Kadoh, Daisuke, Yoshinobu Kuramashi, Yoshifumi Nakamura, Ryo Sakai, Shinji Takeda, and Yusuke Yoshimura, 2019, "Tensor network analysis of critical coupling in two dimensional ϕ^4 theory," J. High Energy Phys. 05, 184.

Kadoh, Daisuke, Yoshinobu Kuramashi, Yoshifumi Nakamura, Ryo Sakai, Shinji Takeda, and Yusuke Yoshimura, 2020, "Investigation of complex ϕ^4 theory at finite density in two dimensions using TRG," J. High Energy Phys. 02, 161.

Kadoh, Daisuke, and Katsumasa Nakayama, 2019, "Renormalization group on a triad network," arXiv:1912.02414.

Kandala, Abhinav, Kristan Temme, Antonio D. Corcoles, Antonio Mezzacapo, Jerry M. Chow, and Jay M. Gambetta, 2019, "Error mitigation extends the computational reach of a noisy quantum processor," Nature (London) **567**, 491–495.

Kaplan, David B., and Jesse R. Stryker, 2020, "Gauss's law, duality, and the Hamiltonian formulation of U(1) lattice gauge theory," Phys. Rev. D **102**, 094515.

Kasper, V., F. Hebenstreit, F. Jendrzejewski, M. K. Oberthaler, and J. Berges, 2017, "Implementing quantum electrodynamics with ultracold atomic systems," New J. Phys. **19**, 023030.

Kaufman, Bruria, 1949, "Crystal statistics. II. Partition function evaluated by spinor analysis," Phys. Rev. **76**, 1232–1243.

Kawauchi, Hikaru, and Takeda Shinji, 2018, "Loop-TNR analysis of CP(1) model with theta term," EPJ Web Conf. **175**, 11015.

Keesling, Alexander, *et al.*, 2019, "Quantum Kibble-Zurek mechanism and critical dynamics on a programmable Rydberg simulator," Nature (London) **568**, 207–211.

Keldysh, L. V, 1965, "Ionization in the field of a strong electromagnetic wave," Sov. Phys. JETP **20**, 1307–1314.

Kharzeev, Dmitri E., and Yuta Kikuchi, 2020, "Real-time chiral dynamics from a digital quantum simulation," Phys. Rev. Research **2**, 023342.

Kim, Hyosub, Kyungtae Kim, Woojun Lee, and Jaewook Ahn, 2017, "Quantum simulation with $N = 19$ Rydberg atoms for quantum Ising dynamics," in *Proceedings of the Conference on Lasers and Electro-Optics (CLEO), San Jose, 2017* (Optical Society of America, Washington, DC), p. JTh5C.1.

Kim, K., M.-S. Chang, S. Korenblit, R. Islam, E. E. Edwards, J. K. Freericks, G.-D. Lin, L.-M. Duan, and C. Monroe, 2010, "Quantum simulation of frustrated Ising spins with trapped ions," Nature (London) **465**, 590–593.

Kim, K., *et al.*, 2011, "Quantum simulation of the transverse Ising model with trapped ions," New J. Phys. **13**, 105003.

Klco, N., E. F. Dumitrescu, A. J. McCaskey, T. D. Morris, R. C. Pooser, M. Sanz, E. Solano, P. Lougovski, and M. J. Savage, 2018, "Quantum-classical computation of Schwinger model dynamics using quantum computers," Phys. Rev. A **98**, 032331.

Klco, Natalie, and Martin J. Savage, 2019, "Digitization of scalar fields for quantum computing," Phys. Rev. A **99**, 052335.

Knolle, J., and R. Moessner, 2019, "A field guide to spin liquids," Annu. Rev. Condens. Matter Phys. **10**, 451–472.

Kogut, John B., 1979, "An introduction to lattice gauge theory and spin systems," Rev. Mod. Phys. **51**, 659–713.

Kogut, John B., 1983, "The lattice gauge theory approach to quantum chromodynamics," Rev. Mod. Phys. **55**, 775–836.

Kogut, John B., and Leonard Susskind, 1975, "Hamiltonian formulation of Wilson's lattice gauge theories," Phys. Rev. D **11**, 395–408.

Korenblit, Simcha, 2013, "Quantum simulations of the Ising model with trapped ions: Devil's staircase and arbitrary lattice proposal," Ph.D. thesis (University of Maryland, College Park).

Kramers, H. A., and G. H. Wannier, 1941, "Statistics of the two-dimensional ferromagnet. Part I," Phys. Rev. **60**, 252–262.

Kühn, Stefan, J. Ignacio Cirac, and Mari Carmen Bañuls, **2015**, "Non-Abelian string breaking phenomena with matrix product states," J. High Energy Phys. 07, 130.

Kuramashi, Yoshinobu, and Yusuke Yoshimura, 2019, "Three-dimensional finite temperature Z_2 gauge theory with tensor network scheme," J. High Energy Phys. 08, 023.

Lamm, Henry, Scott Lawrence, and Yukari Yamauchi (NuQS Collaboration), 2019, "General methods for digital quantum simulation of gauge theories," Phys. Rev. D **100**, 034518.

Lamm, Henry, Scott Lawrence, and Yukari Yamauchi (NuQS Collaboration), 2020, "Parton physics on a quantum computer," Phys. Rev. Research **2**, 013272.

Lay, William, and Joseph Rudnick, 2002, "Analysis of a Continuous Field Theory in Two Dimensions with Use of the Density Matrix Renormalization Group," Phys. Rev. Lett. **88**, 057203.

Leibfried, D., R. Blatt, C. Monroe, and D. Wineland, 2003, "Quantum dynamics of single trapped ions," Rev. Mod. Phys. **75**, 281–324.

Levin, Michael, and Cody P. Nave, 2007, "Tensor Renormalization Group Approach to 2D Classical Lattice Models," Phys. Rev. Lett. **99**, 120601.

Li, Tracy, Lucia Duca, Martin Reitter, Fabian Grusdt, Eugene Demler, Manuel Endres, Monika Schleier-Smith, Immanuel Bloch, and Ulrich Schneider, 2016, "Bloch state tomography using Wilson lines," Science **352**, 1094–1097.

Li, Ying, and Simon C. Benjamin, 2017, "Efficient Variational Quantum Simulator Incorporating Active Error Minimization," Phys. Rev. X **7**, 021050.

Li, Zi-Qian, Li-Ping Yang, Z. Y. Xie, Hong-Hao Tu, Hai-Jun Liao, and T. Xiang, 2020, "Critical properties of the two-dimensional q-state clock model," Phys. Rev. E **101**, 060105.

Lidar, Daniel A., and Ofer Biham, 1997, "Simulating Ising spin glasses on a quantum computer," Phys. Rev. E **56**, 3661–3681.

Linke, N. M., S. Johri, C. Figgatt, K. A. Landsman, A. Y. Matsuura, and C. Monroe, 2018, "Measuring the Rényi entropy of a two-site Fermi-Hubbard model on a trapped ion quantum computer," Phys. Rev. A **98**, 052334.

Liu, Yuzhi, Y. Meurice, M. P. Qin, J. Unmuth-Yockey, T. Xiang, Z. Y. Xie, J. F. Yu, and Haiyuan Zou, 2013, "Exact blocking formulas for spin and gauge models," Phys. Rev. D **88**, 056005.

Lloyd, Seth, 1996, "Universal quantum simulators," Science **273**, 1073–1078.

Lüscher, M., 1990, "Selected topics in lattice field theory," in *Champs, Cordes, Et Phénomènes Critiques*, Proceedings of the Les Houches Summer School 1988, Session 49, edited by E. Brezin and J. Zinn-Justin (North-Holland, Amsterdam).

Magnifico, Giuseppe, Marcello Dalmonte, Paolo Facchi, Saverio Pascazio, Francesco V. Pepe, and Elisa Ercolessi, 2020, "Real time dynamics and confinement in the $\mathbb{Z}_n$ Schwinger-Weyl lattice model for $1 + 1$ QED," Quantum **4**, 281.

Magnifico, Giuseppe, Timo Felser, Pietro Silvi, and Simone Montangero, 2021, "Lattice quantum electrodynamics in $(3 + 1)$-dimensions at finite density with tensor networks," Nat. Commun. **12**, 3600.

Marchis, Carlotta, and Christof Gattringer, 2018, "Dual representation of lattice QCD with worldlines and worldsheets of Abelian color fluxes," Phys. Rev. D **97**, 034508.

Martinez, Esteban A., *et al.*, 2016, "Real-time dynamics of lattice gauge theories with a few-qubit quantum computer," Nature (London) **534**, 516–519.

Meurice, Y., 2007, "Nonlinear aspects of the renormalization group flows of Dyson's hierarchical model," J. Phys. A **40**, R39.

Meurice, Y., 2013, "Accurate exponents from approximate tensor renormalizations," Phys. Rev. B **87**, 064422.

Meurice, Yannick, 1994, "Duality in long-range Ising ferromagnets," J. Math. Phys. (N.Y.) **35**, 769–779.

Meurice, Yannick, 2019, "Examples of symmetry-preserving truncations in tensor field theory," Phys. Rev. D **100**, 014506.

Meurice, Yannick, 2020a, "Discrete aspects of continuous symmetries in the tensorial formulation of Abelian gauge theories," Phys. Rev. D **102**, 014506.

Meurice, Yannick, 2020b, *Quantum Field Theory: A Quantum Computation Approach* (Institute of Physics, London).

Meurice, Yannick, 2021, "Theoretical methods to design and test quantum simulators for the compact Abelian Higgs model," Phys. Rev. D **104**, 094513.

Migdal, Alexander A., 1975, "Gauge transitions in gauge and spin lattice systems," Sov. Phys. JETP **42**, 743.

Mishra, Chinmay, Shane Thompson, Raphael Pooser, and George Siopsis, 2020, "Quantum computation of an interacting fermionic model," Quantum Sci. Technol. **5**, 035010.

Molnar, Andras, José Garre-Rubio, David Pérez-García, Norbert Schuch, and J. Ignacio Cirac, 2018, "Normal projected entangled pair states generating the same state," New J. Phys. **20**, 113017.

Montangero, S., 2018, *Introduction to Tensor Network Methods: Numerical Simulations of Low-Dimensional Many-Body Quantum Systems* (Springer, New York).

Montvay, Istvan, and Gernot Münster, 1994, *Quantum Fields on a Lattice*, Cambridge Monographs on Mathematical Physics (Cambridge University Press, Cambridge, England).

Morita, Satoshi, and Naoki Kawashima, 2019, "Calculation of higher-order moments by higher-order tensor renormalization group," Comput. Phys. Commun. **236**, 65–71.

Morita, Satoshi, and Naoki Kawashima, 2021, "Global optimization of tensor renormalization group using the corner transfer matrix," Phys. Rev. B **103**, 045131.

Mostame, Sarah, and Ralf Schützhold, 2008, "Quantum Simulator for the Ising Model with Electrons Floating on a Helium Film," Phys. Rev. Lett. **101**, 220501.

Mueller, Niklas, Andrey Tarasov, and Raju Venugopalan, 2020, "Deeply inelastic scattering structure functions on a hybrid quantum computer," Phys. Rev. D **102**, 016007.

Nachman, Benjamin, Davide Provasoli, Wibe A. De Jong, and Christian W. Bauer, 2021, "Quantum Algorithm for High Energy Physics Simulations," Phys. Rev. Lett. **126**, 062001.

Nakamoto, Norihiro, and Shinji Takeda, 2016, "Computation of correlation functions by tensor renormalization group method," Sci. Rep. Kanazawa Univ. **60**, 11–25.

Nakamura, Yoshifumi, Hideaki Oba, and Shinji Takeda, 2019, "Tensor renormalization group algorithms with a projective truncation method," Phys. Rev. B **99**, 155101.

Nambu, Yoichiro, 1960, "Quasi-particles and gauge invariance in the theory of superconductivity," Phys. Rev. **117**, 648–663.

Nielsen, M. A., and I. L. Chuang, 2000, *Quantum Computation and Quantum Information*, Cambridge Series on Information and the Natural Sciences (Cambridge University Press, Cambridge, England).

Niemeijer, Th., and J. van Leeuwen, 1976, "Renormalization: Ising-like spin systems," in *Phase Transitions and Critical Phenomena*, Vol. 6, edited by C. Domb and M. Green (Academic Press, New York).

Nishino, Tomotoshi, 1995, "Density matrix renormalization group method for 2D classical models," J. Phys. Soc. Jpn. **64**, 3598.

Nishino, Tomotoshi, and Kouichi Okunishi, 1996, "Corner transfer matrix renormalization group method," J. Phys. Soc. Jpn. **65**, 891.

Nishiyama, Yoshihiro, 2001a, "Quantum-fluctuation-induced repulsive interaction of a quantum string between walls," Phys. Rev. B **64**, 064510.

Nishiyama, Yoshihiro, 2001b, "Strong-coupling-expansion analysis of the false-vacuum decay rate of the lattice ϕ^4 model in $1+1$ dimensions," J. Phys. A **34**, 11215–11223.

Orland, Peter, and Daniel Rohrlich, 1990, "Lattice gauge magnets: Local isospin from spin," Nucl. Phys. **B338**, 647–672.

Orus, Roman, 2014, "A practical introduction to tensor networks: Matrix product states and projected entangled pair states," Ann. Phys. (Amsterdam) **349**, 117–158.

Paeckel, Sebastian, Thomas Köhler, Andreas Swoboda, Salvatore R. Manmana, Ulrich Schollwöck, and Claudius Hubig, 2019, "Time-evolution methods for matrix-product states," Ann. Phys. (Amsterdam) **411**, 167998.

Parisi, G., 1998, *Statistical Field Theory* (Avalon Publishing, New York).

Perez, Alejandro, 2013, "The spin-foam approach to quantum gravity," Living Rev. Relativity **16**, 3.

Perez-Garcia, D., F. Verstraete, M. M. Wolf, and J. I. Cirac, 2007, "Matrix product state representations," Quantum Inf. Comput. **7**, 401–430.

Peskin, Michael E., and Daniel V. Schroeder, 1995, *An Introduction to Quantum Field Theory* (Addison-Wesley, Reading, MA).

Peter, F., and H. Weyl, 1927, "The completeness of the primitive representations of a closed continuous group," Math. Ann. **97**, 737–755.

Pichler, T., M. Dalmonte, E. Rico, P. Zoller, and S. Montangero, 2016, "Real-Time Dynamics in U(1) Lattice Gauge Theories with Tensor Networks," Phys. Rev. X **6**, 011023.

Pirvu, B., G. Vidal, F. Verstraete, and L. Tagliacozzo, 2012, "Matrix product states for critical spin chains: Finite-size versus finite-entanglement scaling," Phys. Rev. B **86**, 075117.

Plenio, M. B., J. Eisert, J. Dreißig, and M. Cramer, 2005, "Entropy, Entanglement, and Area: Analytical Results for Harmonic Lattice Systems," Phys. Rev. Lett. **94**, 060503.

Politzer, H. David, 1973, "Reliable Perturbative Results for Strong Interactions?," Phys. Rev. Lett. **30**, 1346–1349.

Pollmann, Frank, Subroto Mukerjee, Ari M. Turner, and Joel E. Moore, 2009, "Theory of Finite-Entanglement Scaling at One-Dimensional Quantum Critical Points," Phys. Rev. Lett. **102**, 255701.

Polyakov, A. M., 1987, *Gauge Fields and Strings*, Contemporary Concepts in Physics (Taylor & Francis, London).

Polyakov, Alexander M., 1978, "Thermal Properties of Gauge Fields and Quark Liberation," Phys. Lett. **72B**, 477–480.

Pontryagin, L., 1939, *Topological Groups* (Princeton University Press, Princeton, NJ).

Potts, R. B., 1952, "Some generalized order-disorder transformations," Math. Proc. Cambridge Philos. Soc. **48**, 106–109.

Poulin, David, Angie Qarry, Rolando Somma, and Frank Verstraete, 2011, "Quantum Simulation of Time-Dependent Hamiltonians and the Convenient Illusion of Hilbert Space," Phys. Rev. Lett. **106**, 170501.

Preskill, John, 2018, "Quantum computing in the NISQ era and beyond," Quantum **2**, 79.

Prokof'ev, Nikolay, and Boris Svistunov, 2001, "Worm Algorithms for Classical Statistical Models," Phys. Rev. Lett. **87**, 160601.

Rahman, Sarmed A., Randy Lewis, Emanuele Mendicelli, and Sarah Powell, 2021, "SU(2) lattice gauge theory on a quantum annealer," Phys. Rev. D **104**, 034501.

Ran, Shi-Ju, Emanuele Tirrito, Cheng Peng, Xi Chen, Luca Tagliacozzo, Gang Su, and Maciej Lewenstein, 2020, "*Tensor Network Contractions*," Lecture Notes in Physics Vol. 964 (Springer, New York).

Raychowdhury, Indrakshi, and Jesse R. Stryker, 2020a, "Loop, string, and hadron dynamics in SU(2) Hamiltonian lattice gauge theories," Phys. Rev. D **101**, 114502.

Raychowdhury, Indrakshi, and Jesse R. Stryker, 2020b, "Solving Gauss's law on digital quantum computers with loop-string-hadron digitization," Phys. Rev. Research **2**, 033039.

Rebbi, C., 1983, *Lattice Gauge Theories and Monte Carlo Simulations* (World Scientific, Singapore).

Reed, M., and B. Simon, 1980, *Methods of Modern Mathematical Physics, Vol. 1: Functional Analysis* (Academic Press, New York).

Rico, E., T. Pichler, M. Dalmonte, P. Zoller, and S. Montangero, 2014, "Tensor Networks for Lattice Gauge Theories and Atomic Quantum Simulation," Phys. Rev. Lett. **112**, 201601.

Robaina, Daniel, Mari Carmen Bañuls, and J. Ignacio Cirac, 2021, "Simulating $2+1$D Z_3 Lattice Gauge Theory with an Infinite Projected Entangled-Pair State," Phys. Rev. Lett. **126**, 050401.

Sachdev, S., 2001, *Quantum Phase Transitions* (Cambridge University Press, Cambridge, England).

Sakai, Ryo, 2019, "Renormalization of tensor networks and applications to particle physics," Ph.D. thesis (Kanazawa University).

Sakai, Ryo, Shinji Takeda, and Yusuke Yoshimura, **2017**, "Higher order tensor renormalization group for relativistic fermion systems," Prog. Theor. Exp. Phys. 063B07.

Samuel, Stuart, and Fu-Goul Yee, 1985, "A theoretical and numerical analysis of disorder operators in the chiral models," Nucl. Phys. **B257**, 85–122.

Savit, Robert, 1977, "Topological Excitations in U(1)-Invariant Theories," Phys. Rev. Lett. **39**, 55–58.
Savit, Robert, 1980, "Duality in field theory and statistical systems," Rev. Mod. Phys. **52**, 453–487.
Schaich, David, and Will Loinaz, 2009, "Improved lattice measurement of the critical coupling in ϕ_2^4 theory," Phys. Rev. D **79**, 056008.
Schauss, Peter, 2018, "Quantum simulation of transverse Ising models with Rydberg atoms," Quantum Sci. Technol. **3**, 023001.
Schollwöck, U., 2005, "The density-matrix renormalization group," Rev. Mod. Phys. **77**, 259–315.
Schollwöck, Ulrich, 2011a, "The density-matrix renormalization group: A short introduction," Phil. Trans. R. Soc. A **369**, 2643–2661.
Schollwöck, Ulrich, 2011b, "The density-matrix renormalization group in the age of matrix product states," Ann. Phys. (Amsterdam) **326**, 96–192.
Schumacher, Benjamin, 1995, "Quantum coding," Phys. Rev. A **51**, 2738–2747.
Schützhold, R., and S. Mostame, 2005, "Quantum simulator for the O(3) nonlinear sigma model," J. Exp. Theor. Phys. Lett. **82**, 248–252.
Schweizer, Christian, Fabian Grusdt, Moritz Berngruber, Luca Barbiero, Eugene Demler, Nathan Goldman, Immanuel Bloch, and Monika Aidelsburger, 2019, "Floquet approach to $\mathbb{Z}_2$ lattice gauge theories with ultracold atoms in optical lattices," Nat. Phys. **15**, 1168–1173.
Serre, J. P., 1973, *A Course in Arithmetic*, Graduate Texts in Mathematics (Springer, New York).
Sewell, Troy J., and Stephen P. Jordan, 2021, "Preparing renormalization group fixed points on NISQ hardware," arXiv:2109.09787.
Shi, Y. Y., L. M. Duan, and G. Vidal, 2006, "Classical simulation of quantum many-body systems with a tree tensor network," Phys. Rev. A **74**, 022320.
Shimizu, Yuya, 2012, "Analysis of the $(1+1)$-dimensional lattice ϕ^4 model using the tensor renormalization group," Chin. J. Phys. **50**, 749.
Shimizu, Yuya, and Yoshinobu Kuramashi, 2014a, "Critical behavior of the lattice Schwinger model with a topological term at $\theta=\pi$ using the Grassmann tensor renormalization group," Phys. Rev. D **90**, 074503.
Shimizu, Yuya, and Yoshinobu Kuramashi, 2014b, "Grassmann tensor renormalization group approach to one-flavor lattice Schwinger model," Phys. Rev. D **90**, 014508.
Shimizu, Yuya, and Yoshinobu Kuramashi, 2018, "Berezinskii-Kosterlitz-Thouless transition in lattice Schwinger model with one flavor of Wilson fermion," Phys. Rev. D **97**, 034502.
Silvi, Pietro, Enrique Rico, Marcello Dalmonte, Ferdinand Tschirsich, and Simone Montangero, 2017, "Finite-density phase diagram of a $(1+1)$-d non-Abelian lattice gauge theory with tensor networks," Quantum **1**, 9.
Silvi, Pietro, Yannick Sauer, Ferdinand Tschirsich, and Simone Montangero, 2019, "Tensor network simulation of an SU(3) lattice gauge theory in 1D," Phys. Rev. D **100**, 074512.
Silvi, Pietro, Ferdinand Tschirsich, Matthias Gerster, Johannes Jünemann, Daniel Jaschke, Matteo Rizzi, and Simone Montangero, 2019, "The Tensor Networks Anthology: Simulation techniques for many-body quantum lattice systems," SciPost Phys. Lect. Notes 8.
Simon, Jonathan, Waseem S. Bakr, Ruichao Ma, M. Eric Tai, Philipp M. Preiss, and Markus Greiner, 2011, "Quantum simulation of antiferromagnetic spin chains in an optical lattice," Nature (London) **472**, 307–312.
Sjostrand, Torbjorn, Stefan Ask, Jesper R. Christiansen, Richard Corke, Nishita Desai, Philip Ilten, Stephen Mrenna, Stefan Prestel, Christine O. Rasmussen, and Peter Z. Skands, 2015, "An introduction to PYTHIA 8.2," Comput. Phys. Commun. **191**, 159–177.
Smith, Adam, M. S. Kim, Frank Pollmann, and Johannes Knolle, 2019, "Simulating quantum many-body dynamics on a current digital quantum computer," npj Quantum Inf. **5**, 106.
Sulejmanpasic, Tin, and Christof Gattringer, 2019, "Abelian gauge theories on the lattice: θ-terms and compact gauge theory with(out) monopoles," Nucl. Phys. **B943**, 114616.
Surace, Federica M., Paolo P. Mazza, Giuliano Giudici, Alessio Lerose, Andrea Gambassi, and Marcello Dalmonte, 2020, "Lattice Gauge Theories and String Dynamics in Rydberg Atom Quantum Simulators," Phys. Rev. X **10**, 021041.
Suzuki, Masuo, 1976, "Generalized Trotter's formula and systematic approximants of exponential operators and inner derivations with applications to many-body problems," Commun. Math. Phys. **51**, 183–190.
Tagliacozzo, L., A. Celi, and M. Lewenstein, 2014, "Tensor Networks for Lattice Gauge Theories with Continuous Groups," Phys. Rev. X **4**, 041024.
Tagliacozzo, L., A. Celi, P. Orland, and M. Lewenstein, 2013, "Simulations of non-Abelian gauge theories with optical lattices," Nat. Commun. **4**, 2615.
Tagliacozzo, L., A. Celi, A. Zamora, and M. Lewenstein, 2013, "Optical Abelian lattice gauge theories," Ann. Phys. (Amsterdam) **330**, 160–191.
Tagliacozzo, L., Thiago. R. de Oliveira, S. Iblisdir, and J. I. Latorre, 2008, "Scaling of entanglement support for matrix product states," Phys. Rev. B **78**, 024410.
Tagliacozzo, L., and G. Vidal, 2011, "Entanglement renormalization and gauge symmetry," Phys. Rev. B **83**, 115127.
Takeda, Shinji, and Yusuke Yoshimura, **2015**, "Grassmann tensor renormalization group for the one-flavor lattice Gross-Neveu model with finite chemical potential," Prog. Theor. Exp. Phys. 043B01.
Temme, Kristan, Sergey Bravyi, and Jay M. Gambetta, 2017, "Error Mitigation for Short-Depth Quantum Circuits," Phys. Rev. Lett. **119**, 180509.
Thirring, Walter E., 1958, "A soluble relativistic field theory," Ann. Phys. (Amsterdam) **3**, 91–112.
Trotter, H., 1959, "On the product of semi-groups of operators," Proc. Am. Math. Soc. **10**, 545–551.
Ueda, Hiroshi, Kouichi Okunishi, and Tomotoshi Nishino, 2014, "Doubling of entanglement spectrum in tensor renormalization group," Phys. Rev. B **89**, 075116.
Unmuth-Yockey, J., Jin Zhang, P. M. Preiss, Li-Ping Yang, S. W. Tsai, and Y. Meurice, 2017, "Probing the conformal Calabrese-Cardy scaling with cold atoms," Phys. Rev. A **96**, 023603.
Unmuth-Yockey, Judah, Jin Zhang, Alexei Bazavov, Yannick Meurice, and Shan-Wen Tsai, 2018, "Universal features of the Abelian Polyakov loop in $1+1$ dimensions," Phys. Rev. D **98**, 094511.
Unmuth-Yockey, Judah F., 2019, "Gauge-invariant rotor Hamiltonian from dual variables of 3D $U(1)$ gauge theory," Phys. Rev. D **99**, 074502.
Unmuth-Yockey, Judah F., 2020, "Four-dimensional U(1) gauge theory as a rotor gauge theory" (to be published).
Unmuth-Yockey, Judah Francis, 2017, "Duality methods and the tensor renormalization group: Applications to quantum simulation," Ph.D. thesis (University of Iowa).
Unmuth-Yockey, Judah Francis, Yannick Meurice, James Osborn, and Haiyuan Zou, **2015**, "Tensor renormalization group study of

the 2D O(3) model," Proc. Sci. LATTICE2014, 325 [arXiv:1411.4213].
Vaks, V. G., and A. I. Larkin, 1965, "On phase transitions of second order," Zh. Eksp. Teor. Fiz. **49**, 975 [Sov. Phys. JETP **22**, 678 (1966)].
Vanhecke, Bram, Jutho Haegeman, Karel Van Acoleyen, Laurens Vanderstraeten, and Frank Verstraete, 2019, "Scaling Hypothesis for Matrix Product States," Phys. Rev. Lett. **123**, 250604.
Verstraete, F., and J. I. Cirac, 2004a, "Renormalization algorithms for quantum-many body systems in two and higher dimensions," arXiv:cond-mat/0407066.
Verstraete, F., and J. I. Cirac, 2004b, "Valence-bond states for quantum computation," Phys. Rev. A **70**, 060302.
Verstraete, F., V. Murg, and J. I. Cirac, 2008, "Matrix product states, projected entangled pair states, and variational renormalization group methods for quantum spin systems," Adv. Phys. **57**, 143–224.
Verstraete, F., M. M. Wolf, D. Perez-Garcia, and J. I. Cirac, 2006, "Criticality, the Area Law, and the Computational Power of Projected Entangled Pair States," Phys. Rev. Lett. **96**, 220601.
Verstraete, Frank, J. Ignacio Cirac, and José I. Latorre, 2009, "Quantum circuits for strongly correlated quantum systems," Phys. Rev. A **79**, 032316.
Vidal, G., 2007, "Entanglement Renormalization," Phys. Rev. Lett. **99**, 220405.
Vidal, Guifré, 2003, "Efficient Classical Simulation of Slightly Entangled Quantum Computations," Phys. Rev. Lett. **91**, 147902.
Vidal, Guifré, 2004, "Efficient Simulation of One-Dimensional Quantum Many-Body Systems," Phys. Rev. Lett. **93**, 040502.
Villani, C., 2012, *Théorème Vivant*, Littérature Franćaise (Grasset, Paris).
Wang, Jianwei, Fabio Sciarrino, Anthony Laing, and Mark G. Thompson, 2020, "Integrated photonic quantum technologies," Nat. Photonics **14**, 273–284.
Wang, Xiaoqun, and Tao Xiang, 1997, "Transfer matrix DMRG for thermodynamics of one-dimensional quantum systems," arXiv:cond-mat/9705301.
Wegner, F. J., 1971, "Duality in generalized Ising models and phase transitions without local order parameters," J. Math. Phys. (N.Y.) **12**, 2259–2272.
Wen, X. G., 2004, *Quantum Field Theory of Many-Body Systems: From the Origin of Sound to an Origin of Light and Electrons*, Oxford Graduate Texts (Oxford University Press, Oxford).
Wen, Xiao-Gang, 2017, "Colloquium: Zoo of quantum-topological phases of matter," Rev. Mod. Phys. **89**, 041004.
White, Steven R., 1992, "Density Matrix Formulation for Quantum Renormalization Groups," Phys. Rev. Lett. **69**, 2863–2866.
White, Steven R., 1993, "Density-matrix algorithms for quantum renormalization groups," Phys. Rev. B **48**, 10345–10356.
Wiese, Uwe-Jens, 2013, "Ultracold quantum gases and lattice systems: Quantum simulation of lattice gauge theories," Ann. Phys. (Berlin) **525**, 777–796.
Wilson, K. G., and John B. Kogut, 1974, "The renormalization group and the epsilon expansion," Phys. Rep. **12**, 75–199.
Wilson, Kenneth G., 1974, "Confinement of quarks," Phys. Rev. D **10**, 2445–2459.
Wilson, Kenneth G., 1975, "The renormalization group: Critical phenomena and the Kondo problem," Rev. Mod. Phys. **47**, 773.
Witten, Edward, 1982, "Constraints on supersymmetry breaking," Nucl. Phys. **B202**, 253.
Wolff, Ulli, 1990, "Asymptotic freedom and mass generation in the O(3) nonlinear σ-model," Nucl. Phys. **B334**, 581–610.
Wolff, Ulli, 2008, "Cluster simulation of relativistic fermions in two space-time dimensions," Nucl. Phys. **B789**, 258–276.
Wolff, Ulli, 2010, "Simulating the all-order strong coupling expansion III: O(N) sigma/loop models," Nucl. Phys. **B824**, 254–272.
Wozar, Christian, and Andreas Wipf, 2012, "Supersymmetry breaking in low dimensional models," Ann. Phys. (Amsterdam) **327**, 774–807.
Wu, Xiaoling, Xinhui Liang, Yaoqi Tian, Fan Yang, Cheng Chen, Yong-Chun Liu, Meng Khoon Tey, and Li You, 2021, "A concise review of Rydberg atom based quantum computation and quantum simulation," Chin. Phys. B **30**, 020305.
Xie, Z. Y., J. Chen, M. P. Qin, J. W. Zhu, L. P. Yang, and T. Xiang, 2012, "Coarse-graining renormalization by higher-order singular value decomposition," Phys. Rev. B **86**, 045139.
Xie, Z. Y., H. C. Jiang, Q. N. Chen, Z. Y. Weng, and T. Xiang, 2009, "Second Renormalization of Tensor-Network States," Phys. Rev. Lett. **103**, 160601.
Yang, Li-Ping, Yuzhi Liu, Haiyuan Zou, Z. Y. Xie, and Y. Meurice, 2016, "Fine structure of the entanglement entropy in the O(2) model," Phys. Rev. E **93**, 012138.
Yang, Shuo, Zheng-Cheng Gu, and Xiao-Gang Wen, 2017, "Loop Optimization for Tensor Network Renormalization," Phys. Rev. Lett. **118**, 110504.
Yoshimura, Yusuke, Yoshinobu Kuramashi, Yoshifumi Nakamura, Shinji Takeda, and Ryo Sakai, 2018, "Calculation of fermionic Green functions with Grassmann higher-order tensor renormalization group," Phys. Rev. D **97**, 054511.
You, Hao, Michael R. Geller, and P. C. Stancil, 2013, "Simulating the transverse Ising model on a quantum computer: Error correction with the surface code," Phys. Rev. A **87**, 032341.
Yu, J. F., Z. Y. Xie, Y. Meurice, Yuzhi Liu, A. Denbleyker, Haiyuan Zou, M. P. Qin, and J. Chen, 2014, "Tensor renormalization group study of classical XY model on the square lattice," Phys. Rev. E **89**, 013308.
Zhang, J., G. Pagano, P. W. Hess, A. Kyprianidis, P. Becker, H. Kaplan, A. V. Gorshkov, Z.-X. Gong, and C. Monroe, 2017, "Observation of a many-body dynamical phase transition with a 53-qubit quantum simulator," Nature (London) **551**, 601–604.
Zhang, Jin, J. Unmuth-Yockey, J. Zeiher, A. Bazavov, S. W. Tsai, and Y. Meurice, 2018, "Quantum Simulation of the Universal Features of the Polyakov Loop," Phys. Rev. Lett. **121**, 223201.
Zhao, H. H., Z. Y. Xie, Q. N. Chen, Z. C. Wei, J. W. Cai, and T. Xiang, 2010, "Renormalization of tensor-network states," Phys. Rev. B **81**, 174411.
Zhou, Yi, Kazushi Kanoda, and Tai-Kai Ng, 2017, "Quantum spin liquid states," Rev. Mod. Phys. **89**, 025003.
Zohar, Erez, and Michele Burrello, 2015, "Formulation of lattice gauge theories for quantum simulations," Phys. Rev. D **91**, 054506.
Zohar, Erez, and Michele Burrello, 2016, "Building projected entangled pair states with a local gauge symmetry," New J. Phys. **18**, 043008.
Zohar, Erez, Michele Burrello, Thorsten Wahl, and J. Ignacio Cirac, 2015, "Fermionic projected entangled pair states and local U(1) gauge theories," Ann. Phys. (Amsterdam) **363**, 385–439.
Zohar, Erez, Alessandro Farace, Benni Reznik, and J. Ignacio Cirac, 2017a, "Digital lattice gauge theories," Phys. Rev. A **95**, 023604.
Zohar, Erez, Alessandro Farace, Benni Reznik, and J. Ignacio Cirac, 2017b, "Digital Quantum Simulation of $\mathbb{Z}_2$ Lattice Gauge Theories with Dynamical Fermionic Matter," Phys. Rev. Lett. **118**, 070501.

Zohar, Erez, and J. Ignacio Cirac, 2018a, "Combining tensor networks with Monte Carlo methods for lattice gauge theories," Phys. Rev. D **97**, 034510.

Zohar, Erez, and J. Ignacio Cirac, 2018b, "Eliminating fermionic matter fields in lattice gauge theories," Phys. Rev. B **98**, 075119.

Zohar, Erez, and J. Ignacio Cirac, 2019, "Removing staggered fermionic matter in U(N) and SU(N) lattice gauge theories," Phys. Rev. D **99**, 114511.

Zohar, Erez, J. Ignacio Cirac, and Benni Reznik, 2012, "Simulating Compact Quantum Electrodynamics with Ultracold Atoms: Probing Confinement and Nonperturbative Effects," Phys. Rev. Lett. **109**, 125302.

Zohar, Erez, J. Ignacio Cirac, and Benni Reznik, 2013a, "Cold-Atom Quantum Simulator for SU(2) Yang-Mills Lattice Gauge Theory," Phys. Rev. Lett. **110**, 125304.

Zohar, Erez, J. Ignacio Cirac, and Benni Reznik, 2013b, "Quantum simulations of gauge theories with ultracold atoms: Local gauge invariance from angular momentum conservation," Phys. Rev. A **88**, 023617.

Zohar, Erez, J. Ignacio Cirac, and Benni Reznik, 2016, "Quantum simulations of lattice gauge theories using ultracold atoms in optical lattices," Rep. Prog. Phys. **79**, 014401.

Zohar, Erez, and Benni Reznik, 2011, "Confinement and Lattice QED Electric Flux-Tubes Simulated with Ultracold Atoms," Phys. Rev. Lett. **107**, 275301.

Zohar, Erez, Thorsten B. Wahl, Michele Burrello, and J. Ignacio Cirac, 2016, "Projected entangled pair states with non-Abelian gauge symmetries: An SU(2) study," Ann. Phys. (Amsterdam) **374**, 84–137.

Zou, Haiyuan, Yuzhi Liu, Chen-Yen Lai, J. Unmuth-Yockey, A. Bazavov, Z. Y. Xie, T. Xiang, S. Chandrasekharan, S. W. Tsai, and Y. Meurice, 2014, "Progress towards quantum simulating the classical O(2) model," Phys. Rev. A **90**, 063603.